Stability and variability of spatially-modulated neuronal firing patterns

Revekka Ismakov

Stability and variability of spatially-modulated neuronal firing patterns

Research Thesis

IN PARTIAL FULFILLMENT OF THE REQUIREMENTS FOR
THE DEGREE OF MASTER OF SCIENCE OF MEDICAL
SCIENCES

Revekka Ismakov

SUBMITTED TO THE SENATE OF THE TECHNION-
ISRAEL INSTITUTE OF TECHNOLOGY

CHESVAN 5776, HAIFA, NOVEMBER 2015

THE RESEARCH THESIS WAS DONE UNDER THE SUPERVISION OF DORI DERDIKMAN IN THE DEPARTMENT OF NEUROSCIENCE, RAPPAPORT FACULTY OF MEDICINE, TECHNION, HAIFA, ISRAEL.

THE GENEROUS FINANCIAL HELP OF TECHNION IS GRATEFULLY ACKLOWLEDGED.

ACKNOWLEDGMENT

I wish to express my gratitude to my adviser, Dori Derdikman, for his devoted guidance and assistance throughout my work.

I would also like to thank Omri Barak for his insights and advice, particularly in [CHAPTER 3.5] of this thesis.

Many thanks to all the lab members for their help when required, in particular Sophia Rapaport for her assistance in the DREADDs project.

Much love and gratitude to my parents, Arthur and Zoya Ismakov, for their continuous love and support throughout my academic studies.

** This page intentionally left blank **

LIST OF PUBLICATIONS:

- Ismakov, R.,Rappoport, S., Derdikman, D. *Using DREADDs to silence hippocampal place cells*. (Technion Medical Retreat, Nazareth- Israel, 2014).

- Ismakov, R., Derdikman, D. *Patterns of overdispersion in grid cells.* (Israel Society for Neuroscience, Eilat- Israel, 2014).

- Ismakov, R.,Rappoport, S., Derdikman, D. *Using DREADDs to silence hippocampal place cells.* (Technion Medical Research Day, Haifa- Israel, 2015).

- Ismakov, R., Omri Barak, Derdikman, D. *Evidence for a pivot in grid cell firing patterns.* (Society for Neuroscience, Chicago- USA, 2015).

** This page intentionally left blank **

Table of Contents

Table of Contents (cont.)

List of Figures and Tables

Abstract

The spatially-modulated neurons within the hippocampal formation of the brain are believed to be a mechanism by which memory is consolidated and physical space is perceived. These neurons include place cells, which are pyramidal neurons in the hippocampus that fire whenever the animal transverses a given location of an arena; and grid cells, located in the entorhinal cortex, which fire in a specific pattern spanning the entire environment whose firing fields form a periodic, equal-distanced hexagonal array.

These neurons have been shown to play a significant role in spatial navigation and in the perception of self-location. The system is also referred to as an "internal GPS," as it is the means by which an animal forms a cognitive map within the brain. Beyond purely mapping out space, these neurons have also been suggested to be involved in the formation and consolidation of memory.

The firing properties of these cells tend to be stable and reliable when the animal is in the same environment, exhibiting neuronal activity when the animal traverses inside the firing fields, and remaining virtually silent when outside of them. As a means by which to signify change, the neurons change the location of their firing fields when placed in a different environment. This phenomenon is known as "remapping."

In this research, we investigate how robust, reliable, and stable the firing fields of these neurons tend to be. We examined this through two different methods: a chemogenetic approach using DREADDs (Designer Receptors Exclusively Activated by Designer Drugs) to silence hippocampal cells, and a computational method, analyzing firing activity patterns of individual grid cell fields.

DREADDs is an engineered G protein-coupled receptor that responds exclusively to synthetic small molecules, while remaining inert to its natural ligands. It allows for spatial and temporal control of neurons through noninvasive means. In addition, its effects are reversible, with no damage to the system. We used an inhibitory type of DREADD to inactivate hippocampal place cells and observe the effects on the firing fields after recovery. Specifically, we wanted to see whether the fields returned to the same location or rather, remapped. Results found that both cases occur, with fields sometimes remapping and other times reverting to the same place.

In the second part of the research, we examined the firing patterns of a set of grid cells. We were interested in testing the variability between different firing fields of a single grid cell. We found that the activity between firing fields of individual grid cells exhibited a larger variability than would have been expected by shuffle measures. Here we investigated the overlaying patterns and possible source of this overdispersion. Further analysis revealed that this overdispersion is mainly the result of one specific strongly-firing grid field. Tending to be located near the borders of the environment, this field hints at the possibility that it may act as an anchoring point, or pivot point, for the formation of the grid cell orientation and phase.

These findings expose that the firing fields of both place cells and grid cells are not as static as previously assumed. The firing patterns of place cells do not remain the same when neuronal activity is manipulated through pharmacological means, grid cells do not exhibit uniform firing rates among the fields, and both suggest that other information is being relied aside from purely spatial that results in this instability and non-uniformity.

Abbreviations and Symbols

AAV	adeno-associated virus
Ach	acetylcholine
CA	*Cornu Ammonis* (areas of the hippocampus)
CCh	carbachol
CNO	clozapine N-oxide
DAPI	4', 6-diamidino-2-phenylindole
DDW	double-distilled water
DG	Dentate Gyrus
DMSO	dimethyl sulfoxide
DREADDs	Designer Receptors Exclusively Activated by Designer Drugs
EC	Entorhinal Cortex
GIRKs	G protein inwardly rectifying potassium channels
GPCR	G protein-coupled receptor
HD cells	head direction cells
hM3	human M3 muscarinic receptor
HPC	Hippocampal Cortex
IP	intraperitoneal
LSM	laser-scanning microscope
mAchR	muscarinic acetylcholine receptor
MEC	Medial Entorhinal Cortex
mm	millimeters
PBS	phosphate buffered saline
PC	place cells
Sub	subiculum
°C	degrees Celsius
µl	microliters
µm	micrometers

Preface

The organization of this thesis is divided into three sections: the introduction followed by two other chapters detailing the methods and findings of two separate research projects. The first section, [CHAPTER 1], beginning on the following page, provides a background of the hippocampal formation and of the neurons located in the brain region. The distinctive firing patterns of these neurons are detailed in this section, which relate to both of the projects that the thesis will go on to explain.

The next part, [CHAPTER 2], reports the details of the first research project concerned with using DREADDs to silence hippocampal place cells. This research is the smaller project of the two, and was mainly conducted as a proof of principle. It is an ongoing project, and as such, the findings are not entirely conclusive, and further research needs to be conducted to provide more clear and concise findings.

Lastly, the third section, [CHAPTER 3], aims to explain and understand specifications of grid cell firing patterns by investigating the variability of the activity. It elaborates on specific findings pertaining to grid cell firing activity. This is the larger of the two projects, and delivers more conclusive results.

I hope this research manages to shed light on the tools it applies, as well as adds to the understanding of the spatially-modulated neurons it examines, and more broadly, to the knowledge of spatial perception and memory in general.

In the words of neuroscientist Santiago Ramón y Cajal, "*As long as our brain is a mystery, the universe, the reflection of the structure of the brain will also be a mystery*" [1].

Introduction

Hippocampal neurons' role in space and memory

'It is place, permanent position in both the social and topographical sense, which gives us our identity." — J.B. Jackson

Chapter [1.1]

Hippocampal formation

The hippocampus is a region in the brain found to be highly involved in spatial navigation and the consolidation of memory from short-term to long-term [2]. It is via neurons located within this region that spatial representations of the environment are encoded and formed in the brain. For these reasons, it is one of the most highly studied regions in the brain, and of strong interest in the field of neuroscience.

The name of the region means "seahorse" in Latin, alluding to its distinctive, S-shaped curve. Included in this structure is the dentate gyrus (DG), CA1, CA3, and the subiculum [3]. The dentate gyrus is a tightly packed layer of small granule cells, while the CA areas are filled with densely packed pyramidal cells.

The pathways of signaling form a loop within the hippocampus, with external input entering mainly through the entorhinal cortex, and then exiting from the pyramidal cells in CA1 back into the subiculum and layers of the entorhinal cortex. The signal pathway of subicular neurons also flows into the entorhinal cortex. These feedback loops demonstrate that there is information flowing in both directions within the hippocampal cortex, and that the neurons in the different sub-regions receive signals from each other. FIGURE 1.1 provides an illustration of the region and a simplified diagram of basic circuity and directions of signal flow.

The hippocampus' specific role in the function of memory was realized when an epileptic patient, known as H.M., underwent surgery at the site of his seizures. He had a bilateral medial temporal lobectomy removing almost entirely the hippocampal regions and some associated areas. The surgery resulted in an inability to form any new episodic memories.

While his retrograde memory, the memory formed before the time of the surgery, remained relatively intact, he was unable to consolidate new episodic and declarative memories into long-term storage [4]. Thus, though some types of memory were undisrupted, including working memory and procedural memory, new events were unable to be recorded into explicit storage.

In addition to this specific and special case, disorders relating to loss of memory function are seen to have a strong effect on the hippocampus. In Alzheimer's diseases, where memory loss is the main symptom, the hippocampus and entorhinal cortex are the first to suffer damage [5]. This exposes the strong and highly specific function of the hippocampal formation in memory encoding and retention.

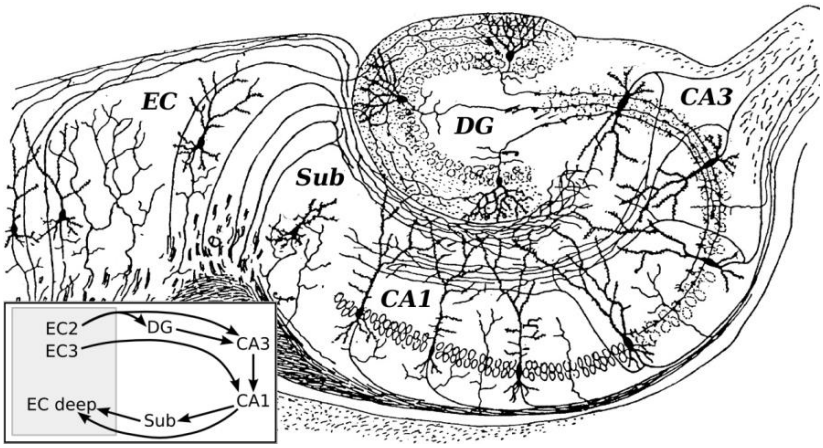

FIGURE 1.1 *Depiction of the hippocampal structure illustrated by Santiago Ramón y Cajal. Lower left corner shows simplified diagram of the basic circuitry and signal flow projections between hippocampal regions. Wikipedia-modified image from Histologie du Système nerveux de l'Homme et des Vertébrés,, Santiago Ramón y Cajal., 1909 [6].*

Chapter [1.2]

Spatially-modulated neurons

Within the hippocampal formation are specific spatially and directionally modulated neurons. These include place cells, grid cells, head direction (HD) cells, and border cells. This section will outline the basic characteristics of these four cell types. These neurons, and the circuits underlying them, may have significant implications for memory. The spatial context for memories and past experiences are embedded in their activity, and thus they may play a pivotal role in memory processes, in conjunction with mapping out space and location.

The 2014 Nobel Prize in Medicine and Physiology has been awarded for the discovery of place cells and grid cells, indicating their strong impact in scientific knowledge and understanding.

{1.2.i} Head Direction Cells

Head Direction (HD) cells are located in multiple brain regions, including the anterior thalamus, presubiculum, and entorhinal cortex. Their firing activity is tuned to the animal's head direction, with a specific preferred head direction for an individual HD cell [7].

They are strongly dependent on the vestibular system, specifically the semicircular canals of the inner ear. The direction and position of the animal's body in relation to its head appears to be less influential on the neuron's firing. HD cells continue operating even in the absence of light, responding to rotations of the head, although the HD alignment may drift slowly over time [8].

The role of sensory input in their function is complex; sensory input doesn't purely drive HD firing activity, but is also not entirely independent of it [9, 10].

{1.2.ii} Place Cells

Place cells are pyramidal neurons located mainly in the CA1 and CA3 regions of the hippocampus. They fire whenever the animal enters a specific location of the environment, and are virtually silent when the animal is anywhere outside this region. This area is called the "firing field" of the cell. Most place cells have one

firing field, although they can sometimes have two or more. The larger the arena, the more likely the cell will have more than one firing field [11]. The entire population of place cells is thought to span out the entire environment.

When placed into a different arena, the place cells change the location of the firing fields, or may become entirely silent, while other cells silent beforehand may start firing [12]. This is known as "remapping". When placed back into the original arena, they resume their original firing patterns.

This is thought to be the mechanism by which the cells recognize similar environments, and signify novelty for novel arenas.

{1.2.iii} Grid Cells

Grid cells are neurons located within the medial entorhinal cortex (MEC) and additional regions. Their firing activity spans out the entire arena and forms a periodic hexagonal-array of firing fields that are equi-distanced from each other. The sizes of the fields tend to be similar in size for an individual neuron with a regular spacing between them. This specific firing pattern tends to be rather robust, and these neurons have even been described as the "crystals of the brain" [13].

The grid alignments of the firing fields of these cells have different spacing and different orientations to the walls. Neurons found next to each other in the brain tend to have similar spacing distances, with differing phases. This is dependent on which layer of the MEC the neurons are located; cells more ventral have larger

spacing, while cells more dorsal have smaller spacing. The spacing tends to fall into discrete values, rather than a uniform distribution of values. Groups of grid cells with similar spacing and orientation within a single rat are referred to as "modules." So grid cells are organized by modules within the entorhinal structure.

Some grid cells also code for directionality, in a similar manner to head direction cells. Thus, there are two types of grid cells: pure grid cells, which provide information purely on location, and conjunctive grid cells, which are grid cells with a combined direction-coding characteristic, providing information on both location and head direction. The pure grid cells are found mainly within Layer II of the MEC, while conjunctive grid cells are found in deeper layers. Please reference to FIGURE 1.2 for illustrative examples.

The presubiculum and parasubiculum send out projections into the entorhinal cortex. Thus grid cells most likely receive information about the animals' head direction from the presubicular and parasubicular head direction cells.

In summary, grid cells:

- Have multiple firing fields, as compared to place cells, which have one, or only a few.
- Have firing fields that are organized into a hexagonal pattern, with the fields approximately the same size and same distance from each other.
- Are organized into modules within the MEC by their spacing.
- Come in two types: pure grid cells, with firing independent of head direction, and conjunctive grid cells, exhibiting grid-like firing only when the animal's head is faced in a specific direction.

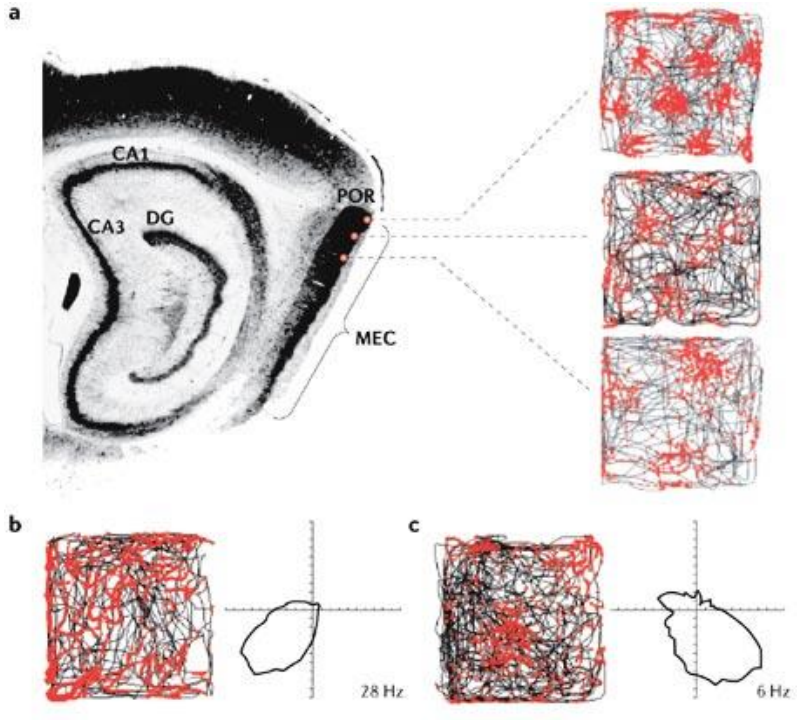

FIGURE 1.2 *Illustrations of the different types of grid cells and where they can be found within the entorhinal cortex. a) Hippocampus, postrhinal cortex, and medial entorhinal cortices labeled, with grid cell examples of various spacing, pointing to the layers of the MEC where they tend to be found. This illustrates that different layers tend to have grid spacing of specific discrete values. (b) and (c) Example of a conjunctive cell, displaying information of both head direction and space. Each panel shows trajectories in black and grid cell spikes in red. Note that the red dots are clustered into groups and the groups form a hexagonal pattern. The polar histograms in (b) and (c) show the head-direction rate of each cell as a function of the head-direction. Figure taken from McNaughton et al., 2006 [14].*

{1.2.iv} Border Cells

Border cells are neurons known to be located in the subiculum, the presubiculum, the parasubiculum, and the entorhinal cortex. They fire when the rat is within a certain distance of a given border of the arena and have been suggested to be significant for planning trajectories or possibly anchoring place and grid fields to a specific boundary reference point. They are intermingled in the entorhinal cortex with grid and head direction cells, encompassing only about 10% of the entire population [15]. FIGURE 1.3 summarizes the four types of cells found in these brain regions.

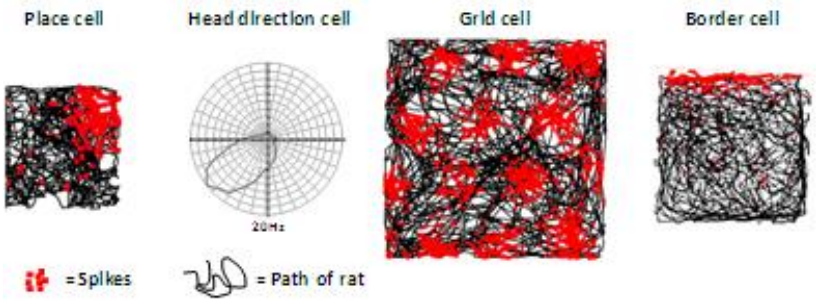

FIGURE 1.3 *Illustrations of the four spatially and directionally-modulated neurons: place, head direction, grid, and border cells. Red dots signify spikes while black line shows trajectory of the animal. In the polar histogram the rate is shown as a function of head direction. Place cells fire in a specific region of the environment. HD cells fire to a preferred head direction. Grid cells have a unique firing pattern that forms a hexagonal array spanning the entire area. Border cells fire to a given distance of a preferred border or boundary of an environment. Figure taken from Jeffery Lab, UCL website [16].*

Chapter [1.3]

Cognitive map

"Sense of place is the sixth sense, an internal compass and map made by memory and spatial perception together."

— Rebecca Solnit, *Savage Dreams*

These neurons all aid in the formation of a cognitive map within the rat's brain. The notion of a cognitive map has been proposed by Tolman. He demonstrated the concept in a series of studies examining how a rat reacts to a change in routes towards a reward, and whether it is able to choose the shortest and most correct path available without ever having crossed through it.

In one such study, the rat was trained to run a maze with one available maze arm leading towards a reward through a convoluted, lengthened path. After the rat was trained in this specific maze, the rat was then introduced to a sunburst maze, which the rat had not been familiarized with. This maze included multiple maze arms placed at even intervals at varying degrees (see FIGURE 1.4 for reference). Although the rat was not familiar with this maze, and had never taken the paths before, he was in some cases able to accurately choose the correct path to the reward, despite the fact that it started and was directed in a different location than the path he had been originally trained to run within the first maze.

This suggested to Tolman that an intrinsic cognitive map exists within the brain. It is through the aid of the spatially-modulated neurons located within the hippocampal cortex that the map originates and through which we are provided with a sense of space. These neurons are capable of achieving this by acting as cognitive representations of place and location.

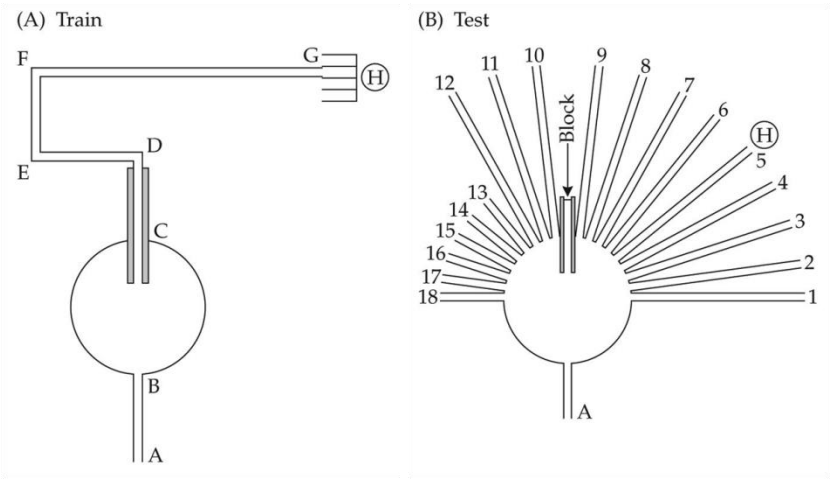

FIGURE 1.4 *Sunburst maze experiment set-up. a) The apparatus the rat was trained to run across, with (H) signifying the location of the reward. b) The sunburst maze the rat was tested on, with maze arms placed at even intervals at varying degrees. The study demonstrated that the rat was able to choose the correct path in the sunburst maze despite being unfamiliar with the path. Image taken from Tolman et al., 1946 [17].*

Chapter [1.4]

Remapping and grid realignment

"There is no mysterious essence we can call a 'place'. Place is change. It is motion killed by the mind, and preserved in the amber of memory."

— J.A. Baker, *The Peregrine*

Place cell firing activity tends to be stable within the same arenas. However, they are known to abruptly change their firing pattern and change the locations of their place fields, in what is referred to as "remapping," as a reaction to changes in the external environment. Usually small changes in sensory input are not enough to enable a response in the system, but strong changes will elicit a reaction in place cell firing [18].

The current space and the shifting environment constantly adjust the firing patterns of these neurons accordingly. There are three main types of remapping or deformation of place cell firing. Space deformation occurs when the environment very rapidly shifts in size or shape. Place cells usually respond to this type of change by elongating or shrinking their firing fields to adjust for the rescaling of the arena. The positions of the different place fields are usually in relatively similar positions from their surrounding boundaries.

Rate remapping (also known as "local remapping") is when the locations of the firing fields remain the same, by changes occur in the firing rate. This usually occurs for a small, local change in the arena, such as a change to the color of the

walls. For a strong external change to the environment, place cells preform global remapping, where the place fields entirely change locations, or might become active or inactive. When returning the animal to the original arena, the place cell firing fields all reverse to the original firing patterns within that arena. FIGURE 1.X provides examples of such cases.

In summary, the three types of remapping or deformation are:

- Rate remapping, where the positions of the fields remain the same, but the firing rate changes.
- Global remapping, where the activity of the place cells entirely change, with change in position of the fields as well as activation or inactivation of cells that were previously firing or were silent.
- Space deformation, where the fields distort through elongation of rescaling while remaining in a similar location relative to the surrounding borders.

Grid cells, with information from place cells, also respond and adjust firing patterns to different environmental changes. Grid patterns are exhibited at the animal's entrance into the arena, and remain more or less stable thereafter. Visual input is not required for their functioning, as they remain firing in the same manner when the lights are turned off in an environment [19], however visual input does exert influence over their patterns of firing. This is seen by the observation that a rotated cue card on the wall of an arena will result in the grid pattern rotating in the same manner.

Place cell rate remapping has no effect on grid cell firing patterns. When an animal is placed into a different arena however, a situation in which place cells

undergo global remapping, the grid pattern will adjust its phase and orientation. Neighboring neurons within the brain all adjust their firing patterns by the same offsets to each other. This was seen in a study recording grid cells from Layer II of the MEC [20]. Whether this localized coherence extends to other layers is still unclear. The findings suggest that during global remapping, the grid cell firing maps realign with environment changes while remaining their intrinsic spatial phase structure.

Space deformation had similar effects in grid cells as in place cells, with the grid pattern in most cases stretching or shrinking to the rescaling of the arena. It rescales with respect to the boundaries, returning to its original shape once returned to the original arena. The grid pattern also distorts and decreases in "gridness" at such changes.

In summary, grid cells in reaction to place cell remapping mechanisms, have specific responses (see FIGURE 1.5 for illustration):

- Rate remapping in place cells causes no change in grid cell firing patterns.
- Global remapping in place cells causes grid cells to adjust their offset, although spacing between grid fields remains the same.
- Space deformation results in most cases in the deformation of the grid cell pattern to rescale in the same manner as the arena change (i.e. elongation of the environment leads to an elongation of the grid pattern).

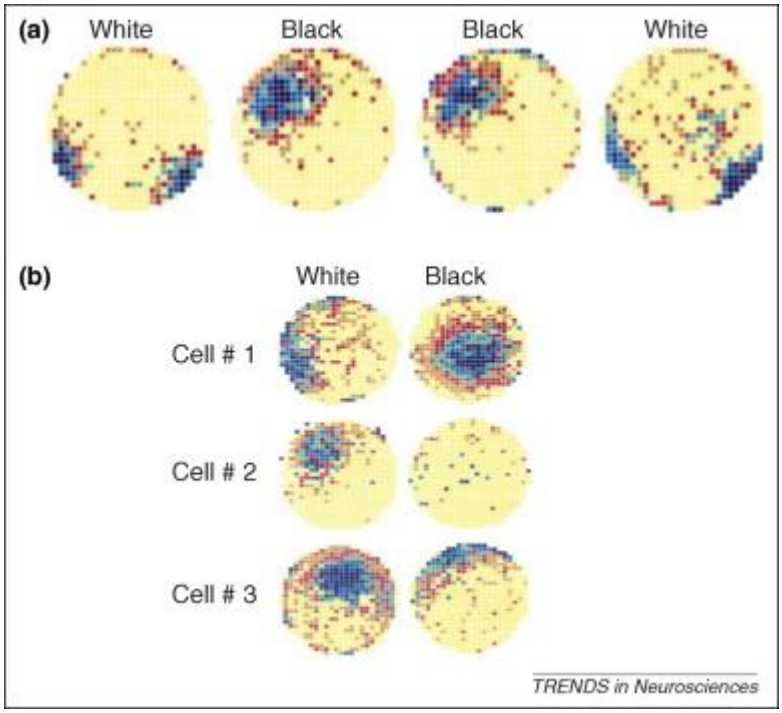

FIGURE 1.5 *Examples of remapping of place cell firing fields. a) demonstrates how the place cell remaps to a different location, and returns to its original firing activity when placed back in the original white room. b) shows three other examples where the field remaps (cell #1 and cell #3) and a case where the cell entirely silences its firing activity (cell #2). Image taken from Colgin et al., 2008 [21].*

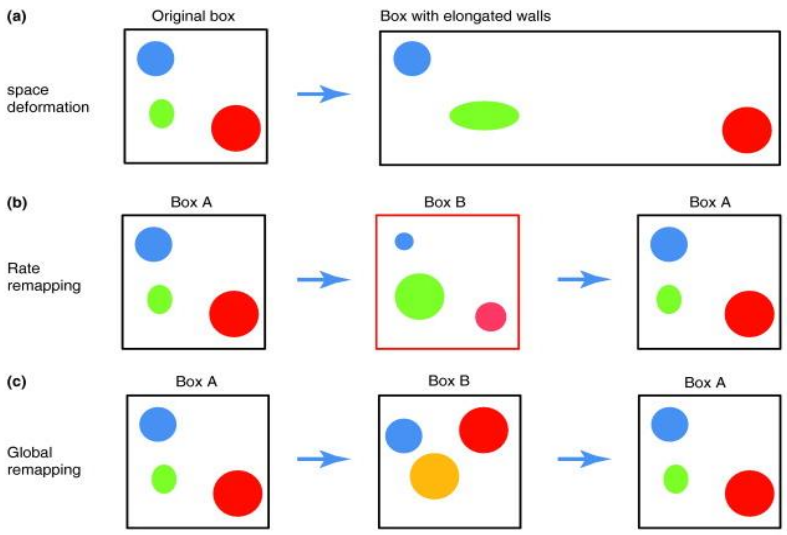

FIGURE 1.6 *Illustrations depicting different types of remapping: space deformation, rate remapping, and global remapping. Each spate color denotes a different place cell. Space deformation leads to the deformation of the fields in relation to the walls. Rate remapping leads to changes in the firing rate of each field. Global remapping leads to the place cells changing location of their firing, or entirely silencing. When returned to the original arena, the neurons resume their original firing patterns. Figure taken from Derdikman and Moser, 2010 [22].*

Part I

Chemogenetic inactivation of hippocampal place cells in rats

"Life is a question of nerves, and fibres, and slowly built-up cells in which thought hides itself..." — Oscar Wilde

Chapter [2.1]

Introduction to DREADDs

DREADDs (Designer Receptors Exclusively Activated by Designer Drugs) are a synthetic chemogenetic tool used for cellular signaling control. They are mutant G-protein coupled receptor (GPCR) drugs which can be activated through the pharmacologically-inert ligand clozapine N-oxide (CNO) [23], while remaining insensitive to endogenous ligands. With this technique, GPCR activity can be moderated in vivo noninvasively.

There are various GPCR signaling cascades that the drug acts on, including those activated by Gq, Gi, and Gs [24]. Directed molecular evolution of the human M3 muscarinic receptor (hM3) in yeast was the method by which the first Gq DREADD was created. Mutants of hM3 underwent multiple cycles of random mutagenesis and were chosen for CNO-mediated agonist activity. Through this directed evolution, they modified the receptors to favor the synthetic CNO substrate over its natural ligand. A few key requirements were necessary of the selected mutant receptors:

- Nanomolar potency for CNO.
- Lack of response to the endogenous muscarinic acetylcholine receptor (mAchR) ligand acetylcholine.
- Low levels of constitutive activity [25].

The goal was for the engineered receptors to react to the otherwise inert ligand CNO, while not responding to the ligand acetylcholine. This would allow for the precise control of the mutant receptors with no interference from the endogenous receptor ligands. In addition, the mutants were also selected to be low in constitutive activity so as for the mutant receptors to be relatively inactive when expressed in vitro and in vivo [26]. This ensured that overexpression of the receptors would not increase activity of the expressed region without controlled injection of CNO, permitting the engineered receptors to mimic the signaling pattern of acetylcholine-activated native muscarinic receptors with precise and defined control.

In neurons, DREADDs acting on Gq-mediated signaling depolarizes the cell. This enhances neuronal firing by increasing excitability of the neurons, and results in the production of burst-like firing. Thus, DREADDs hM3Dq (Gq-mediated) is used as an excitatory tool to increase neuronal firing.

In a similar method, through same point mutations in the M2 and M4 muscarinic acetylcholine receptors, DREADDs acting on Gi-mediated signaling were created. This DREADD subtype, called hM2Di and hM4Di, unlike the Gq-preferring DREADD, silences rather than excites the cells. Muscarinic Gi-coupled GPCRs are able to activate G protein inwardly rectifying potassium channels (GIRKs). DREADD hM4Di is able in a similar manner to activate GIRKs by dissociating beta/gamma subunits, which achieves neuronal silencing [25]. In hippocampal pyramidal neurons, this Gi-preferring DREADD induces hyperpolarization as well as silences spontaneous and depolarization-evoked firing (see FIGURE 2.1 and 2.2 for reference).

The hM4Di receptor was tested in cultured hippocampal neurons. In natural hippocampal neurons, carbachol (CCh), an analog of acetylcholine, rather than CNO induces neuronal inhibition. However, in hippocampal neuron culture expressing the hM4D receptor, CNO induced neuronal hyperpolarization. Inhibition of the neurons mediated by CCh through the native receptors was not affected by the expression of these engineered receptors in the neurons. This shows that the expression of these receptors does not alter natural functioning of the cells. Thus, without disrupting resting membrane potential of untreated neurons infected with DREADDs, CNO was able to prevent excitation of the cultured hippocampal neurons. The ability to directly and precisely control the firing activity of hippocampal neurons with this biologically-engineered means is demonstrated through these studies.

The activity of neurons rises in a dose-dependent manner with the injection of CNO. Onset starts at around ten minutes post-CNO injection and peaks around 45 minutes [27], although this is dependent on the neuronal population in which the DREADDs is expressed. The offset is on the order of hours. The receptors are expressed via viral delivery methods, where an AAV (adeno-associated virus) is loaded with the DREADD gene and a promoter region that are then expressed into the region of interest.

We would like to implement this cellular signaling control drug in active, behaving animals. This chemogenetic tool is a highly appealing candidate for the direction we would like to go for several reasons, including:

- Permits spatial and temporal experimental manipulation of neuronal firing.
- No apparent effects on the morphology, electrophysiological parameters of neuronal health.
- Noninvasiveness, thus permitting behavioral testing in awake, active animals.
- Reversible effects, allowing us the opportunity to investigate effects after recovery.

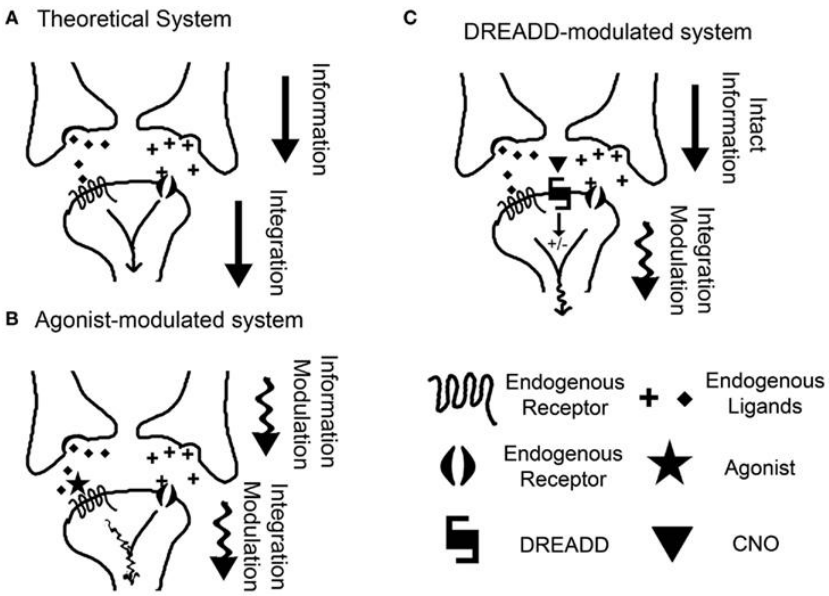

FIGURE 2.1 *Illustration of how the concept of DREADDs works. (a) illustrates how within a theoretical system endogenous ligands (information) act on endogenous receptors (integration). (b) depicts an agonist-modulated system, where agonists act on the endogenous receptors to inactivate and manipulate regular neuronal activity, thereby modulating information and integration of regular signaling. (c) represents the DREADD-modulated system, which allows endogenous ligands to act undisrupted on endogenous receptors, without having any effect on the DREADD receptor, while CNO acts on the DREADD receptor, while being inert to the endogenous receptors. Thus, allowing for incoming information to remain intact, but modulating the integration. Image taken from Farrell, 2011 [28].*

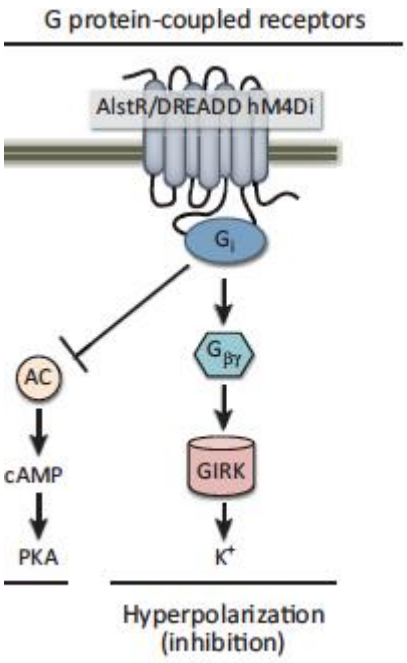

FIGURE 2.2 *Illustration of the mechanism by which DREADDs hM4Di receptors work. They act on G protein-coupled inwardly rectifying potassium channels (GIRKs) through dissociation of G beta/gamma subunits. This induces hyperpolarization, and thus inhibition. Image modified from Pollock et al., 2014 [29].*

Chapter [2.2]

Research goals

Our motivation for this research was primarily a technical one. We wanted to check that DREADDs does in fact operate as it should *in vivo* in awake, behaving rats. We hoped to observe the specific effects of the drug, including time of onset, strength of effect, and recovery of neuronal firing. Majority of previous studies using this tool applied it to cultured brain slices or to anesthetized animals, although few have used it on behaving animals, mostly mice [30-32]. We hoped to expand on the methods and understanding of this technique by studying its effect on hippocampal cells in behaving rats.

Some studies have applied DREADDs *in vivo* in studying behaving animals. One group has demonstrated that neuronal activity can be remotely controlled through these evolved G protein-coupled receptors in mice [26]. It's been further used to show behavioral and physiological differences in memory with the manipulation of neuronal signaling using this tool, including enhancing memory [30], disrupting consolidation of fear memory [31], and generating a synthetic memory [32]. These studies have focused on using mice as the choice of model.

We wanted to expand on the understanding of this chemogenetic approach as a tool by applying it to rats. In addition to confirming its efficiency and examining the details of its effects, we also wanted to examine recovery and how the drug affected the firing activity after the effects were washed out of the system.

Specifically, we wanted to see how place cell fields were affected after resuming their natural firing patterns. Would the fields return to the same location as before injection of the ligand CNO and activation of the engineered receptors, or would they remap to another location? Remapping to a new location is a way for place cells to signify novelty or change of an arena. The question is a significant one as it sheds light on just how reversible the effects of DREADDs actually are, as well as investigates how stable the firing fields of hippocampal place cells tend to be.

Thus, the goals of our research include:

- Confirm that the inhibitory DREADD is able to silence hippocampal cells *in vivo* in awake, behaving rats.

- Test whether place cell firing fields before activation of DREADDs and after recovery remained in their same locations or if they remapped.
- Examine if the neuron's firing rate had any change before DREADD activation and after DREADD recovery.

This will allow us to test the limitations of the chemogenetic technique of silencing neurons, as well as reveal the stability of hippocampal firing fields when manipulated with such pharmacogenetic tools.

Chapter [2.3]

Materials and Methods

{2.3.i} Subjects

Experiments were conducted on five male Long-Evans rats of at least 3 months of age. Animals were housed in the Animal Facility of the Technion Faculty of Medicine in single-housed, transparent cages filled with sawdust where they were maintained on a 12 hour light/dark cycle.

Three of the rats were used for electrophsiological analysis and histology, while the other two were used solely for histology. Rats that undergone intracranial viral injection surgery without the implantation of an electrode microdrive received food and water *ad libitum*. Rats used for behavioral testing and electrophysiological recordings were on a food-restricted diet where they were kept at 85% of their natural weight.

All procedures involving animals were conducted in compliance with the institutional guidelines of the Technion Animal Facility.

{2.3.ii} AAV viral construct

The DREADDs AAV virus was purchased from Bryan Roth's Lab at North Carolina University. The inhibitory AAV-hSyn-hM4D(Gi)-mCherry and AAV-CaMKlla-hM3D(Gi)-mCherry were used.

In order to avoid repeated freeze-thaw cycles, the virus was pipetted from the manufacture's vial into smaller working aliquots in a Class II Biosafety Cabinet and stored in a -80 °C freezer.

{2.3.iii} Intracranial viral injection surgery

Animals were anesthetized in an induction cage at 5% isoflurane, and then transferred to a rodent stereotaxic apparatus, where they were head-fixed with ear bars. Isoflurane was gradually decreased to around 2%, while checking for reflexes. An incision was made to expose the skull, and a hole was drilled above the site of the hippocampus, at coordinates relative to Bregma: 2 mm lateral and 3 mm posterior. Once dura was exposed, a duratomy was performed (see FIGURE 2.3 for illustration).

An AAV viral construct containing DREADDs was delivered with a 5-ml Hamilton syringe that was held in a Quissential Stereotactic Injector (QSI). The virus was injected at between 0.03 and 0.06 µl/second, at depth 2 µm, with the amount

injected ranging from 0.5 to 1.5 µl. The syringe was left in place for about 10 min before and after every injection to limit diffusion into the track of injection.

After injection, the skin was sutured. Animals were removed from the apparatus and monitored for full recovery. Antibiotic injections were administered daily for three days after surgery to facilitate recovery.

{2.3.iv} Histological analysis

Rats were perfused between 3 to 8 weeks after the intracranial injection of the DREADDs viral construct in order to allow receptor translation and trafficking. They were heavily anaesthetized with Pental and then perfused intracardially with saline, heated to body temperature, followed by a 10% formalin solution, used for fixation. Brains were removed from the skull and post-fixed in 10% formalin for at least 2 days. They were then transferred to PBS for about 24 hours, and then cyroprotected in a 10% sucrose solution for another couple of days. The brain was then frozen using liquid nitrogen and isopentane.

After, the brain was coronally sliced at 40-70 µm using a cryostat and each section mounted onto a glass microscope slide. Slides were then mounted with DAPI-infused mounting medium and a coverslip was applied.

Some brain slice slides were additionally stained with Alexa 568 antibody.

High resolution images were acquired using a confocal laser-scanning microscope (LSM 510).

{2.3.v} DREADDs injection and microdrive implantation

Anesthetized rats were placed in a rodent stereotaxic apparatus and the DREADDs viral construct intracranial injection was performed as detailed in [Section 2.3.iii] above. The virus was injected at two or three depths (in mm): 2.1, 2.7, and 3.5, at a rate of 0.06 µl/second.

After injection of the virus, a microdrive was implanted above the area of injection and secured with skull screws and dental acrylic. The anterior most skull screw was used as a ground electrode.

The microdrive contained four tetrodes. Each tetrode was constructed by twisting together four strands of platinum wire. The tetrodes were threaded through a steel cannula, which connected to the ground screw acting as an animal ground.

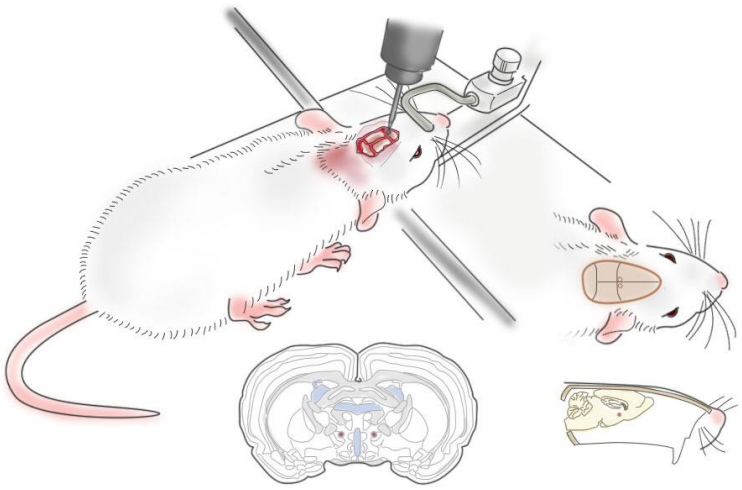

FIGURE 2.3 *An illustration of the stereotactic apparatus used for the viral intracranial injection and the microdrive electrode implantation. The apparatus allowed for precise identification of the necessary coordinates, using Bregma as reference. Image taken from Clodrosome webpage on animal injections [33].*

{2.3.vi} Electrophysiological analysis

After a week for recovery, rats were trained to forage for food rewards in an environment. The environment was a 100-by-100 cm square arena. Electrodes were lowered slowly by 50-100 μm until the first hippocampal place cells could be detected.

Once place cells were obtained, given that it was a minimum 30 days after intracranial surgery to allow for expression of the virus, rats were administered CNO. Neurons were then recorded from at specific time intervals.

All injections were intraperitoneal (IP). CNO was dissolved in dimethylsulfoxide (DMSO) and then diluted in 0.9% saline solution. X (amount) was injected for each rat.

Recording sessions were composed of 30-40 minute explorations of the arena. There were about four recording sessions for each place cell silencing experiment: before CNO injection session, an hour after injection session, two hours after session, and the recovery session. The arena was cleaned with soap and water in between all sessions.

A Neuralynx Cheetah recording system was used to acquire the single unit and positional data. See FIGURE 2.4 for a simplified illustration of the set-up.

Neuronal units were analyzed using Matlab (MathWorks) and Neuralynx.

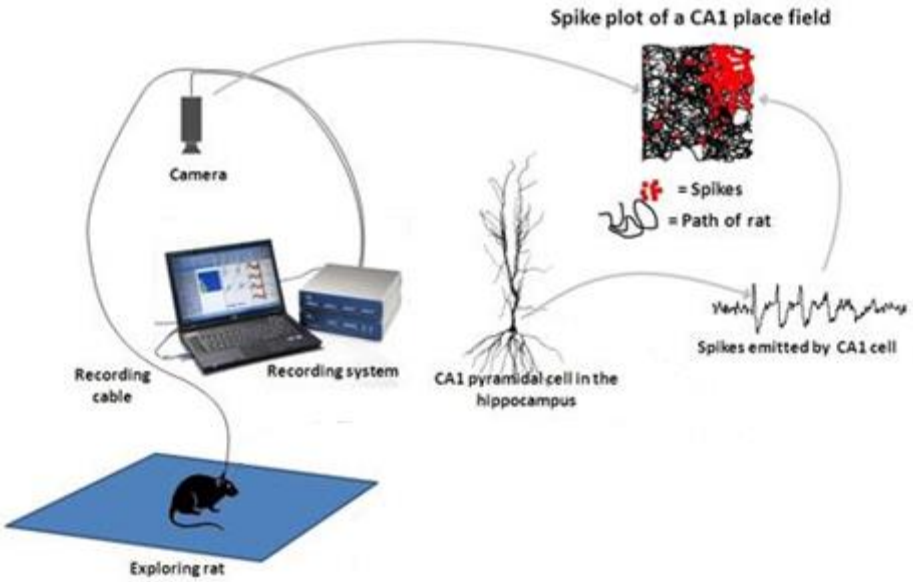

FIGURE 2.4 *An illustration of the electrophysiology recording set-up. The rat runs around the arena, with LED headlights connected to the drive implanted at his skull. The camera records from above, with the LED headlights allowing for head direction and rat position tracking. Information on the neuronal activity is sent to the recording system. Thus, we are able to visualize spike activity emitted from CA1 pyramidal cells overlapped with the position of the animal in order to detect spatially-modulated neuronal activity. Image modified from Jeffery lab, UCL [34].*

Chapter [2.4]

Results

{2.4.i} Histology

Histology was performed to ensure that the virus was indeed expressed in the region of interest. Below are images captured with a Confocal LSM 700 microscope. Images visualize that the pyramidal neurons within the hippocampus were indeed expressed with the DREADDs receptor, delivered through an AAV viral construct (see FIGURE 2.5-2.8 for images).

While the expression in the hippocampus was indeed within the pyramidal cell layer (reference FIGURE 2.7), the expression in the DG was actually most prominent outside of the main granule cell layer (FIGURE 2.6). The virus was expressed in the interneurons.

Most images below show native mCherry florescence, although some were additionally stained with Alexa 568 for more vivid expression.

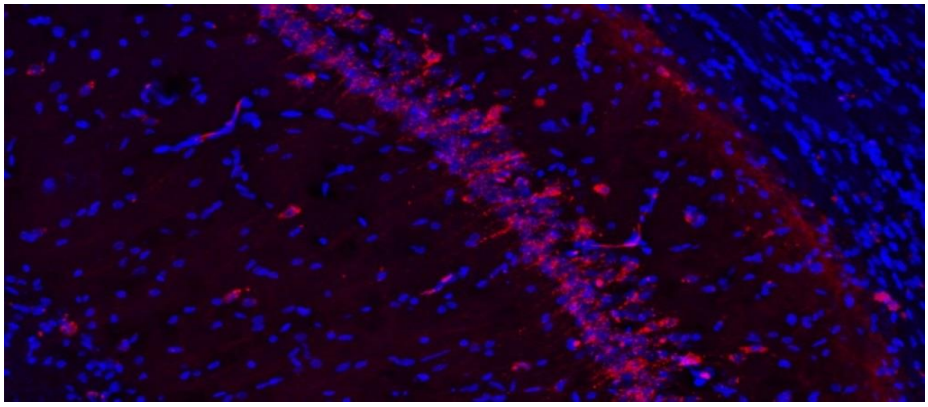

FIGURE 2.5 *Merged image showing co-localization of DAPI stained cell nuclei and native virus mCherry florescence. Pyramidal neurons in the CA1 area of the hippocampus. Taken with a 25x objective.*

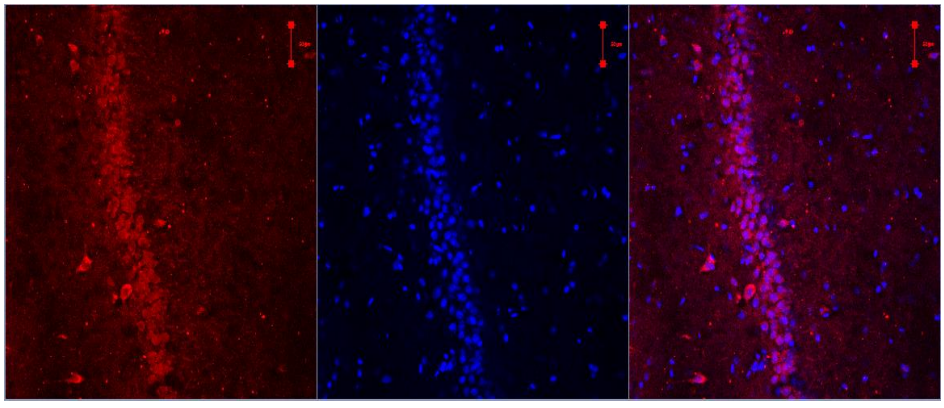

FIGURE 2.6 *Left image shows close up view of hippocampal cells loaded with Alexa 568. Center image shows same view with DAPI staining, outlining cell nuclei. Right image is merged image. Scale bar shown is 50 micrometers. All images were taken with a 25x objective and with the same parameters*.

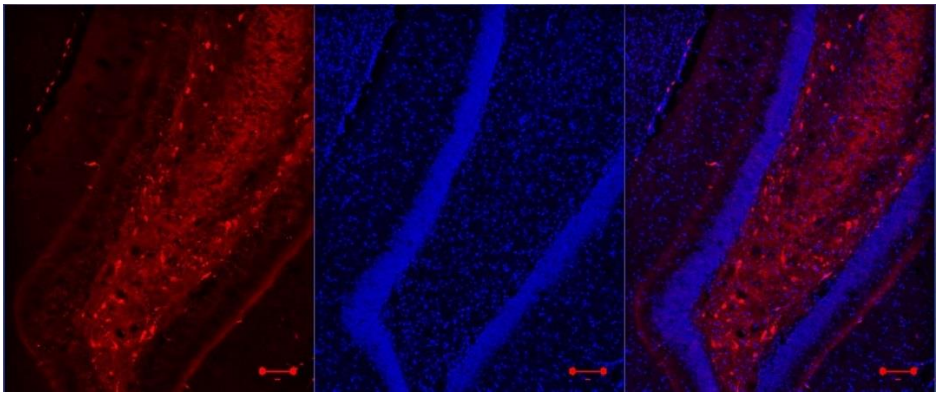

FIGURE 2.7 *Right most image shows the dentate gyrus region of the hippocampus with native mCherry florescence. Center shows the same image with DAPI staining, visualizing cell nuclei. Right most image is the merged images of DAPI staining and native mCherry florescence of the DREADDs virus expression. Viral construct with hSyn promoter used here. Scale bar is at 100 micrometers. All images were taken with a 25x objective and with the same parameters*.

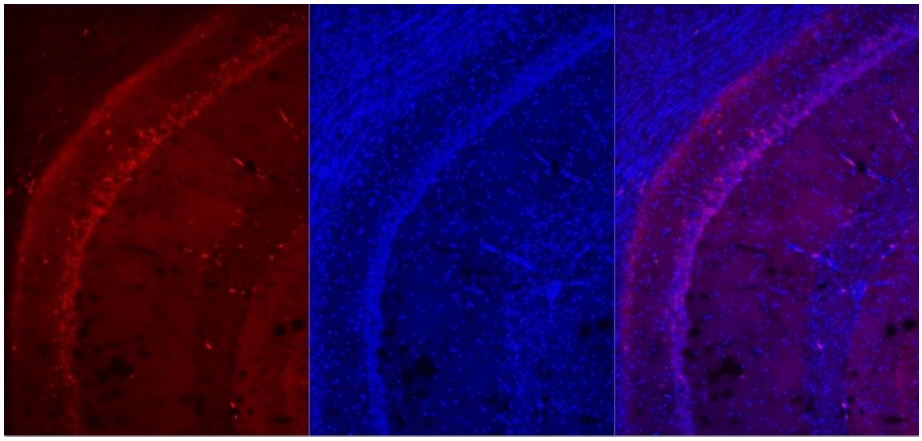

FIGURE 2.8 *Left images shows CA1 region of the hippocampus with native mCherry florescence. Center image shows DAPI staining of same image. Left image is merged image of DAPI staining and mCherry florescence. All images were taken with a 25x objective and with the same parameters*.

{2.4.ii} Electrophysiology

Three rats undergone surgery implanting an electrode microdrive within the CA1 region of the hippocampus. After recovery, they were trained to forage an open arena while the electrodes were lowered until detection of place cells. The cells were then recorded at different timestamps of CNO injection. The experiment yielded thirteen cells (eight place cells and five non-place cells), which were examined for this study.

Place cells were indeed silenced to some degree with the administration of CNO after DREADDs expression in the hippocampal brain region. All the cells strongly diminished their firing rate. The results appear to show rate remapping after DREADDs activation. TABLE 2.1 summarizes the cells recorded in the study.

Recovery of the effect, in half of the cases resulted in the place field remapping to another location, while in the other half it returned to the same place and firing rate.

In order to confirm that the cells remapping were indeed the same cells as the original recorded, we made examined the spike shape and cluster forms during spike sorting. FIGURES 2.12-2.14 plot the spike waveforms and other properties of the spike shape for the cells that remapped.

In addition to some cases remapping, the firing rate appears to vary after recovery from before injection of the ligand. On average, it varies around 43.34% of the original firing rate, both for the peak rate and the overall rate. This variation manifests as both decrease and increase of the original pre-injection

firing rate compared to the recovery rate. FIGURE 2.10 and 2.11 plot the peak firing rate and the overall firing rate, respectively, before CNO injection, during activation of DREADDs, and after recovery. TABLE 2.1 and 2.2 also details the values.

TABLE 2.3 details the information of the non-place cells recorded, which show similar kinetics to place cells. The cells had varying effects, with some sharply decreasing their firing and some only minimally diminishing. The cells decreased their firing from a range of 15 to 90 percent of the original firing rate. This strong variation in the effect of DREADDs was similarly exhibited between all rats.

The effect of inactivation peaked in most cases around after 120 minutes, for both peak rate and overall rate.

After around five to six hours, the activity started to recover. Full recovery regained after at least seven hours.

The fact that recovery of CNO lead in some cases to global remapping, or rate remapping, shows that manipulation of place cell neuronal activity through pharmacogenetic means has an effect both on firing rate as well as location of its firing field after recovery of system from the drug.

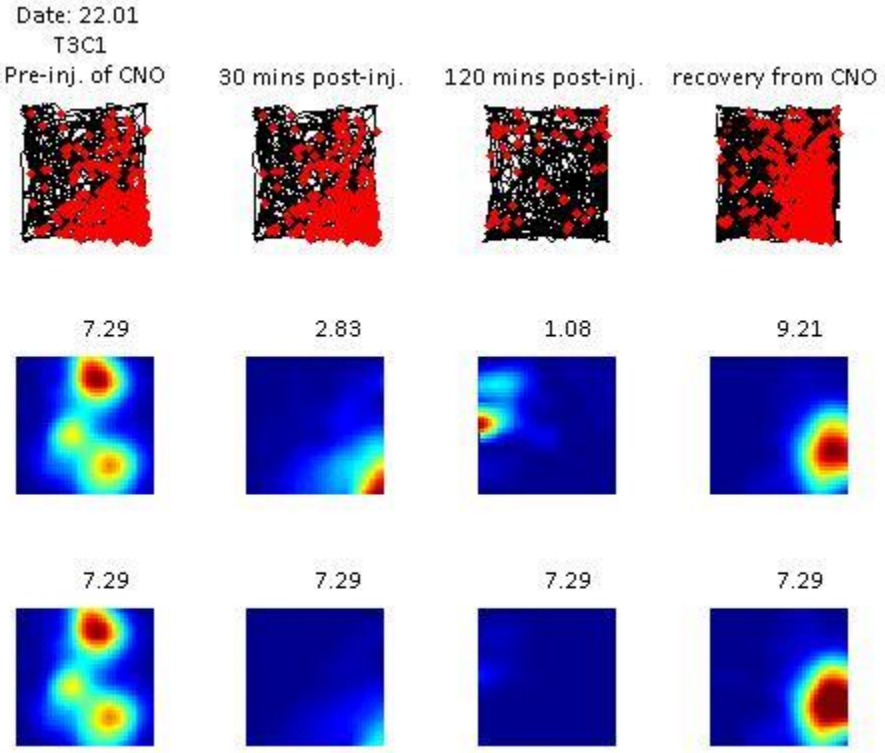
Date: 22.01
T3C1
Pre-inj. of CNO
30 mins post-inj.
120 mins post-inj.
recovery from CNO
7.29
2.83
1.08
9.21
7.29
7.29
7.29
7.29

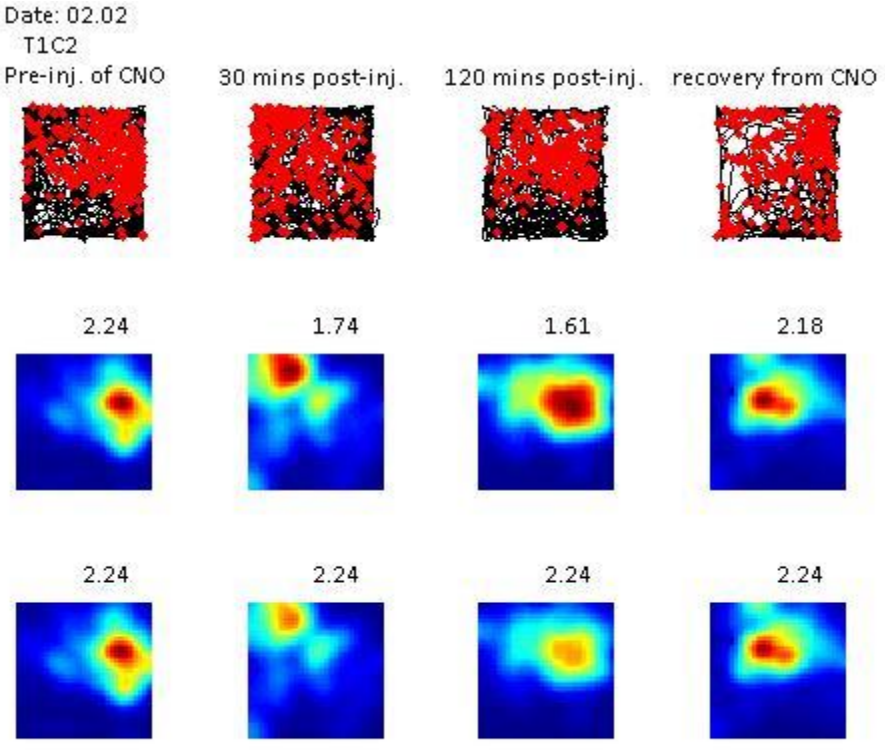
Date: 02.02
T1C2
Pre-inj. of CNO
30 mins post-inj.
120 mins post-inj.
recovery from CNO
2.24
1.74
1.61
2.18
2.24
2.24
2.24
2.24

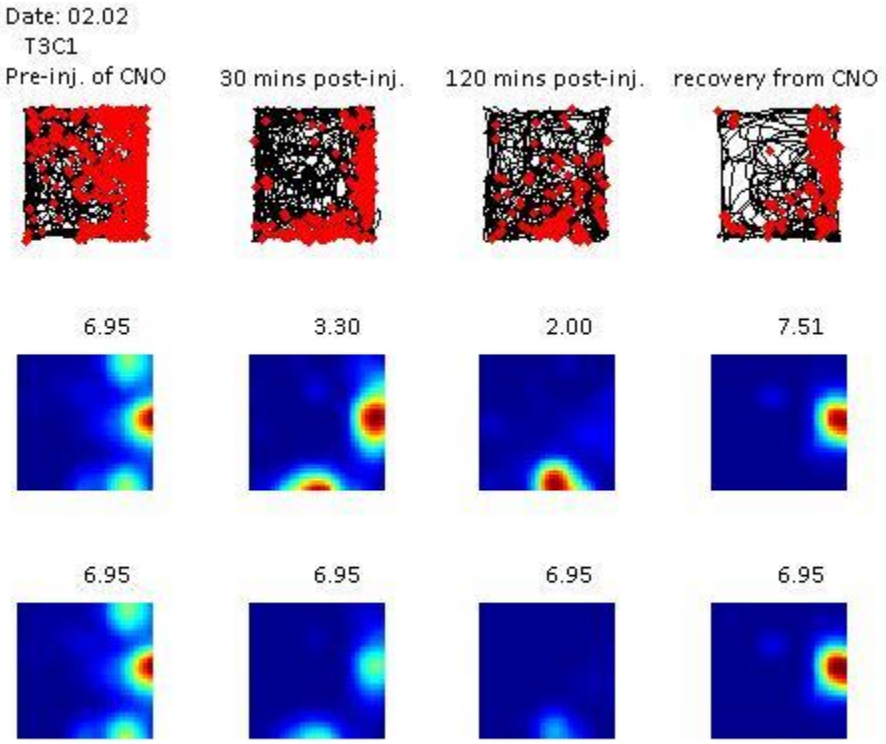
Date: 02.02
T3C1
Pre-inj. of CNO
30 mins post-inj.
120 mins post-inj.
recovery from CNO
6.95
3.30
2.00
7.51
6.95
6.95
6.95
6.95

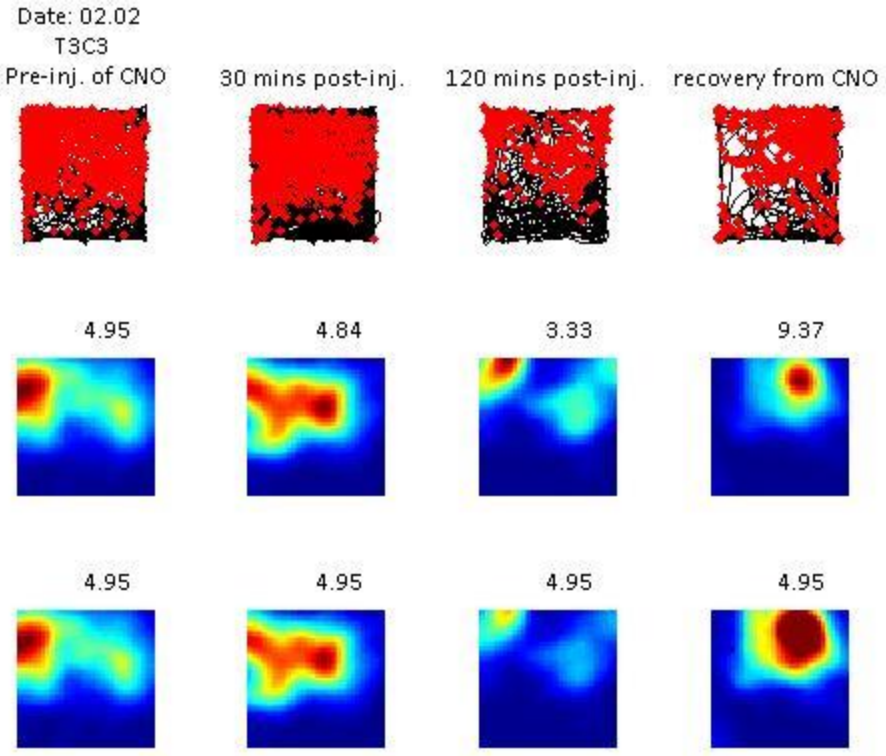
Date: 02.02
T3C3
Pre-inj. of CNO
30 mins post-inj.
120 mins post-inj.
recovery from CNO
4.95
4.84
3.33
9.37
4.95
4.95
4.95
4.95

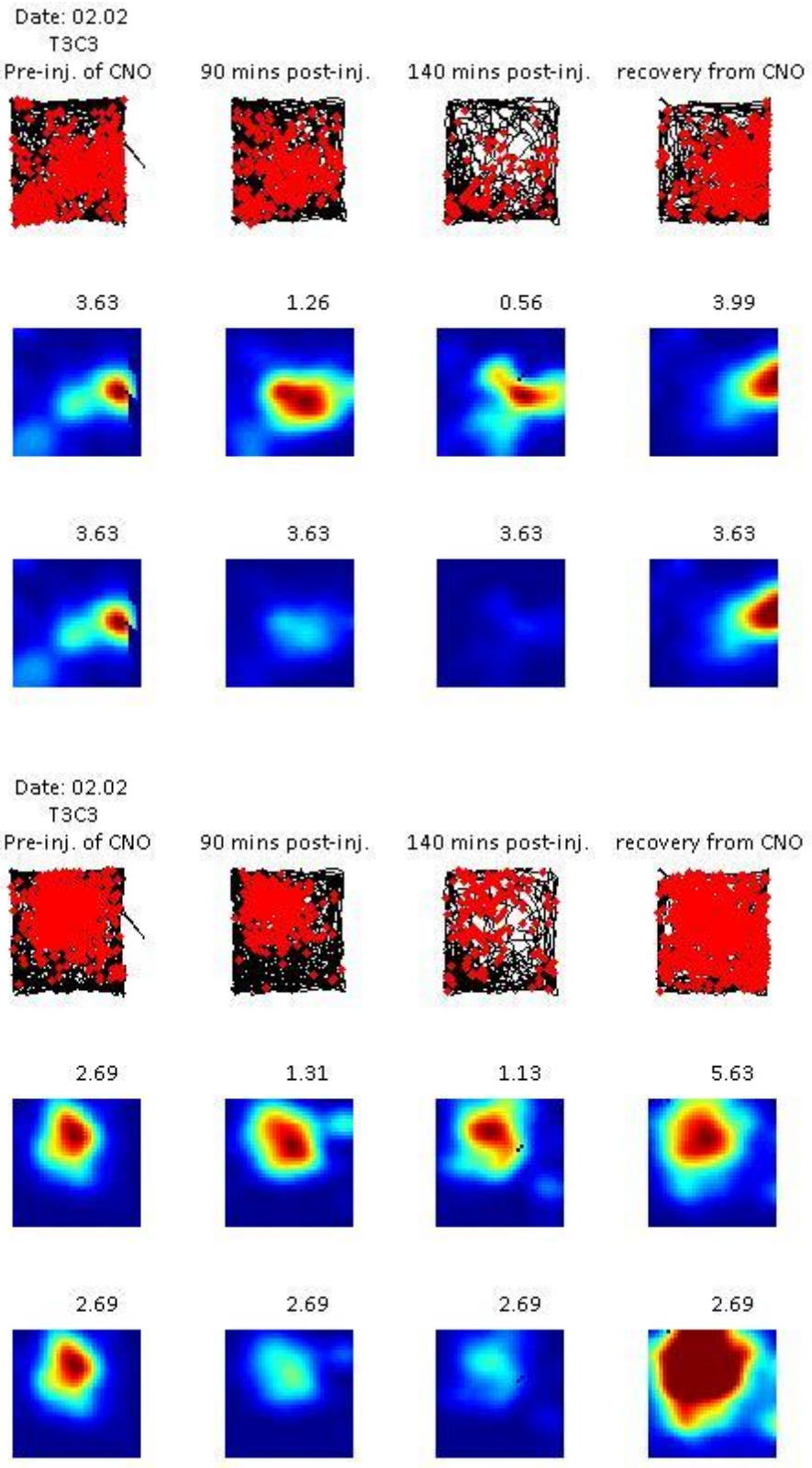

FIGURE 2.9 *Spike plots and rate maps of cell activity before and after CNO injection. Values above figures detail the colorbar max value, where red signifies large and blue low values. Middle row maximum firing rate displayed is normalized to the session, while last row is normalized to the first session (before CNO injection).*

TABLE 2.1: Recorded Place Cells used for DREADDs analysis [peak rate]

Cell no.	Date T/C	Pre-injection firing rate (Hz)	120-140 mins post-inj. rate (Hz)	Recovery rate (Hz)
1	22.01 T3C1	7.28	1.08	9.21
2	02.02 T1C1	6.36	5.26	5.53
3	02.02 T1C2	2.24	1.61	2.18
4	02.02 T2C1	1.93	0.98	1.10
5	02.02 T3C1	6.95	2.00	7.50
6	02.02 T3C3	4.95	3.33	9.37
7	09.02 T3C1	3.63	0.56	3.99
8	09.02 T3C2	2.69	1.13	5.63

TABLE 2.2: Recorded Place Cells used for DREADDs analysis [overall rate]

Cell no.	Date T/C	Pre-injection firing rate (Hz)	120-140 mins post-inj. rate (Hz)	Recovery rate (Hz)
1	22.01 T3C1	1.90	0.08	1.36
2	02.02 T1C1	1.05	0.70	0.89
3	02.02 T1C2	0.44	0.40	0.47
4	02.02 T2C1	0.67	0.41	0.40
5	02.02 T3C1	0.92	0.16	0.50
6	02.02 T3C3	1.37	1.53	0.58
7	09.02 T3C1	0.62	0.12	0.61
8	09.02 T3C2	0.53	0.27	1.80

TABLE 2.3: Non-Place Cells used for DREADDs analysis [peak rate]

Cell no.	Date T/C	Pre-injection firing rate (Hz)	120-180 mins post-inj. rate (Hz)	Recovery rate (Hz)
9	18.05 T2C1	14.04	2.53	N/A
10	18.05 T3C1	27.27	6.37	N/A
11	18.05 T3C2	3.44	1.37	N/A
12	23.06 T2C1	10.52	9.5	N/A
13	23.06 T3C1	10.20	1.96	N/A

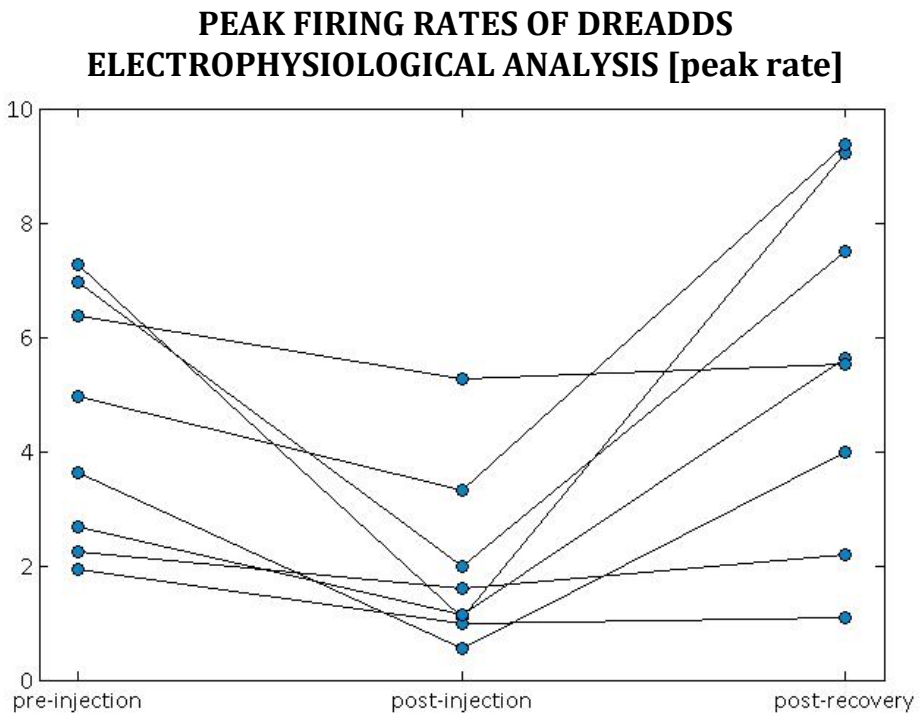

FIGURE 2.10 *The peak firing rates of the place cells before injection of CNO, after injection of CNO, and after recovery from CNO. It can be seen that the peak firing rates drop after injection of the ligand, and then spike again after recovery. The rates after recovery, however, do not return to the same exact values as the original firing rates, and sometimes increase or decrease their firing.*

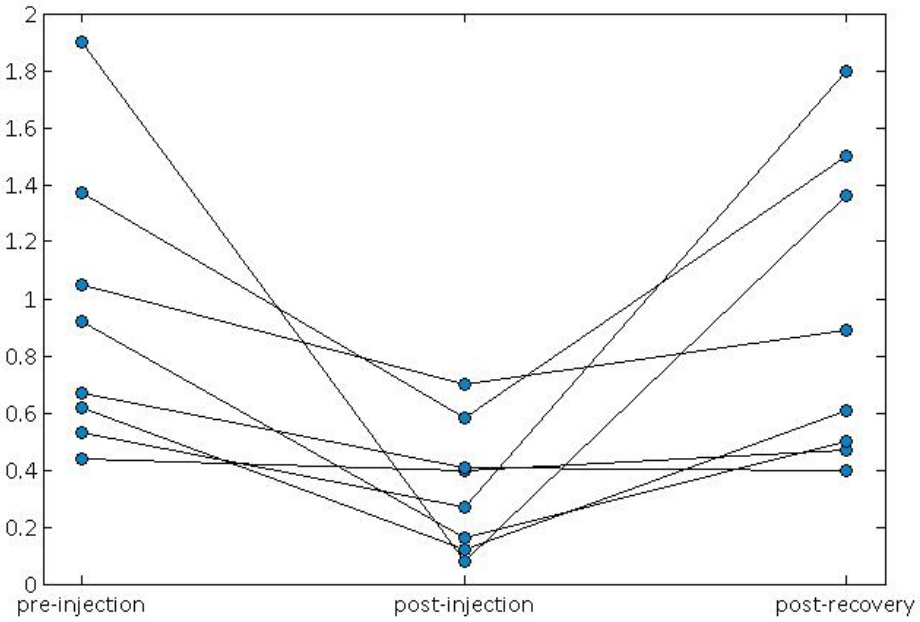

FIGURE 2.11 *The overall firing rates of the place cells at the three different time-stamps (before CNO injection, after CNO injection, and after recovery from CNO). As seen above with the peak firing rates, the overall rates also decrease drastically post-injection, and then recover their firing activity.*

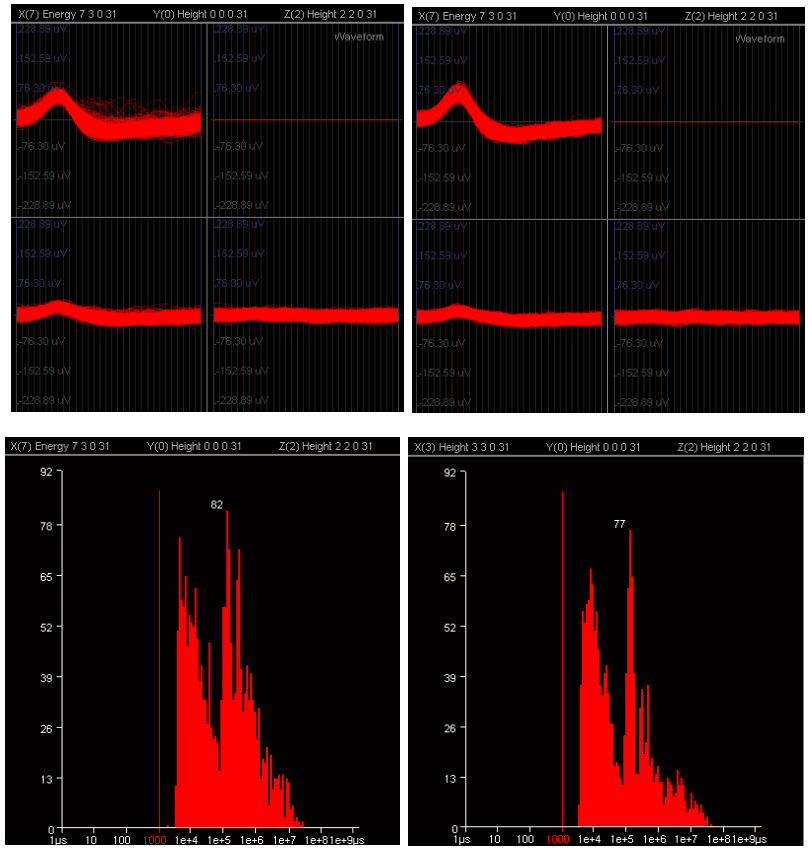

FIGURE 2.12 *Spike shapes from the cell recorded on 22.01.15 and 23.01.15 (T3C1). Left images are before CNO injection, while right images are after recovery from CNO. Top shows the spike shapes, middle shows the 2D cluster plot, and bottom plots the ISI histogram. As can be seen, the spikes shapes and properties of the spike shape are similar. This provides evidence that the cell is the same cell, despite having remapped after recovery.*

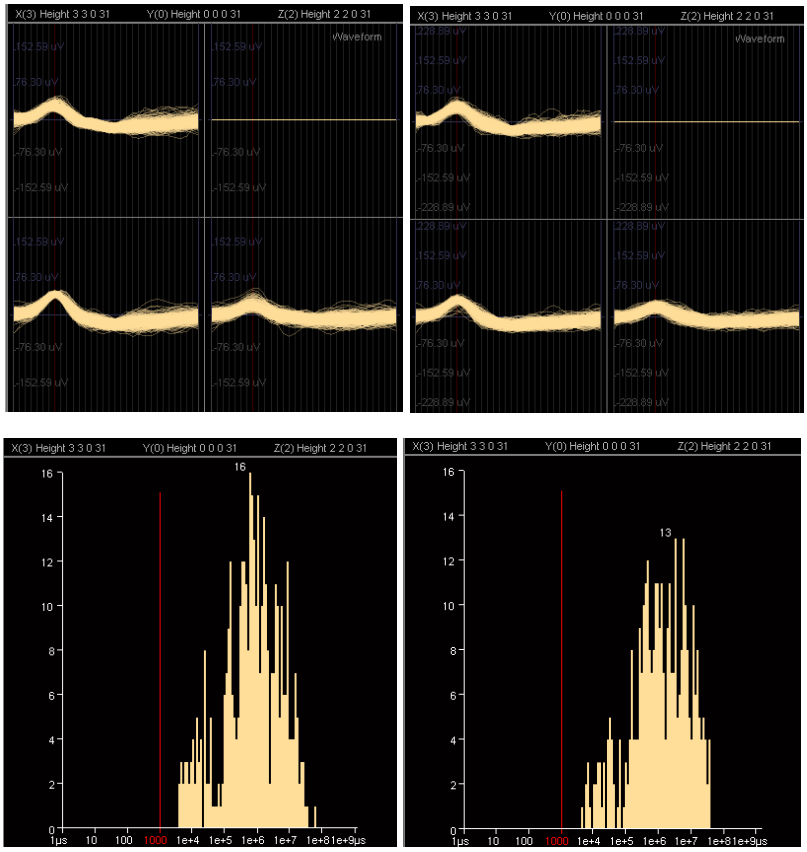

FIGURE 2.13 *Spike shapes from the cell recorded on 02.02.15 and 03.02.15 (T1C2). Left images are before CNO injection, while right images are after recovery from CNO. Top shows the spike shapes, middle shows the 2D cluster plot, and bottom plots the ISI histogram. As can be seen, the spikes shapes and properties of the spike shape are similar. This provides evidence that the cell is the same cell, despite having remapped after recovery.*

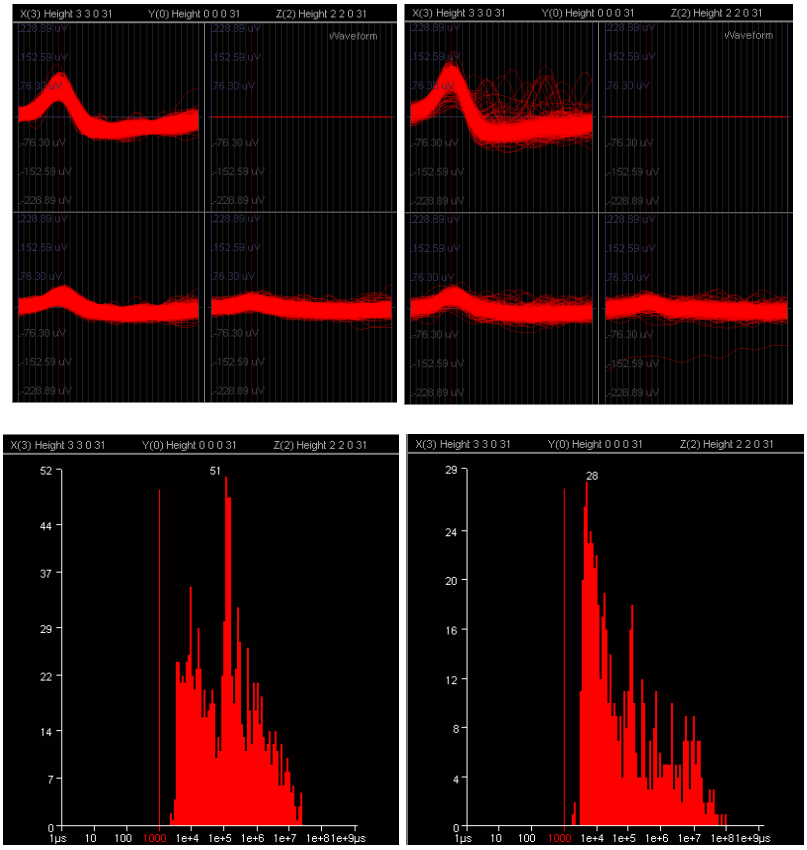

FIGURE 2.14 *Spike shapes from the cell recorded on 02.02.15 and 03.02.15 (T3C1). Left images are before CNO injection, while right images are after recovery from CNO. Top shows the spike shapes, middle shows the 2D cluster plot, and bottom plots the ISI histogram. As can be seen, the spikes shapes and properties of the spike shape are similar. This provides evidence that the cell is the same cell, despite having remapped after recovery.*

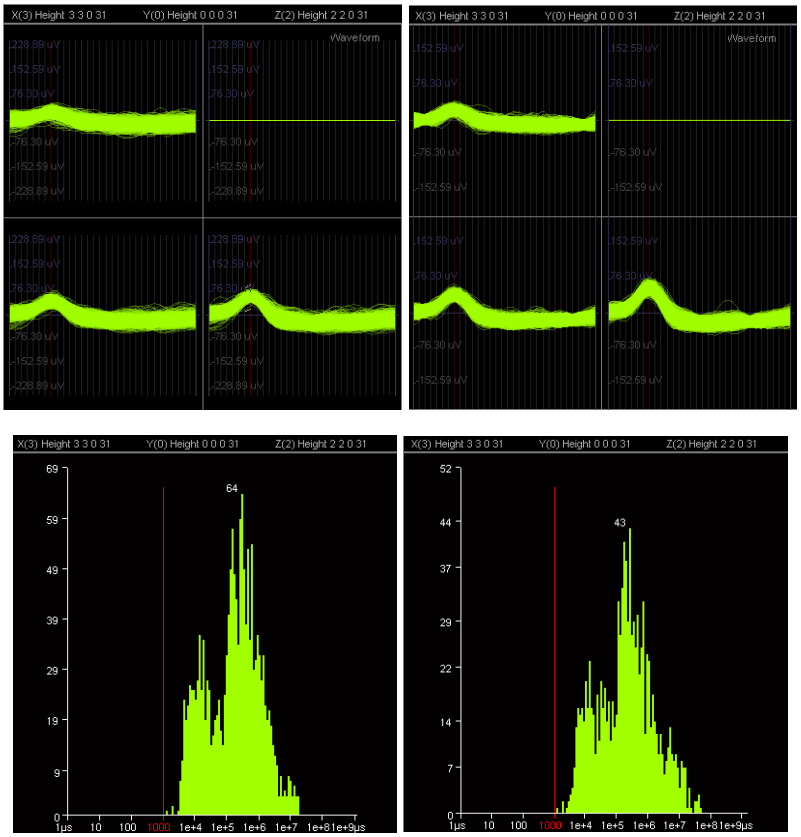

FIGURE 2.15 *Spike shapes from the cell recorded on 02.02.15 and 03.02.15 (T3C3). Left images are before CNO injection, while right images are after recovery from CNO. Top shows the spike shapes, middle shows the 2D cluster plot, and bottom plots the ISI histogram. As can be seen, the spikes shapes and properties of the spike shape are similar. This provides evidence that the cell is the same cell, despite having remapped after recovery.*

Our results revealed that the use of DREADDs and CNO injection in many cases led to global and rate remapping, signifying changes in the functional properties of the neurons. These results can also be observed in a study by the Moser group which investigates place cell remapping after MEC inactivation, using both optogenetic and pharmacogenetic approaches [35]. When optogenetics was utilized to partially inactivate the MEC region, place cell firing activity returned to its original firing after laser simulation. However, the same recovery could not be seen when using DREADDs to do the same experimental procedure. Place cells remapped, and 12 hours after CNO injection did not return to their original firing activity. This suggests that recovery is less reliable using DREADDs as compared to other methods.

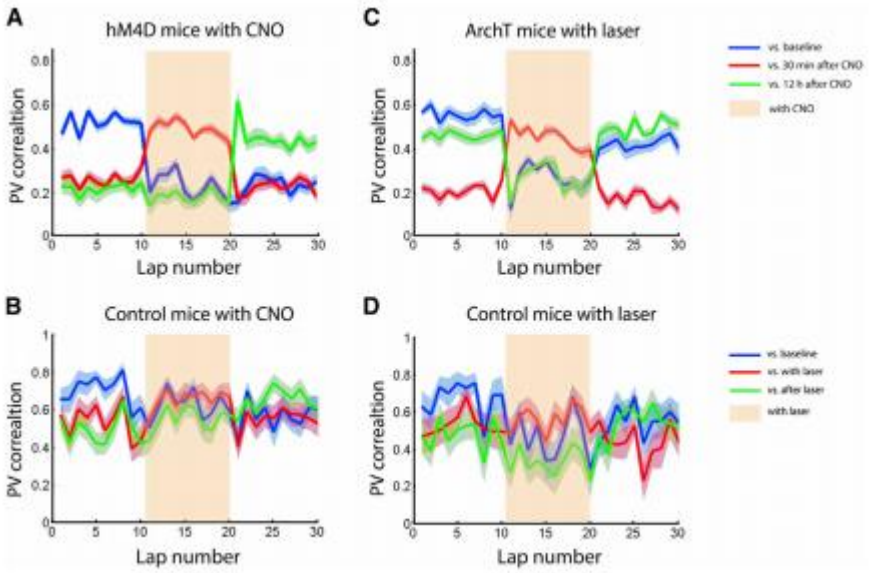

FIGURE 2.16 *Population vector correlations of 10 laps before, 10 laps during, and 10 laps after partial MEC inactivation. With ArchT mice and laser inactivation, the correlation is high between the baseline and the after laser firing activity (C). In the CNO group, the correlation is low between the baseline and 12 hours after CNO injection (A). This suggests that recovery is less reliable with DREADDs.(B,D) are controls showing no clear difference in the PV correlations among the three different cases. Image taken from Miao et al., 2015 [35].*

{2.4.iii} Post-recording histology

After recording from the rat, we performed a perfusion and extraction of the brain, which was then sliced and DAPI stained for further analysis. Histology was performed to examine the florescence and track of the electrodes. Below are images captured with a Confocal LSM 700 microscope. Images show different regions of the hippocampus (CA1, CA3, and the dentate gyrus) which were all expressed with the virus (See FIGURES 2.17-2.20).

The expression visible from the images is the native mCherry florescence of the viral construct containing DREADDs.

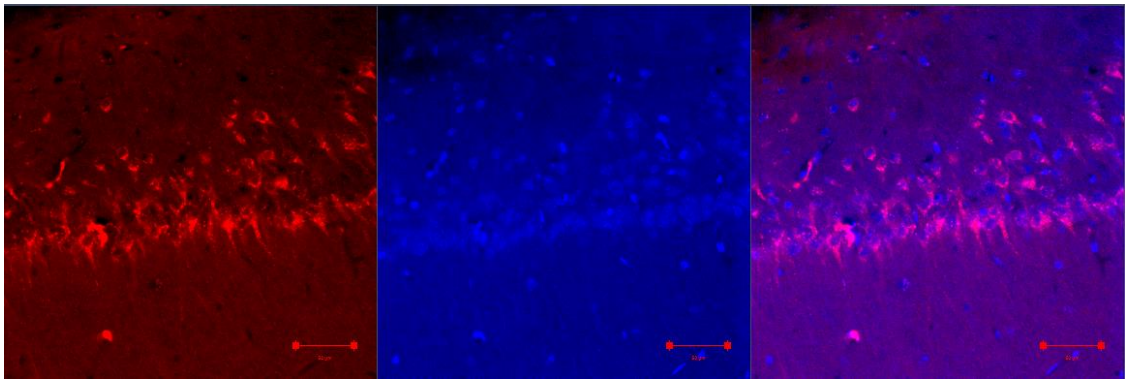

FIGURE 2.17 *Hippocampal cells in CA1 region. Left image shows native mCherry fluorescence of the viral construct containing DREADDs. Center image shows DAPI staining. Right image is merged image. Taken with a 20x objective.*

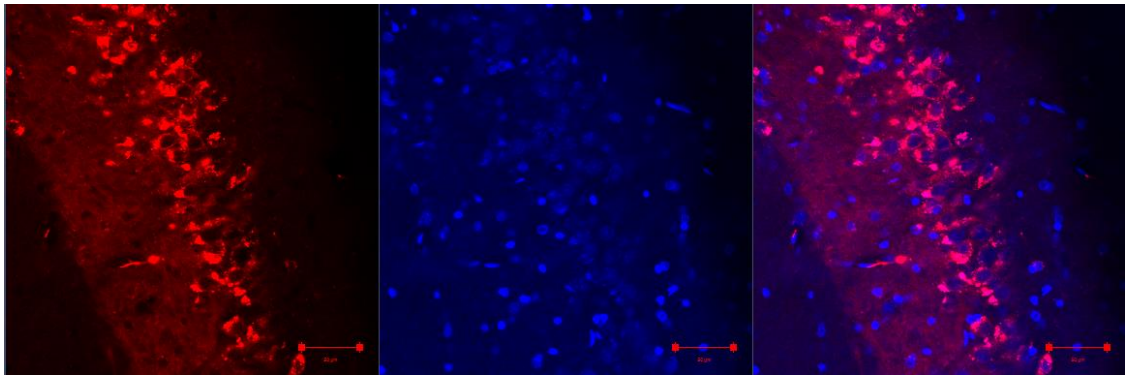

FIGURE 2.18 *Left image shows close up view of hippocampal cells in the CA3 region with the viral construct's native mCherry florescence. Center image shows same view with DAPI staining, outlining cell nuclei. Right image is merged image. Scale bar shown is 50 micrometers. All images were taken with a 20x objective and with the same parameters*.

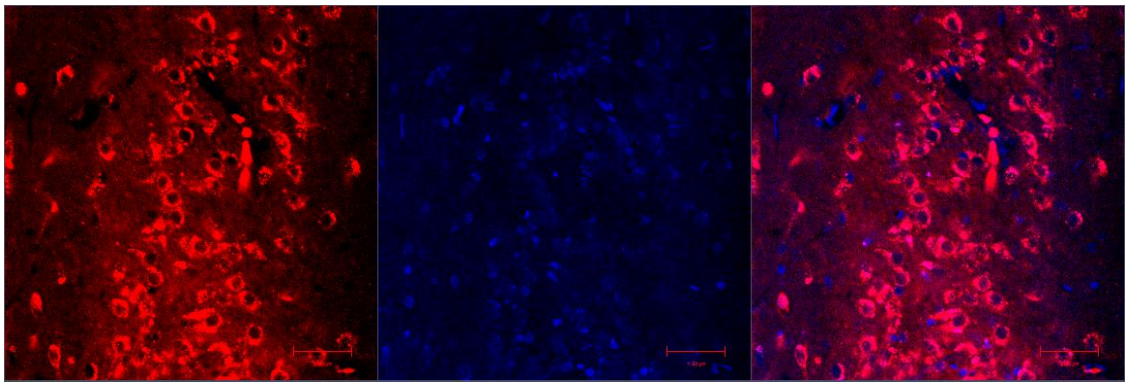

FIGURE 2.19 *Hippocampal cells in the dentate gyrus (DG) region. Left image shows native mCherry fluorescence of the viral construct containing DREADDs. Center image shows DAPI staining. Right image is merged image. Taken with a 20x objective.*

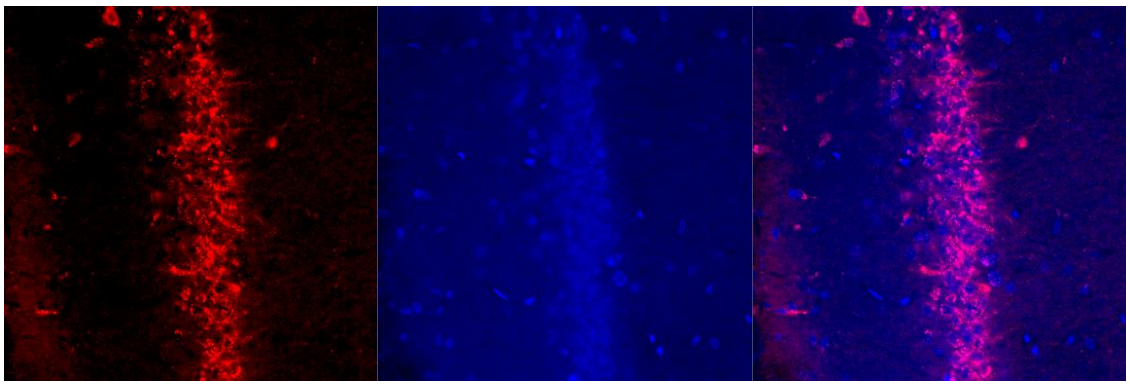

FIGURE 2.20 *Hippocampal cells in CA1 region. Left image shows native mCherry fluorescence of the viral construct containing DREADDs. Center image shows DAPI staining. Right image is merged image. Taken with a 20x objective.*

Chapter [2.5]

Discussion

DREADDs is a good tool for application in the neurosciences for a diverse number of reasons. It allows for manipulation of neuronal firing without disrupting regular neuronal functioning. It also permits for behavior to be turned "on" and "off" without any permanent damage to the system. For these reasons, it's a good candidate for studying both behavior and electrophysiology in behaving animals.

We hoped to observe the specific effects of the drug, including time of onset, strength of effect, and recovery of neuronal firing. In addition, we also hoped to observe the effect recovery had on place cell firing field stability. We found that onset of drug effect usually peaked at around 120-180 minutes, while full recovery was reached at around seven hours after CNO injection.

We have showed here that DREADDs is able to diminish firing in hippocampal place cells in awake, behaving rats. In most cases, however, it was shown that it was not a full inactivation, rather only partial silencing. In addition, recovery of the drug in some cases led to strong difference in the firing rate as compared to the original firing activity. Also, examples showed cases of global remapping after recovery. This suggests that DREADDs may lead to instability of place cell firing.

We made sure to confirm in cases where the field remapped that it was indeed the same cell, through examination of the spike shape, and that it was not a case of the electrodes picking up another cell.

Overall, we have succeeded in answering the main questions we had set out to test. We have shown that DREADDs does work in rats and that DREADDs is able to inactivate place cells. We also showed that this inactivation may result in instability of the cell, even after recovery. These findings are significant as they have strong implications for studies in which cell stability is imperative for the research. When stability of neuronal firing activity is essential for the task, it may be that DREADDs will not be the best approach to use.

In addition to DREADDs, other types of pharmacogenetic drugs used for place cell inactivation include lidocaine and muscimol. Muscimol works by acting as an agonist to the GABA-a receptor and leads to an almost complete reduction of firing rate. Lidocaine, a local anesthetic, by contrast, only results in a partial inactivation, and does not lead to complete diminishment of firing [36]. Lidocaine has a faster recovery time though and thus may be used when a full inactivation is unnecessary and a faster recovery time is preferred.

However, for both lidocaine and muscimol, once the drugs are administered, these agonist-modulated methods lead to both information modulation as well as integration modulation. By contrast, ligands acting on DREADD receptors leave the endogenous receptors unaltered, allowing for the incoming neuronal information to remain unchanged.

Additionally, an advantage of DREADDs is its non-invasiveness. Muscimol and lidocaine both require intracranial injections, and thus are less appealing candidates when used for behaving animals. DREADDs is activated through an IP injection, a less invasive means.

All methods are reversible with the neurons resuming their natural firing patterns after recovery. However, despite the reversible effects of DREADDs, we have shown here that the manipulation of neuronal firing doesn't leave the place cells completely unaltered after recovery. The firing fields of the place cells in some cases don't return to the same location. Since remapping is usually a way of signifying change to the animal, this effect after recovery of the DREADDs may imply that the animal's memory has been affected by the drug.

An interesting follow-up of this study will be to see if behavioral effects that correspond to the remapping of place cells would also be seen after recovery. If memory will also be compromised in the rat with the remapping of place cell firing fields, this will further cement the link between the spatially-modulated cells and their strong foundation in memory.

The application of this tool has promising potential for the study of memory in particular, as it provides a clear method by which to do so. While the instability sometimes visible with use of DREADDs may hinder its use in experiments that require strict stability, it may be beneficial in this specific area of study. Place cells have tools that allow them to be silenced or to be excited. DREADDs may additionally permit another property of the cells to be studied, by observation of the effect of remapping in cases where remapping should not occur. This is something that is more difficult to test since remapping usually requires a change in environment. Investigating the effects of remapping when no change occurs has the potential to reveal new information about place cells, memory, and the brain in general.

In summary, our research has found that DREADDs does indeed lead to deactivation of hippocampal place cells. Recovery of the cells has also been shown. However, we saw that this recovery lead to changes in the location of place cell firing.

These changes may have strong implications about the effects of DREADDs, as well as on the stability of place cells, which is compromised with the administration of the drug. The findings leave us with a gain in knowledge on both the details of the pharmacogenetic application, as well as additional information on place cell functioning.

Part II

Evidence for a pivot field in grid cell firing patterns

"A sense of place results gradually and unconsciously from inhabiting a landscape over time, becoming familiar with its physical properties, accruing history within its confines." — Kent Rydon

Chapter [3.1]

Introduction to overdispersion

While the firing fields of place cells and grid cells tend to be spatially stable, discharging whenever the rat enters the location of the firing field and silent outside of it, the rate of firing exhibits more variability than normally expected. This variability is referred to as "overdispersion." Overdispersion dictates that with each pass through a field, the neuron fires with more unpredictability than expected purely by its spatial firing rate distribution.

This phenomenon was addressed in a few studies, which found that place cell fields display significantly different rates with every pass [37-39]. The overdispersion reveals that place cells relay more information than purely spatial. Studies looking into this phenomenon observed that the rat's attention state plays a role in this firing variability, reflecting alternations from local arena-based cued attention to more global room-based attention [40].

Researchers examined CA1 place cells and investigated whether the type of attention necessary for the task would lead to changes in firing overdispersion. They found that discharge fluctuations strongly decreased when the animals used only distal room-based cues to navigate [38]. The place cell code thus reflects not just space and location, but relays additional information.

The case with grid cells, which have not been investigated much in this respect, is less clear. As these cells have multiple firing fields, it would be of interest to

observe the variability among these fields, as well as the variability among each pass through a field.

Chapter [3.2]

Research goals

Here we wanted to expand on these studies of overdispersion and variability of firing by extending this research towards grid cells. While the phenomenon of overdispersion was studied somewhat in respect to place cells, grid cells' firing activity variability is less understood.

Our research asked if this overdispersion was also seen within grid cells, and if each pass of a grid cell field exhibited more variability than would be expected by chance. In addition, we examined whether there was larger variability in the firing rate between all the fields of an individual grid cell and if some firing fields had larger firing rates than the rest.

In brief, we were asking three main questions:

- Is there overdispersion between individual passes through firing fields?
- Is there strong variability in firing rate between the firing fields of individual grid cells?
- If so, what does it reveal about the mechanism of grid cells and the formation of their fields?

Investigating the variability and overdispersion of grid cells has the potential to provide interesting implications on the mechanism and formation of their highly specific firing pattern. The details of grid cell neuronal activity design may further expose hidden facts about the construction and the very foundation of memory.

Chapter [3.3]

Analysis methods

> *"Grid cells have attracted attention because the crystal-like structure underlying their firing fields is not, like in sensory systems, imported from the outside world, but is created within the brain itself."*
>
> — M.B. Moser and E.I. Moser, *Crystals of the brain* [13]

We used a diverse set of grid cells from multiple recordings and sessions compiled from Bonnevie et al., 2013, Derdikman et al., 2012, and Sargolini et al, 2006 [41-43]. Each grid cell received a gridness score that measures the strength of spatial periodicity, and a head-directionality (HD) Rayleigh score that measures how tuned the cell is to head direction.

A firing rate map was produced by partitioning the arena into bins and taking the number of spikes that fired per bin divided by time spent within the bin to calculate the predicted firing rate at each point within the environment. A bin size of 3-by-3cm was used. The rate map was then smoothed by a two-dimensional convolution of a Gaussian function of a standard deviation of sigma size 1.5 cm.

A gridness score was calculated by taking the correlations of rotational symmetry [42]. This was done by using the spatial autocorrelation maps of each rate map and then comparing it to centered rotated versions of itself at 30° intervals. The gridness score was then defined as the minimum of the higher correlation of the 60° and 120° rotation ($Acorr_{60°}, Acorr_{120°}$) subtracted by the maximum of the lower correlation of the 30°, 90°, and 150° rotations ($Acorr_{30°}, Acorr_{90°}, Acorr_{150°}$) .

$$Gridness\ score = \min(Acorr_{60°}, Acorr_{120°}) - \max(Acorr_{30°}, Acorr_{90°}, Acorr_{150°})$$

(eq. 3.1)

A HD Rayleigh score describes the strength of neuron's head-directionality modulation. It is calculated by plotting the polar plot of the firing responses in relation to head direction. The length of the mean vector (Rayleigh vector) is then taken for the total circular distribution of firing rates.

Only grid cells with a gridness score of above 0.3 and a HD Rayleigh score of less than 0.25 were used for analysis.

Using the rate mat and autocorrelation maps of the cells, the place fields were located finding the centers of firing from the rate map. The place field radius was calculated using 65 percent of half the distance between the center point of the rate map spatial autocorrelation map and the next closest field center peak. In

addition, we calculated the number of place fields, the peak firing rate of each field[1], the module, and the grid orientation.

The grid orientation is obtained by taking the angles between the center point of the autocorrelation map and each of the six closest points that form the hexagonal array. The grid orientation is then defined as the smallest of the six angles.

In addition to parameters such as phase and shift, the spacing and orientation of grid cells allow them to be defined by a particular module. It has been found that grid cells are organized into discrete modules with specific spacing values, as opposed to continuous values as expectedly seen in other sensory systems. The spacing of grid cells is organized within the layers of the entorhinal cortex with discretized step-like increases in grid scaled along the dorsoventral axis [44].

In our analysis, we started by extracting these different parameters for each grid cell in our set. We created a "field map," by simplifying the rate mat into place fields visualized by peak firing rate (using the same color map typical of rate maps, with red representing high firing rate, and blue representing low rates). We also plotted the firing rate of each field in increasing order, and used it to find the variability, Fano factor, and coefficient of variance between the firing fields of each cell.

[1] The peak firing rate was chosen for the analysis as opposed to the mean in order to ensure no potential artifacts would arise from the fields located near the borders, whose centers might be located beyond the boundaries of the arena. Also the mean firing rate is dependent on how the place field size is defined, an issue that is resolved by using the peak rate.

EXTRACTION OF INDIVIDUAL GRID CELL PROPERTIES

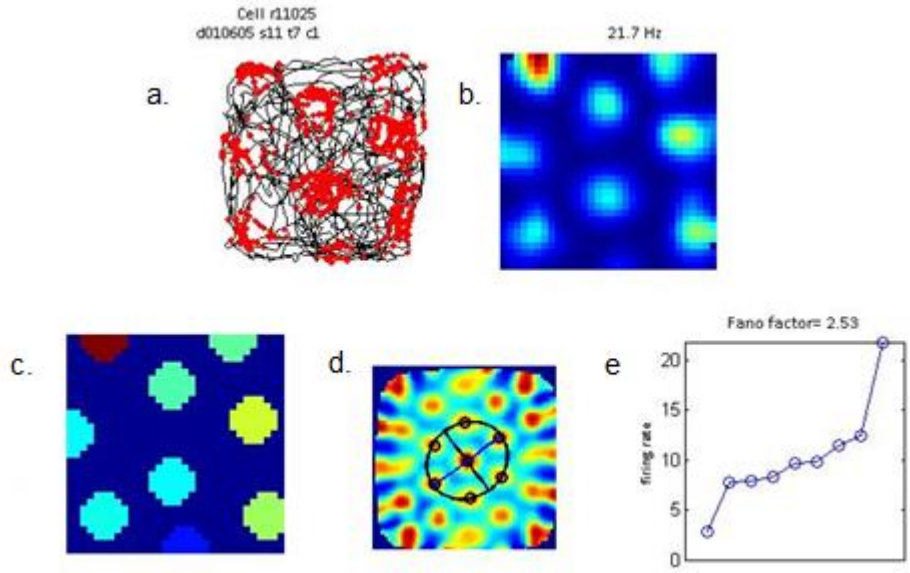

FIGURE 3.1 *The different parameters examined in our analysis for each cell. (a) Depiction of the trajectory of the rat (black line) with the spikes represented in red. The red dots representing the spikes form a hexagonal array spanning the arena. (b) Rate map representation of the firing. Maximum firing rate is detailed above. Color map is standard used (red representing higher values, and blue representing lower). (c) Field peak rate figure shows the peak firing rate of each field, with same color map used as in the rate. (d) the autocorrelation map of the rate map, with the module overlaid on top. (e) Sorted firing fields plot visualizes the peak firing rates calculated using the rate map. The firing rates of each field are plotted in increasing order, with the Fano factor detailed in the title.*

TABLE 3.1: Cells used in variability study

Study	Total number of cells	Cells passing gridness criterion	Grid cells passing HD criterion and recorded in square arena	Remaining cells with at least 8 firing fields
Sargolini et al., 2006	**620**	**111**	**30**	17
Derdikman et al., 2009	**121**	**55**	**50**	30
Bonnevie et al., 2013	**195**	**100**	**83**	39
Total:	936	266	163	86

Chapter [3.4]

Variability between grid cell firing fields

{3.4.i} High variability visible between grid fields

Grid cells have multiple firing fields, organized in a hexagonal pattern spanning the entire environment [19]. These fields are equidistanced and similar in size, and generally considered to be uniform in amplitude [20]. Here we set out to test to what extent the fields are indeed uniform. A set of grid cells compiled from Bonnevie et al. [45], Derdikman et al. [46], and Sargolini et al. [42] were analyzed. These data sets contained entorhinal grid cell recordings of rats foraging in open field arenas, with the position of the animal and the firing activity recorded simultaneously. We were interested in examining the spatial firing patterns in order to extract the variability present among the fields of individual cells.

Since large variability in firing rates may arise from conjunctive grid x HD cells, which in addition to exhibiting typical grid firing pattern are also tuned to a given head direction [42], we eliminated such cells from the study. Only cells with a low head-direction Rayleigh score (less than 0.25) and a high enough gridness score (greater than 0.3), that were recorded in square arenas, were included. Because we were interested in inter-field variability, cells chosen for the study were further screened to include only those with at least eight firing fields. In total, out of 743 cells in the study, 86 remained for analysis. We found that there is larger-than-expected variability present between field firing rates derived from smoothed grid cell rate maps.

Indeed, the majority of our grid cells possessed a Fano factor (variance over mean) larger than 1, indicating a larger variance than expected from a Poisson distribution (75.6% of cells, N=65/86; mean value of 3.35±0.40, FIGURE 3.2).

{3.4.ii} High variability result of mainly one firing field

We further looked at the distribution of this variability in single examples. The large variability was in many cases due to a single strongly-firing field, while the rest of the fields were much more uniform. This is visibly seen in FIGURE 3.3, which shows examples of plots displaying the firing rates of the fields organized in increasing order.

To further ensure that the effect was not due to an artifact of the analysis, we simulated grid cells. The analysis was repeated using simulated spike trains on the same rat trajectories. Simulated spikes trains were produced for each grid cell by using a generated rate map that had the firing field centers at the same locations and had a mean firing rate similar to the original rate map of the cell (see FIGURE 3.4 for examples). Using this contrived rate map, the real rat trajectories were used to simulate spike trains using a Poisson distribution given the rate map probabilities. The analysis was then run again with the simulated spike trains and the results compared to the actual results from the original data.

The median Fano factor (variance over mean) observed from the set was shown to be significant when plotted against the distribution of the simulated data: The real value was larger than 500 out of 500 simulated runs (FIGURE 3.5). This pattern suggests that one field might have a specific function to the grid cell that results in it exhibiting a larger firing rate than the rest.

{3.4.iii} Maximum-firing fields fall near border

Since the large variability was observed to be mainly the result of a single maximum-firing field, we looked at the location of this field and examined whether there was a higher propensity for the field to manifest in certain places within the environment. We found that many of the grid cells had their maximum-firing field near the border of the arena, with "near-border" defined as less than 0.1 normalized distance from the wall (66.28% <0.1, mean value at 0.085±0.016 from border; FIGURE 3.6-3.8). The result did not change when changing the near-border threshold to 0.05 or 0.15 (reference to Appendix II).

The normalized distance of the hyperfield from the arena boundary is also negatively correlated with the firing rate of the hyperfield compared to the mean of the entire set of fields for each grid cell (see FIGURE 3.9).

For statistical evaluation, we shuffled the data to test the probability of this occurring by chance. The shuffling procedure had the peak firing rates randomly mixed among the different fields for each individual grid cell so that each field rate was assigned a different firing field. The number of cells with the distances of the maximum firing field close to from the border (defined as less than 0.1 of the normalized distance from the boundary) was counted for each shuffle procedure and compared to the actual data result.

We found that in the original data the number of cells with a maximum firing-field near the border (N=57 out of 86) was higher than in 1000 out of 1000 shuffles (FIGURE 3.10). This effect was observed to also be significant against the

simulated-data distribution, where the real result was higher than 500 out of 500 simulations (FIGURE 3.11).

We concluded from this part that the large variability observed between different firing fields of a single grid cell was mostly due to one strong field, which tended to be located near the boundary of the arena. We termed this field the 'hyperfield' (we note here that we use this term without any functional implications at this stage, just to denote the phenomenological property). We next tried to determine what the source of this strong field is.

This result may be due to:

- Precision?
- Anchor point?

Since the borders provide clues to the exact location to the animal more precisely than the center of the arena does, the higher firing rates may be due to less drift and less error accumulation [47]. To test whether this was the case, we looked at the fields located near the borders compared to central fields. We wanted to examine whether this effect encompasses other border fields aside from just the maximum-firing field.

We conjectured that this tendency of the maximum-firing field to be found near the border of the arena might be due to border-located fields firing more strongly in general compared to center-located fields, which could occur if, for example, conjunctive grid-cells X border-cells exist in the cell population [15]. In order to investigate whether this border-effect would extend to other fields as well as the maximum-firing field, we examined the second-maximum firing field, to see if it

also exhibited the same tendency to remain near the boundaries of the environment. If the effect was due to border-located fields firing higher in general, the second-maximum firing field should have also displayed a higher tendency to manifest near the borders. We found that the number of cells with second-maximum-firing fields located near the borders was not significantly more than expected from shuffle procedures (result was worse than 180 shuffles out of 1000; FIGURE 3.12). We concluded that the border preference was specific to the hyperfield, and did not extend to the second-maximum firing field.

Next we compared the mean firing rate of border-located fields versus center-located fields. We wanted to see whether there was a trend for the average firing rate of border-located fields to be higher than for the center-located ones. The analysis demonstrated that contrary to expectation, the mean firing rate of border-located fields was not larger than those of center-located ones (Center-located: 9.57 ± 0.67 Hz; Border located: 8.84 ± 0.70 Hz; $p=0.177$, Wilcoxon signed-rank test; FIGURE 3.13).

In addition to examining the maximum-firing and second-maximum-firing fields in isolation, we also investigated whether the top-ranked strongest firing fields in general tended to be situated closer to the borders. This was achieved by observing the top 25% strongest firing fields, excluding the hyperfield (we also looked at 20%, 30% and 40% strongest and this did not change the result: see Appendix II). We found that there were not more border-located fields in the top quarter of maximum-firing fields than expected from shuffle measures (actual mean value 0.5082 was less than 308 shuffles out of 1000; FIGURE 3.14). These observations revealed that the tendency for the maximum-firing field to be

located at the borders was not due to border-located fields firing being stronger in general, but rather due to something specific related to that particular field.

Thus, as this effect does not project to the second-maximal-firing field, it appears to be exclusive to the maximal-firing field. Also, results showed that border-located fields, aside from the maximum-firing field, do not tend to fire stronger than the central fields.

This reveals that the case with the maximum firing field is unrelated to a dimension of its location, and rules out the theory that the stronger-firing field is due to better precision or any other property of its border location.

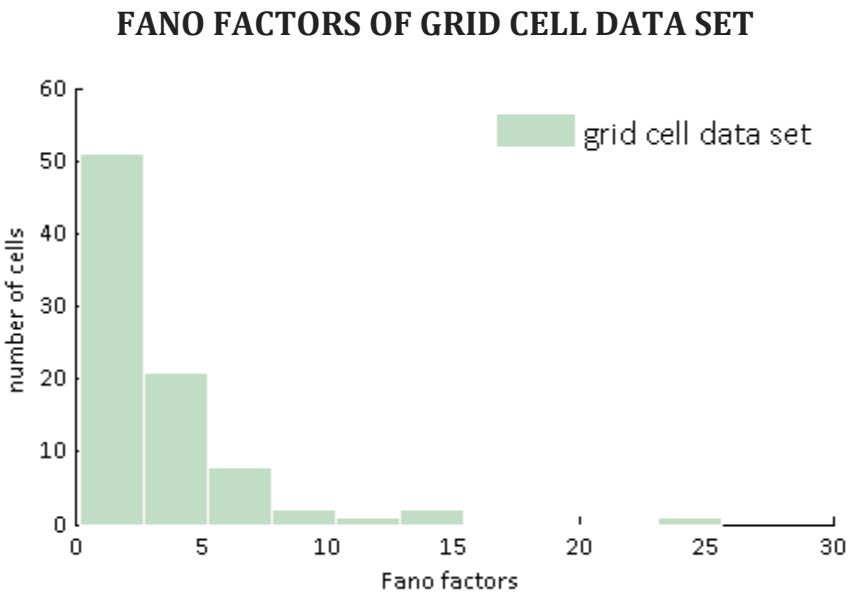

FIGURE 3.2 *Histogram of Fano factors (variance over mean) of the firing rates between the fields of the grid cell data set. 80.23% of the population of the grid cell data set has a Fano factor of larger than one, signifying large variance. Mean value (3.3529) is represented with the dashed red line. This shows that the grid cells tend to exhibit large variability.*

FIRING RATES OF GRID CELL FIELDS PLOTS

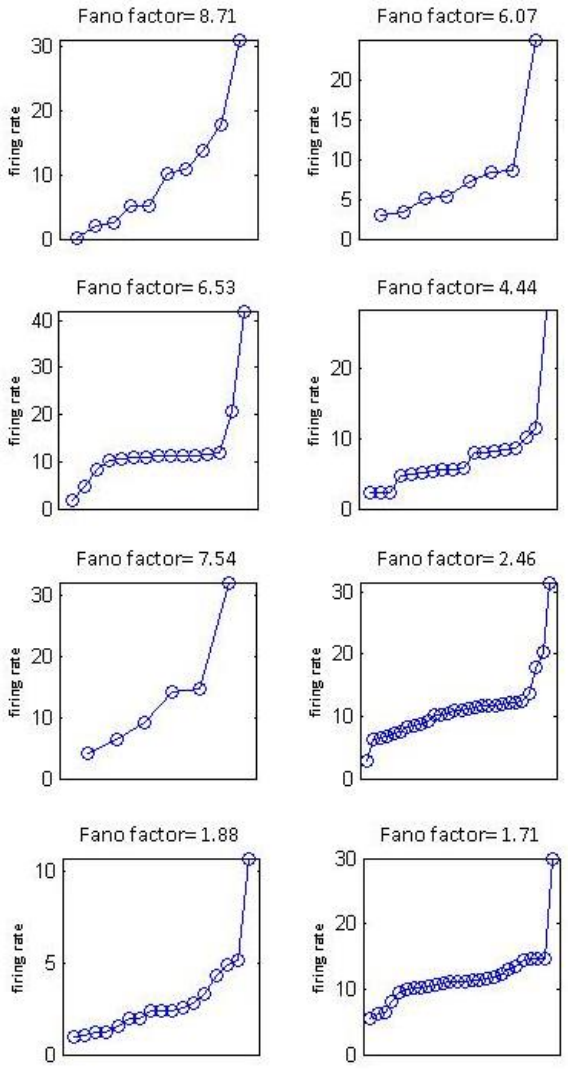

FIGURE 3.3 *Figures plotting the firing rates of each field. X axis is numbered fields in order of increasing firing rate. Y axis is firing rate. A sharp increase is seen in the maximally-firing field. This suggests that the main source of the variability lies in the maximum-firing field. This field tends to fire much higher than expected from just expected variability and might suggest it has another function in the grid cell formation.*

EXAMPLES OF RATE MAPS PRODUCED FROM SIMULATED SPIKE TRAINS

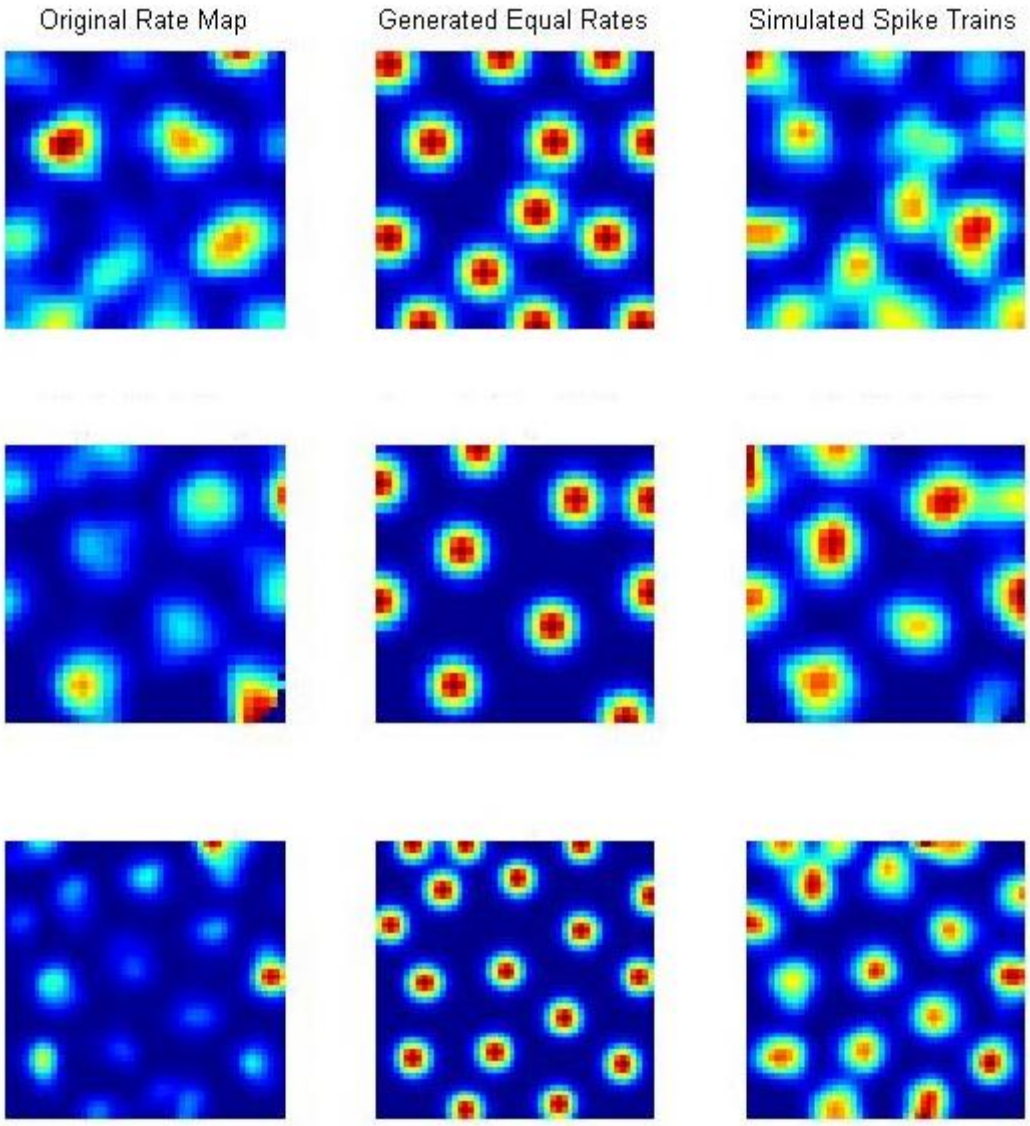

FIGURE 3.4 Examples of simulated rate maps. The first columns shows the original rate map, which was used to generate the rate map of equal firing rates (middle column) with field centers at same locations. This generated equal rates map was then used to simulate spike trains. The simulated rate map is shown in last column.

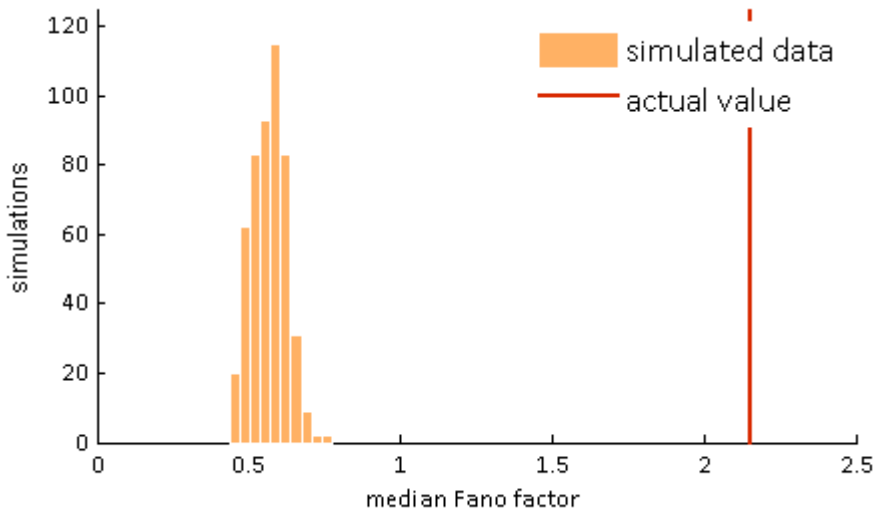

FIGURE 3.5 *Histogram of the median Fano factors of the simulated grid cells, created using rate maps of equal firing rate probabilities. Real value of real data is depicted with red dashed line. The median Fano factor of the real data is much larger than those of the simulated cells. This shows that the large variability seen in the data set is not present in grid cells simulated from rate maps of same probabilities, with smoothing and bin size kept at the same parameters.*

METHOD OF DETERMINING IF GRID CELL MAX-FIRING FIELD FALLS NEAR BORDER

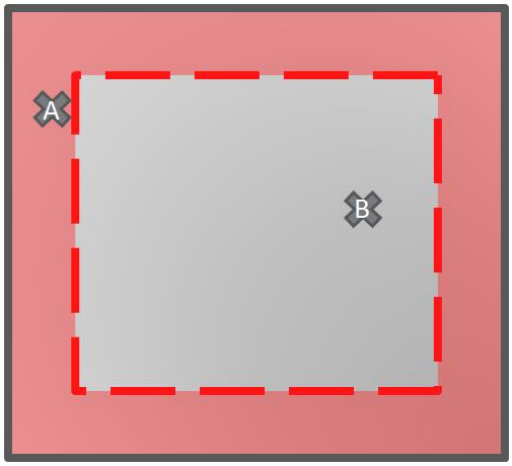

FIGURE 3.6 *Illustration of the method of determining if a cell has a maximum-firing field near the borders of an arena. If the location of the field falls within the given boundaries of the arena, it is considered near the border. In this example, the gray x's mark the location of the maximum-firing field of the cell. Cell A, with marked maximum-firing field location, would be considered containing a max-firing field near the border, while cell B doesn't have a max-firing field near the border.*

LOCATIONS OF MAXIMUM-FIRING FIELDS

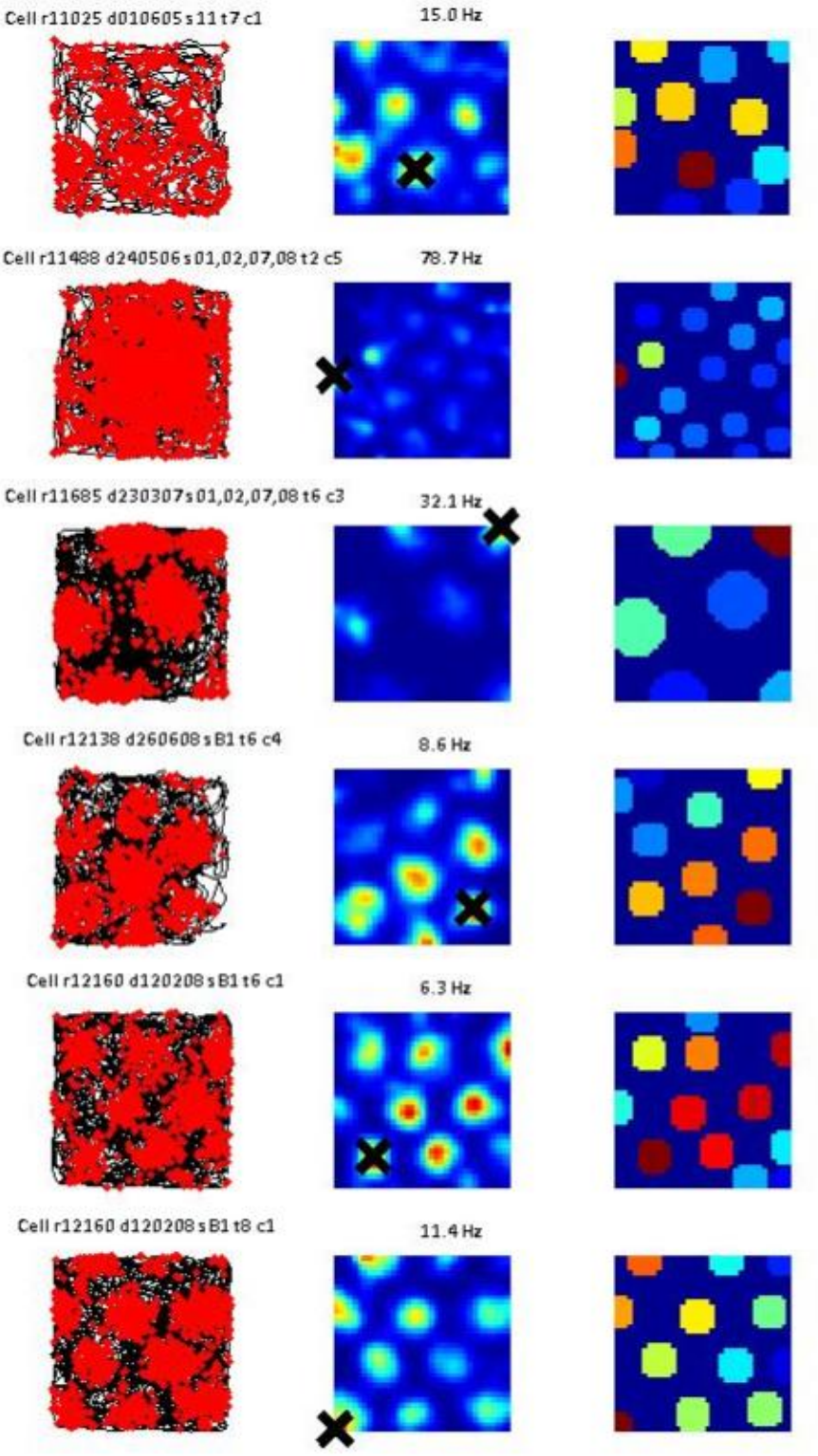

FIGURE 3.7 *Spike maps are plotted alongside rate maps and field map figures. Black x's mark the maximum-firing field in the rate maps. It appears that these max-firing fields tend to be located near the boundaries of the arenas.*

NORMALIZED DISTANCE OF HYPERFIELDS FROM ENVIRONMENT BOUNDARIES

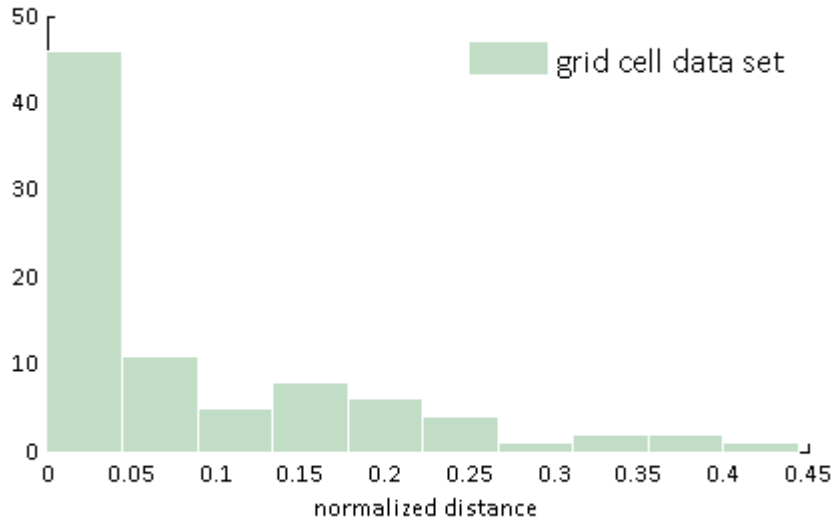

FIGURE 3.8 *Histogram of the normalized distance from the arena borders of all cells in the data set. Non-smoothed data set was used for this analysis. As can be seen, majority of cells have their hyperfields located near the environment boundaries.*

FIRING RATE OF HYPERFIELD OVER MEAN VS. NORMALIZED DISTANCE FROM BORDER

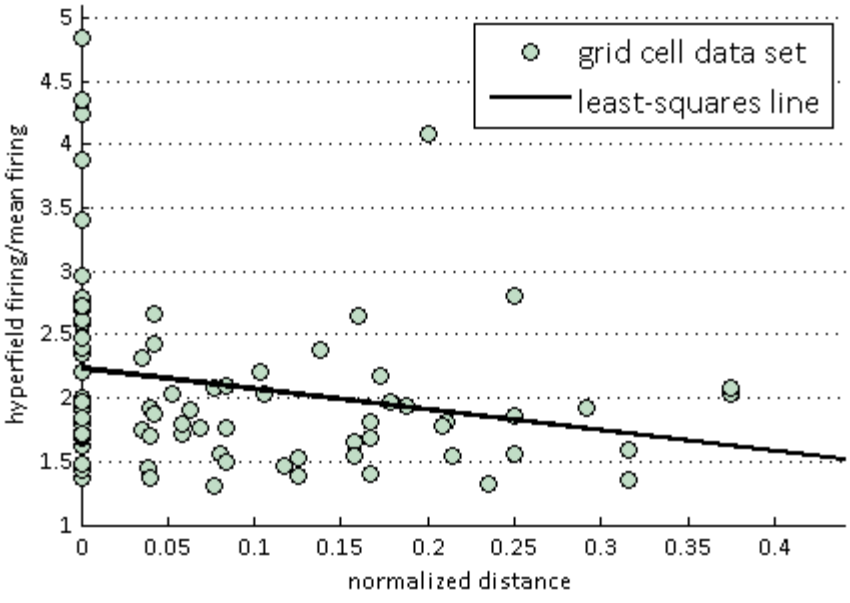

FIGURE 3.9 *Scatterplot of the normalized distance of the hyperfield from the arena boundary versus its firing rate divided by the mean giring rate of all the gird cell's fields. The stronger the hyperfield's firing rate is above the other fields, the more likely it is to be closer to the arena border.*

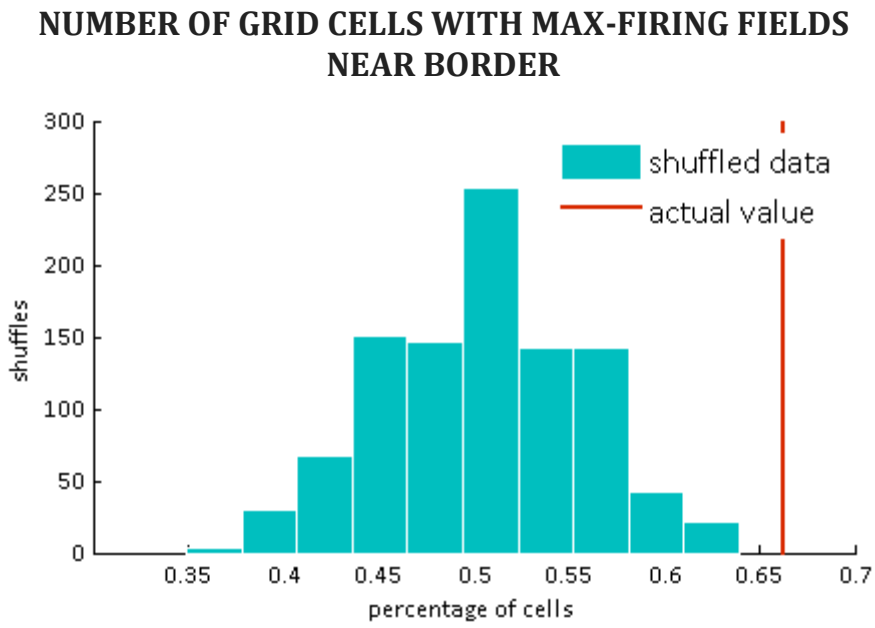

FIGURE 3.10 *Histogram of shuffled data counting the number of cells from the set whose maximum-firing fields fell near the border (defined as less than 0.1 normalized distance from the wall). The red dashed line indicates the actual value.*

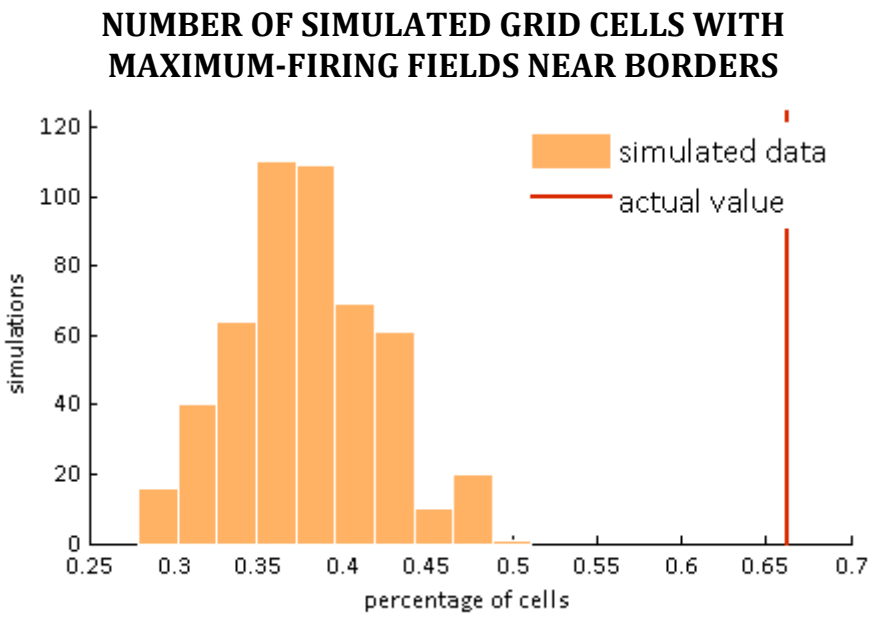

FIGURE 3.11 *Histogram of the number of cells in the simulated data set with maximum-firing fields near the border of the arena. Real value of non-simulated data set depicted with red dashed line.*

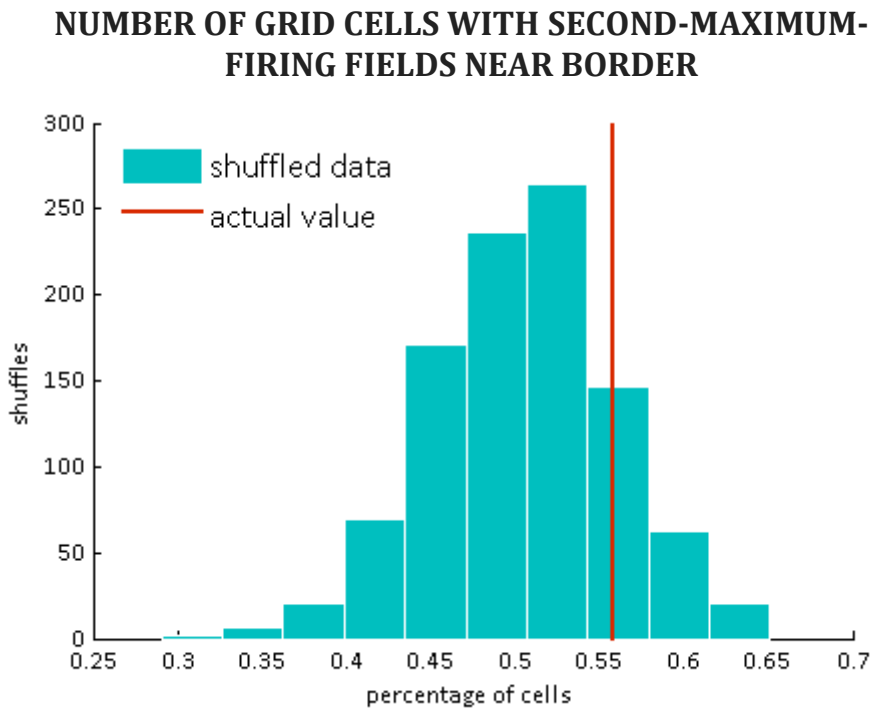

FIGURE 3.12 *Histogram of shuffled data counting the number of cells whose second-maximum-firing fields fell near the border (defined same as above). The red dashed line represents the actual value. As can be seen, the value does not appear to be significant from the shuffled results.*

BORDER AND CENTRAL-LOCATED FIELD MEAN FIRING RATES SCATTERPLOT

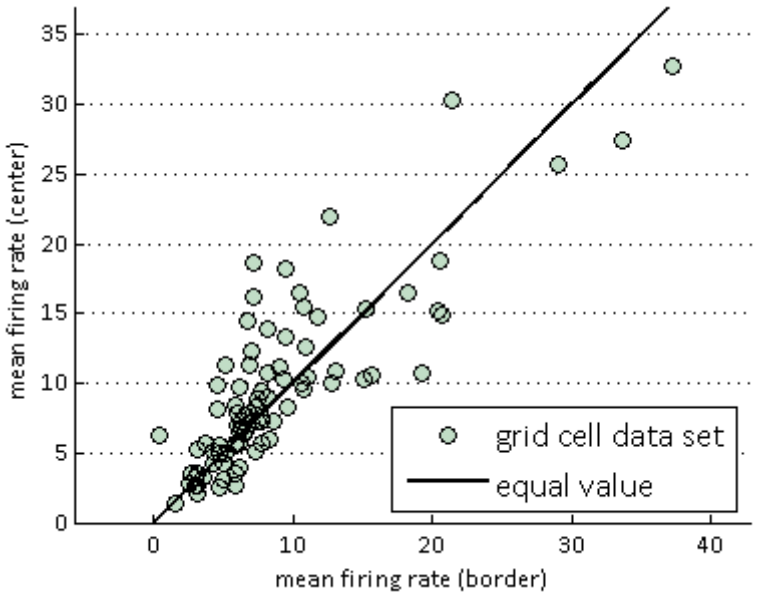

FIGURE 3.13 *Scatterplot of mean firing rates of border-located fields vs. central-located fields. Red dashed line indicates where the values are the same. Plot shows that the rates appear to be scattered around this line, with many points even above it (indicating central-located fields exhibit higher firing rate). This reveals that border-located fields do not tend to fire higher in general.*

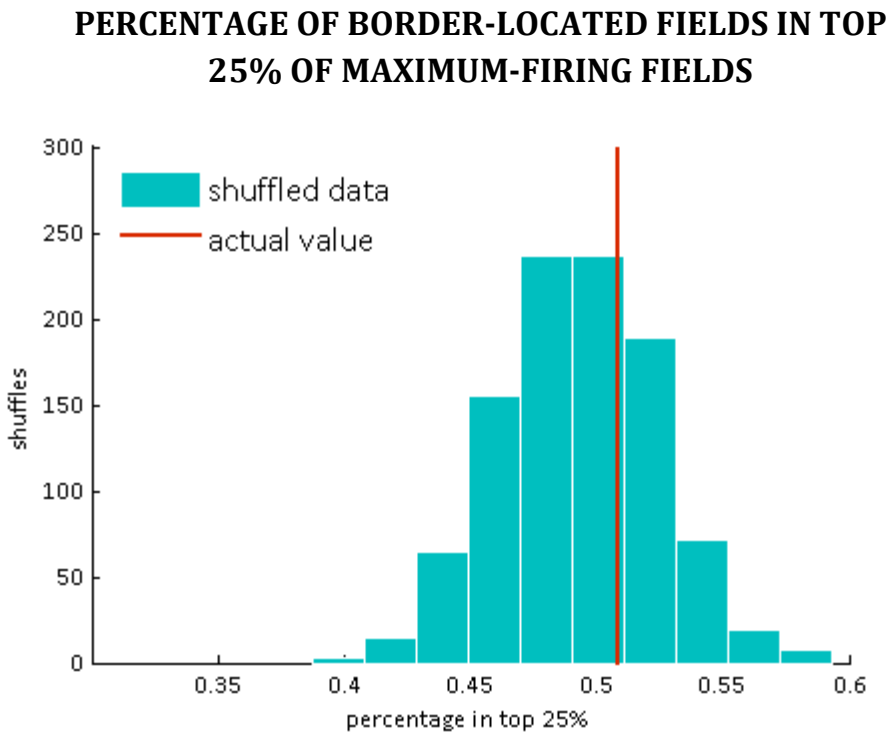

FIGURE 3.14 *Histogram of shuffled data counting the percentage of the top 25% maximum-firing fields that are located on the borders. Real value depicted with red dashed line. This illustrates that most border-located fields do not tend to have large firing, excluding the maximum firing field, and that the top most maximally-firing fields tend to be mainly central-located fields.*

{3.4.iv} Space deformation reveals anchor point

To investigate and further understand the properties of the hyperfield, we wanted to examine how this field would react to a change within an arena. For this analysis, we used data from Barry et al. [48], in which grid cells were recorded in re-scaled environments after the animal had been familiarized in a specific environment. The different arena configurations comprised of a vertical South-North rectangular box, a horizontal West-East rectangular box, a larger square box, and a smaller square box, with most sessions usually starting with the larger square or vertical rectangle box. Each session comprised four arena transformations, with the last arena matching the first. This study found that the grid pattern stretched or compressed on average to about 80% of the new arena configuration change. We used the data from this study to observe how the maximum-firing field changed its position following each arena deformation.

Grid cells were included in the analysis only if they passed a quality criterion ("gridness score") of at least 0.3 in at least one of the five arena configurations.

Examination revealed that in many cases the maximum-firing field remained in the same relative location when the arenas were normalized to the same size, and remained the maximum-firing field, even after the arena box resized (FIGURE 3.15). It was common for the hyperfield to remain the strongest firing field in the majority of transformed arenas. Thus, despite the arena transformation, the hyperfield seemed stable.

As a means by which to define this maximum-firing field stability, we used a measure we referred to as a "cluster score." This score was calculated by taking the number of maximum-firing field normalized locations that fell near each other, divided by the total number of such values ('near' was defined as cases in which the normalized distance between the fields was less than 0.35). Thus, a cluster score of 0 denoted a complete lack of stability in maximum-field location between the changing arenas, while 1 represented strong stability (see FIGURE 3.16).

A score of 1 corresponds to all the points being located in the same normalized location, or "clustered" together when the arenas, normalized along the two dimensions, are projected over each other. A score of 0.6 means that 4 of the 5 points are clustered together, while 0.4 or 0.3 means 3 of the 5 are, with 0.4 indicating the remaining two points remap together to the same location (creating two total clusters), whereas 0.3 indicates they remap separately (creating 3 clusters).

$$Cluster\ score = \frac{sum\ (dist_{norm} < 0.35)}{length\ (dist_{norm})}$$

(eq. 3.2)

We found at the level of the population a high number of cells with large cluster scores among the data set (80.0% >= 0.3, mean=0.474; FIGURE 3.17). In order to observe the statistical significance of this, the data underwent a shuffling process by which the firing rates were randomly mixed between the fields for each session. Compared to the distribution of the shuffled data, the mean field stability

score from the original data was found to be much better than 1000 out of 1000 shuffles (FIGURE 3.18). These results did not change much if using different thresholds for defining 'nearness' (see Appendix II).

These results reveal that the hyperfield remained anchored to its relative position and continued to strongly fire above the rest of the fields.

EXAMPLE OF CLUSTER SCORE ILLUSTRATION

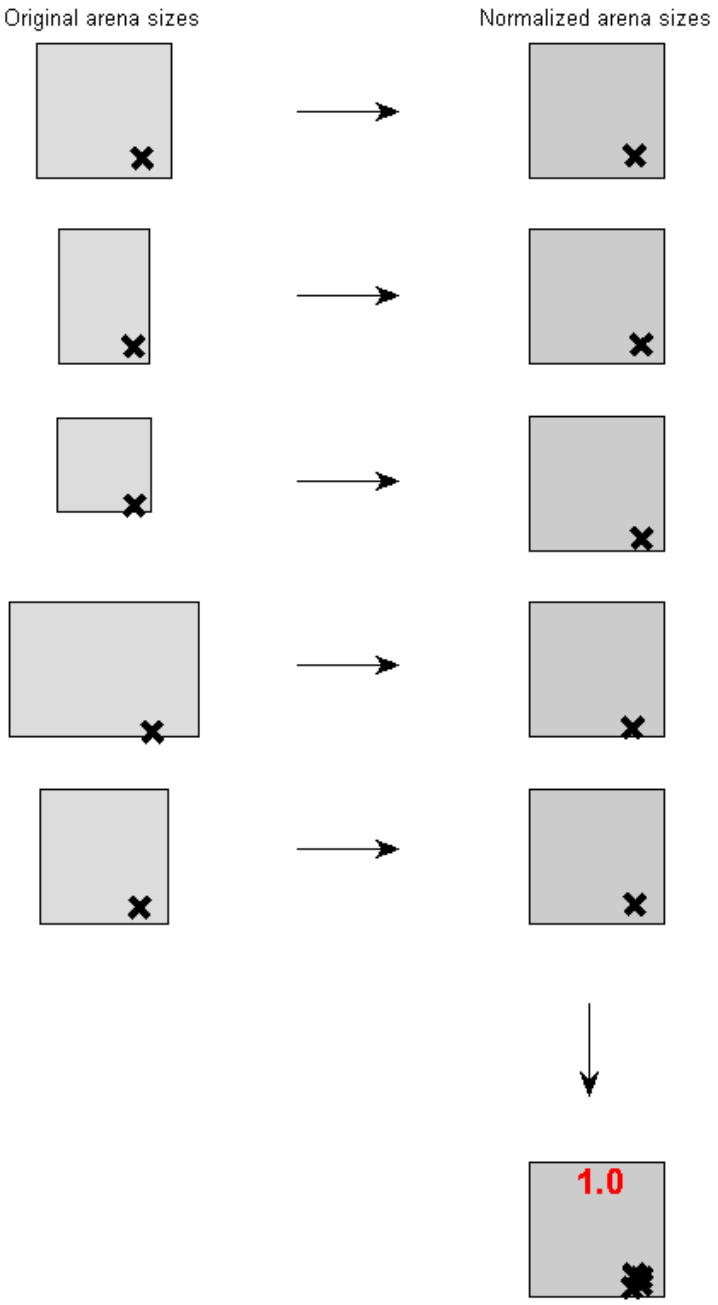

FIGURE 3.15 *Example of how a Cluster score is calculated. The locations of the hyperfield (depicted by black x's) are normalized to the same arena size. The Cluster score is then calculated by how clustered the locations are when overlaid on top of eachhother (as shown in the last row, last column). The Cluster score is displayed in red.*

MAXIMUM-FIRING FIELD AMONG DIFFERENT ARENA CONFIGURATION CHANGES

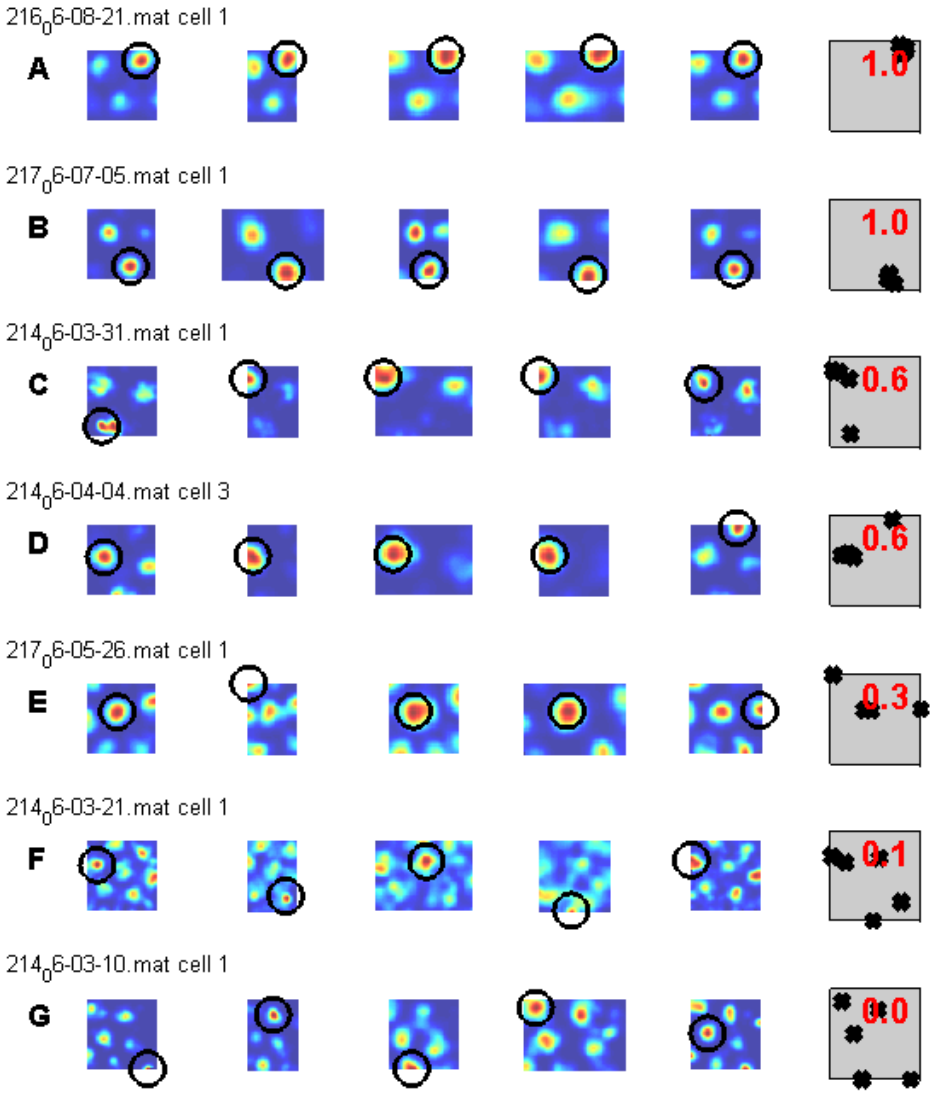

FIGURE 3.16 *Examples of the rate mpas of grid cells in different arena configurations with the hyperfield circled in each map. The normalized locations of the hyperfields are plotted overlaid over eachother in the last column with the Cluster score displayed in red.*

CLUSTER SCORES OF GRID CELL DATA SET

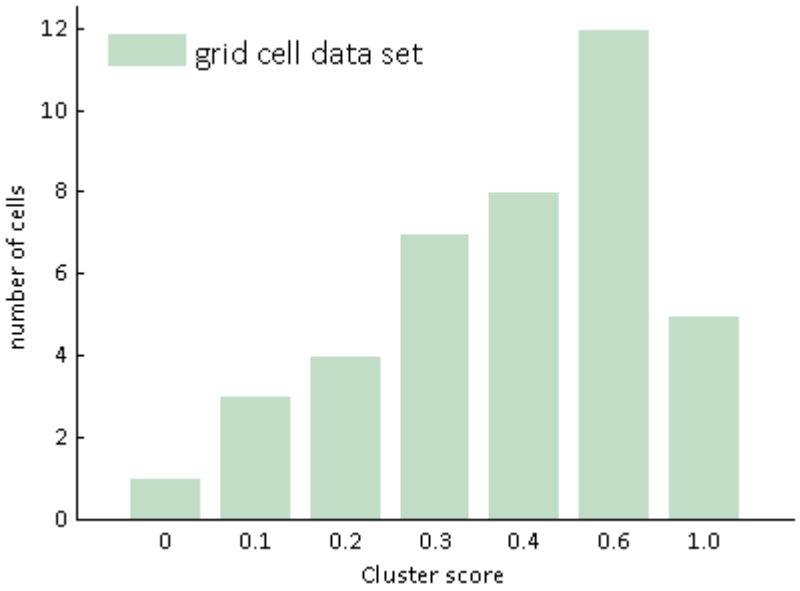

FIGURE 3.17 *Bar graph of Cluster scores of the population data set. Cluster scores range from 0 to 1, in discrete values. As can be seen, there are many cells that exhibit a Cluster score of at least 0.6.*

AVERAGE CLUSTER SCORE OF SHUFFLED DATA SET

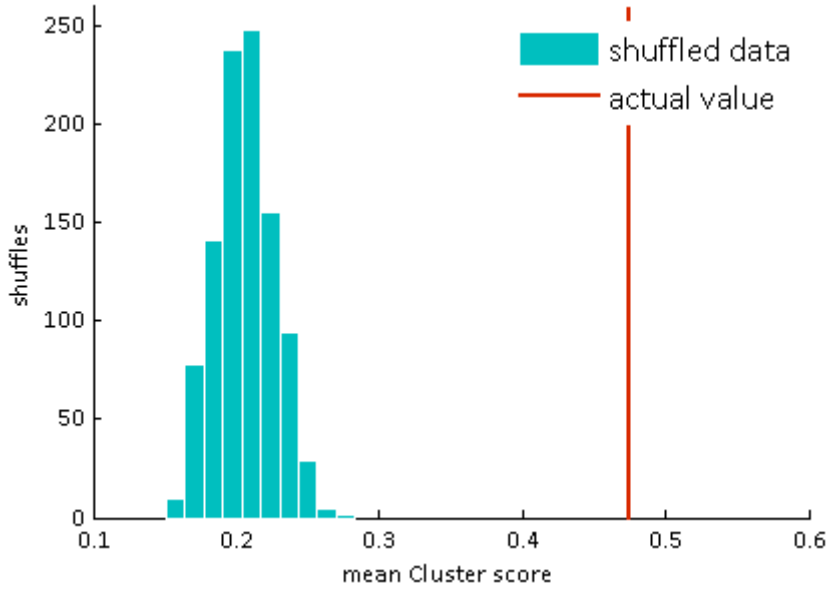

FIGURE 3.18 *Average cluster score of grid cell data set. Shuffled results are reported by the red bars. Green dashed line represents the actual mean cluster score of the data set.*

{3.4.v} Grid cells exhibit stable firing profiles

We further investigated whether the firing rates of the other fields also retained stability across single sessions and across arena changes. We looked at the correlation coefficient of the firing rates of the fields in the first half of the session versus the firing rates of the corresponding fields from the second half to see if fields tended to remain firing in a similar fashion. In addition, we also looked at the original arenas versus the rescaled arenas from the Barry et al. study [48], and the original arenas versus the last identical arena. Examples of the firing rates of the original arena plotted alongside the firing rates of the rescaled arena, in increasing order of the original firing rates, suggested that there is a pattern that is retained between the two environmental variations (see FIGURE 3.19).

To observe the statistical significance of this, we compared the results to the distribution of the shuffling procedure in which the firing rates were shuffled between the different fields. Looking at the first half of the session versus the second half, we found that there tended to be a larger mean correlation coefficient between the two halves than expected from shuffling measures (see FIGURE 3.20). This reveals that the variability is stable across the session and that fields tend to retain a similar firing rate profile across time. The results remained stable even when the hyperfield was excluded from the analysis (FIGURE 3.20), confirming that this high correlation coefficient was not solely the result of its strong amplitude.

Next we observed whether this was also true across arena changes in data from the Barry et al. study [48]. We took paired original arenas with rescaled arenas

that had a similar number of fields (no more than 30% difference) and stretched the rescaled arena to the size of the original. We found the pairs of fields by pairing each with its nearest neighbor. As before, we looked at the mean correlation coefficient compared to the shuffled distribution. We saw that again, the firing fields retained a similar firing profile. This was also the case with the hyperfield excluded (FIGURE 3.20).

Results were also similar when observing the correlation coefficient of the first arena to the last identical arena, also when hyperfield was excluded from the analysis (FIGURE 3.20). These results reveal that fields remain firing in a similar fashion between single sessions, between different sessions of the same arena, and between sessions of a rescaling environment. In all the above cases, and for both the full data and data with the hyperfield excluded, the means of the actual data were better than all 1000 shuffles for all analyses.

CORRELATIONS BETWEEN FIRING RATES IN DIFFERENT ARENA VARIATIONS

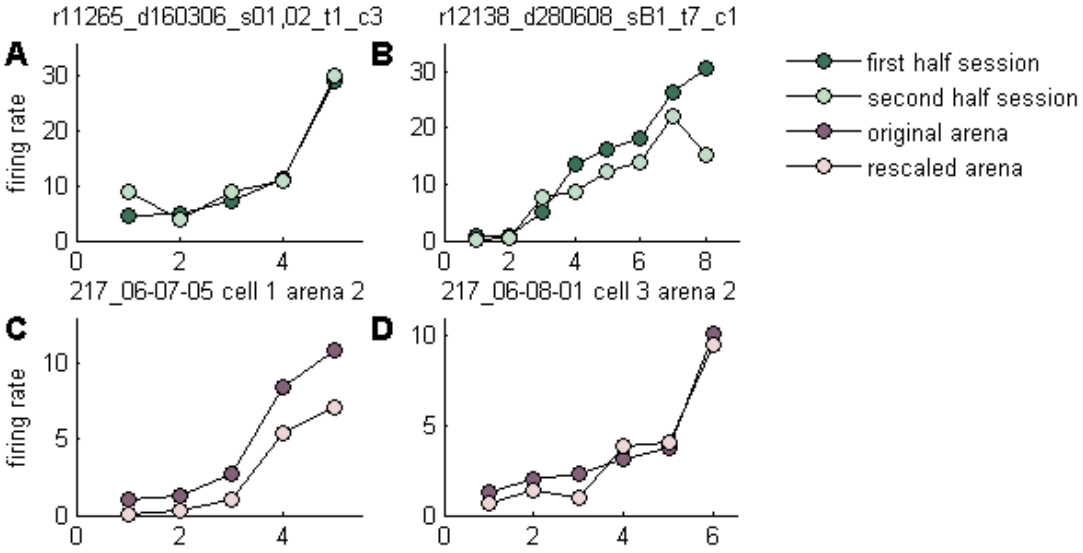

FIGURE 3.19 *(A-D) Examples of firing rate of the first half of the session and the second half of the session. P, plotted in increasing order of the total session peak firing rate. (C-D) Examples of the firing rate of all the fields within the original arena plotted in increasing order compared to firing rates of a rescaled arena plotted according to the original arena. Examples show that firing fields tend to remain firing in a similar fashion throughout both arena configurations.*

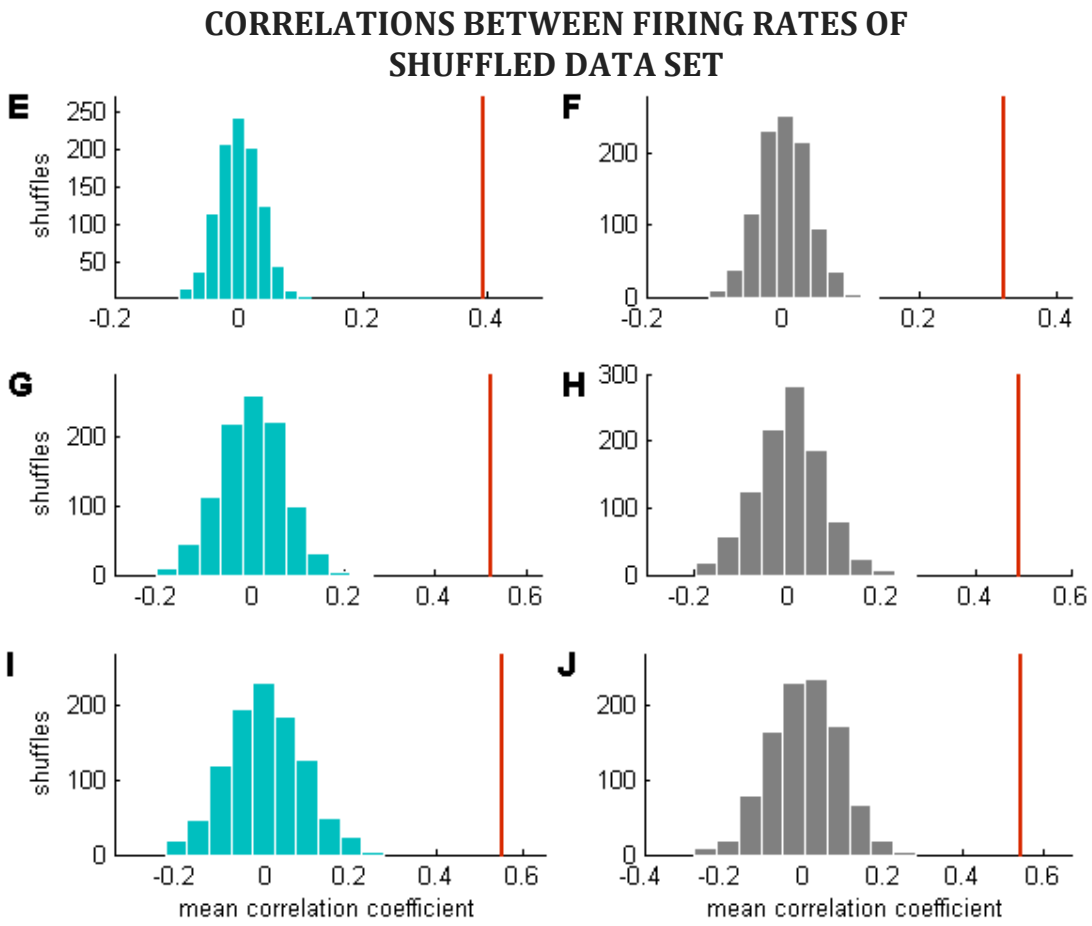

FIGURE 3.20 *(E) The distribution of the mean correlation coefficient of the firing rates among the fields in the first half of the session and the same fields in the second half from the shuffled data compared to the actual value. (F) Same as (E) but with exclusion of the hyperfield. (G) The distribution of the mean correlation coefficient of the firing rates in the original arena against the firing rates of the same corresponding fields in a rescaled environment from the shuffled data compared to the actual value. (H) Same as (G) but with hyperfield excluded. (I) The distribution of the mean correlation coefficient of the firing rates in the original arena against the firing rates of the same corresponding fields in the last identical arena from the shuffled data compared to the actual value. (J) Same as (I) but with hyperfield removed from analysis. The results remain statistically significant, providing evidence that this strong correlation coefficient is not solely due to the hyperfield.*

{3.4.vi} Evidence of anchor with place cell inactivation

A study by the Moser group has found that excitatory drive from the hippocampus is necessary for the formation of the grid cell firing pattern, showing that with the inactivation of the hippocampus and the place cells within it, the grid pattern breaks down [41]. In most cases it appears that the grid cells strongly diminish their firing rate with the breakdown of the grid pattern. However, some cases found that the grid pattern breaks down, but the cell retains a spatial dynamic with no decrease in firing rate. An example is provided in FIGURE 23, which shows a grid cell that breaks down its firing pattern after hippocampus inactivation, but still remains spatially-tuned.

It is interesting to note that in this example provided in the paper, it appears that the location of the firing field that remains after the hippocampal inactivation is located in the same place as the maximum-firing field of the original grid pattern. This may point to the excitatory drive from the hippocampus as the mechanism for how this anchor point is able to aid in the formation of typical grid cell firing activities. A specific place/grid metric may exist, which in cases may fail to fully break down as place cells are silenced. Alternatively, the source of the pivot point may be non-hippocampal and may stem from a different brain structure.

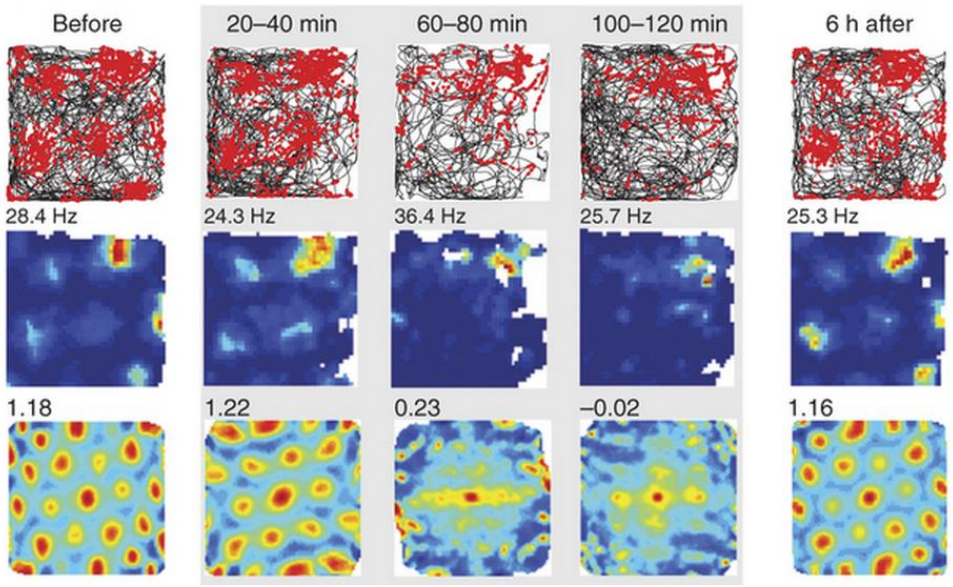

FIGURE 3.21 *An example of a grid cell that remains firing at a similar rate and remains spatially-tuned after inactivation of excitatory information from the hippocampus, but loses its grid pattern. It is interesting to note that the location of the firing field after inactivation is located in the same location as the maximum-firing field of the original grid pattern before inactivation. Figure taken from Bonnevie et al., 2013 [41].*

Chapter [3.5]

Overdispersion of firing field passes

{3.5.i} Field passes adaptation

We wanted to investigate how the firing activity is reflected in the length and manner of the pass. Specifically, we wanted to see if the firing activity diminished with the length of time through the field. If so, this would suggest that adaptation occurs in grid cell fields. Also, we wanted to examine how the method of traversing through the field (i.e. straight through vs in and out from same direction) affected the activity of firing.

We examined this by looking at the firing rate at each single pass, compared to the firing rate that would have been expected. The expected firing rate was calculated from the rate map of the total combined session. We looked at the ratio of the actual firing rate per pass to the predicted firing rate compared to the length of time within the field.

We used a larger data set for this analysis as we included cells from circular arenas. We only used cells with a gridness score of at least 0.4 and a HD Rayleigh score of at least less than 0.2.

Results showed that the ratio of actual versus predicted firing rate diminished as the length of time of pass increased. This suggests that adaptation does indeed occur and that the fields do show fatigue over time.

TABLE 3.2: Cells in the overdispersion study

Study	Total number of cells	Cells passing gridness and HD criterion	Grid cells remaining for study
Sargolini et al., 2006	**620**	**42**	42
Derdikman et al., 2009	**121**	**39**	39
Bonnevie et al., 2013	**195**	**76**	76
Total:	936	157	157

EXAMPLES OF ACTUAL TO EXPECTED FIRING RATE RATIO AS A FUNCTION OF LENGTH OF TIME SPENT IN INDIVIDUAL PASSES

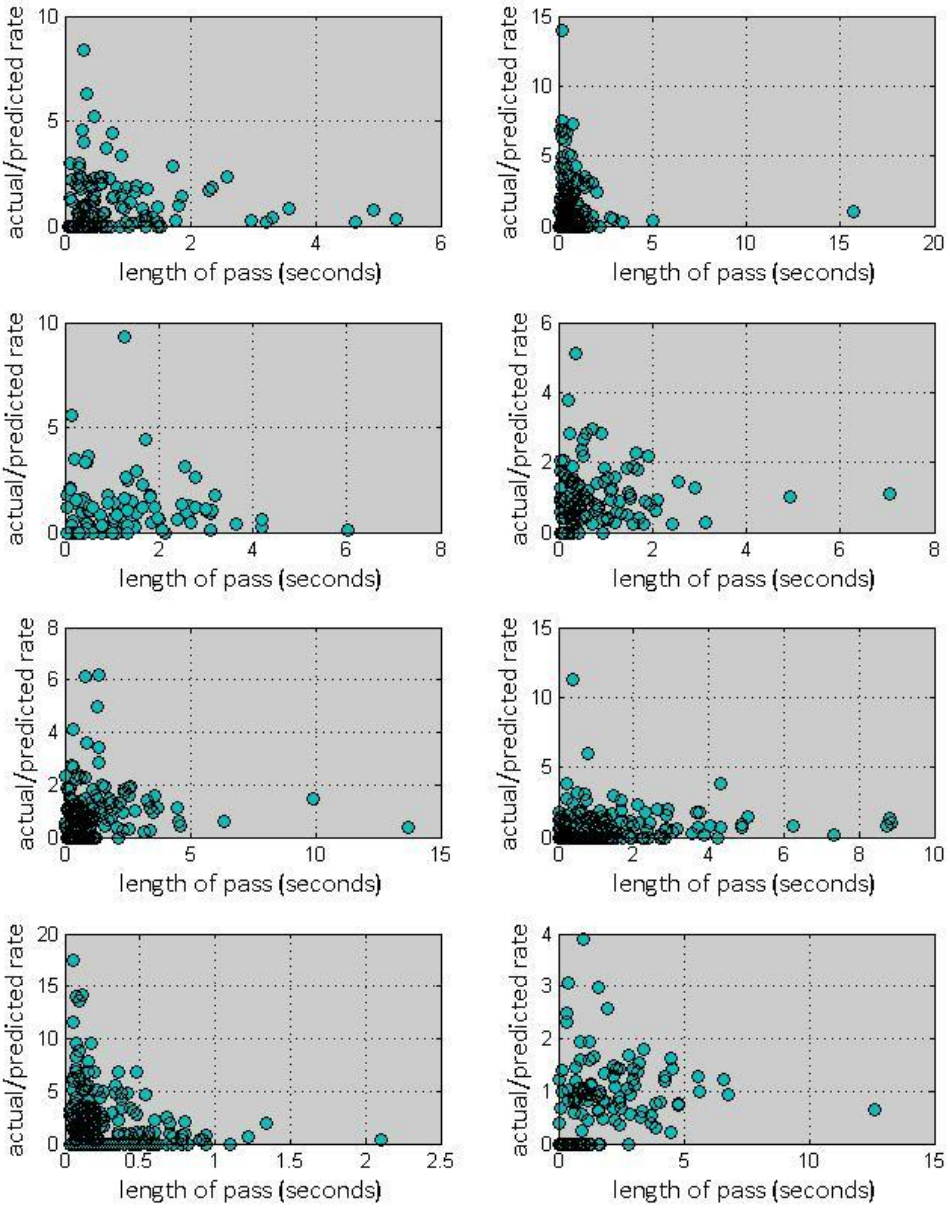

Figure 3.22 *Scatterplots of actual versus predicted firing rate as a function of length of time spent through pass. As the length of time within pass increases, the actual over predicted firing rate decreases. The cell fires at a lower rate than expected the longer he is within an individual field, suggesting fatigue occurs for individual passes.*

CORRELATION COEFFICIENTS OF ACTUAL TO EXPECTED FIRING RATE RATIO VS LENGTH OF TIME IN PASS FOR INDIVIDUAL RUNS

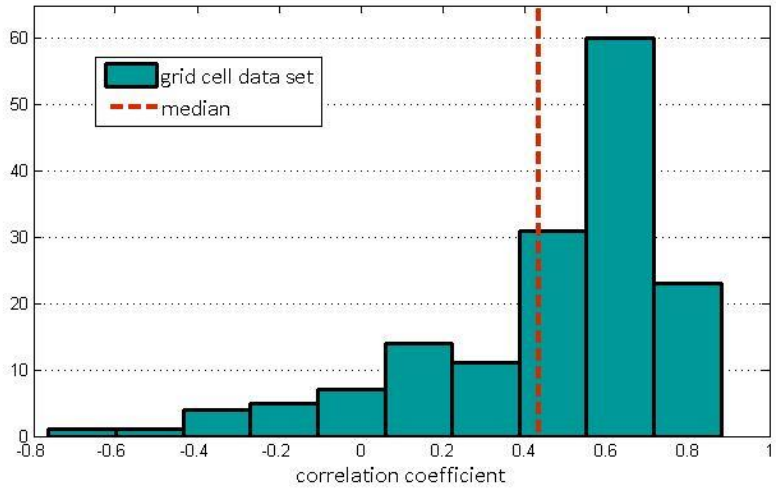

Figure 3.23 *Histogram of the correlation coefficients of actual firing rate over expected actual firing rate as a function of the length of time of individual passes. You can see most fall in the positive correlation values and the median of the data set is at 0.4354. This shows that most of the cells in the data set show a positive correlation between length of time for a pass and the ratio of actual to expected firing rate, suggesting that adaptation may occur within passes.*

Chapter [3.6]

Discussion

Grid cell firing patterns have a specific orientation and phase in respect to the boundaries of the environment. The mechanism by which the properties of this pattern arise is still unclear. Here we provided evidence that this strongly-firing field may be the anchor and pivot point for the formation of this grid cell pattern. Different studies have looked into various properties of grid cell firing activity, finding certain patters and characteristics in the orientation and phase of its specific hexagonal array. An example of this includes a study that examined the orientation of grid cells. The orientation was defined as the smallest angle between the walls and the six points that form the hexagonal, taken from the autocorrelation of the grid cell rate map. The researchers found that this orientation tends to be around 7.5 degrees, which happens to provide the most information about the walls of the arena [49]. Seven degrees means that the angles of the other walls will not be the same, and as such, allows that the maximum information is provided about the room.

However, the way in which the cell is able to adjust its hexagonal array firing pattern is unclear. The cell must in some way be anchored to a wall as it shears its orientation, or a mechanism must exist that permits it to pivot the grid-aligned firing. A method by which this may be possible is if a firing field acts as an anchor or pivot point. We have found evidence that one specific field tends to fire stronger than the rest of the firing fields.

This field may be the mechanism by which the grid cell is able to align itself to the arena boundaries. Its border location and its tendency to remain in the same location as the arena rescales reveals that the strong firing rate it exhibits is not purely noise and something specific to the field. Thus, it stands as a strong candidate as the method by which the grid pattern is able to align itself to a specific orientation and phase, even as subtle changes occur within the environment.

This effect is seen regardless of the variability exhibited between the grid cell fields, exposing that it's not purely a consequence of strong variation, but intrinsic to the cell even when the rest of the fields show more uniformity in firing rates. We investigated the way this field changes as the arena rescales. A study observed how grid cell firing patterns change when an environment that rat was trained in expanded or shrunk. We used this data to further look into how the maximum-firing field changes. We saw that the field remains in the same location and remains the strongest-firing field above the rest.

The fact that this field remains in the same relative location as the arena changes and rescales provides strong evidence that it is not just normal deviation among the fields, since it would in such a case vary among the fields. Rather we see that the fields of the cell retain a specific firing pattern amongst them. The maximum-firing field doesn't just vary between fields as would be expected if it were solely noise and normal variation, but remains connected to the same location throughout.

This suggests that this field may be the anchor or pivot point of the grid firing pattern of the cell. This also provides an explanation for how the cell is able to

retain its grid pattern through changes to the same arena, as well as provide a mechanism through which the grid cell is able to orient and pivot to a specific phase and orientation.

In addition to this, we also looked at the variability between single passes of a grid cell. For individual passes, we found that there were differences between the expected firing rate, calculated using the spatial firing distribution, and the actual firing. We further showed that the ratio of actual to expected firing rate decreased with the length of time spent through pass, suggesting that adaptation occurs for single passes.

Both between individual passes and between the firing fields of grid cells, we see large variability. We have shown here that the variability among the fields is larger than seen in cells simulated from equal-rate firing fields, as well as larger than data acquired through shuffle measures. The fact that the specific field exhibits strong firing and remains in the same location as the space deforms may have strong implications to its precise function and its role in the formation of the grid cell pattern. These findings all expose new knowledge on the unique firing patterns of these neurons.

The non-uniformity and relative stability of this non-uniformity reveals that the grid cell fields are not as static and equal in their firing rates. This has strong implications for the function of grid cells and may reveal new details about their structure not considered before. Grid cells are generally attributed to possessing similar firing rates between fields, which we show does not appear to be the case.

These cells are believed to play a strong role in spatial navigation, perception of self-location, and memory itself. Thus, these results might reveal information not purely on the mechanisms of these neurons, but rather additionally expose something of the phenomenon of space perception and memory.

Appendix I

Plots and spike shapes of DREADDs analysis cells

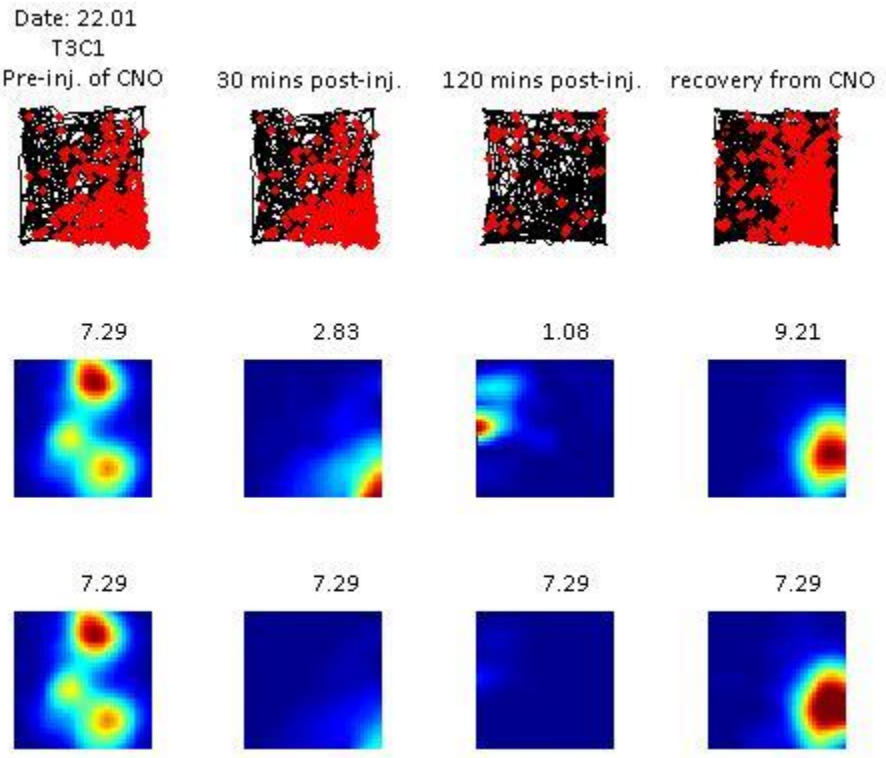
Date: 22.01
T3C1
Pre-inj. of CNO
30 mins post-inj.
120 mins post-inj.
recovery from CNO
7.29
2.83
1.08
9.21
7.29
7.29
7.29
7.29

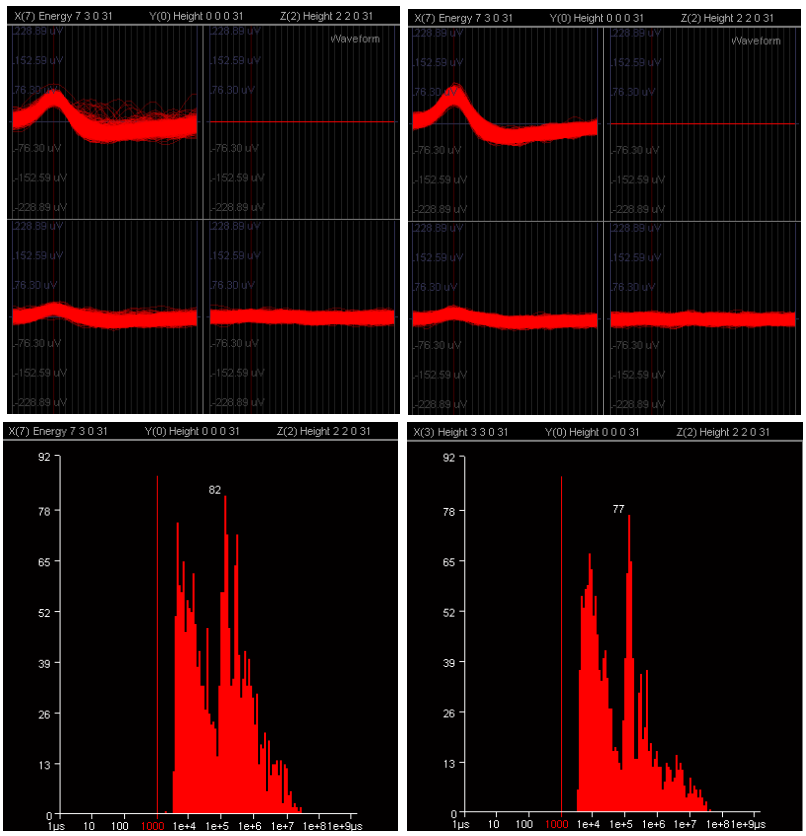
X(7) Energy 7 3 0 31
Y(0) Height 0 0 0 31
Z(2) Height 2 2 0 31
vWaveform
X(3) Height 3 3 0 31
82
77

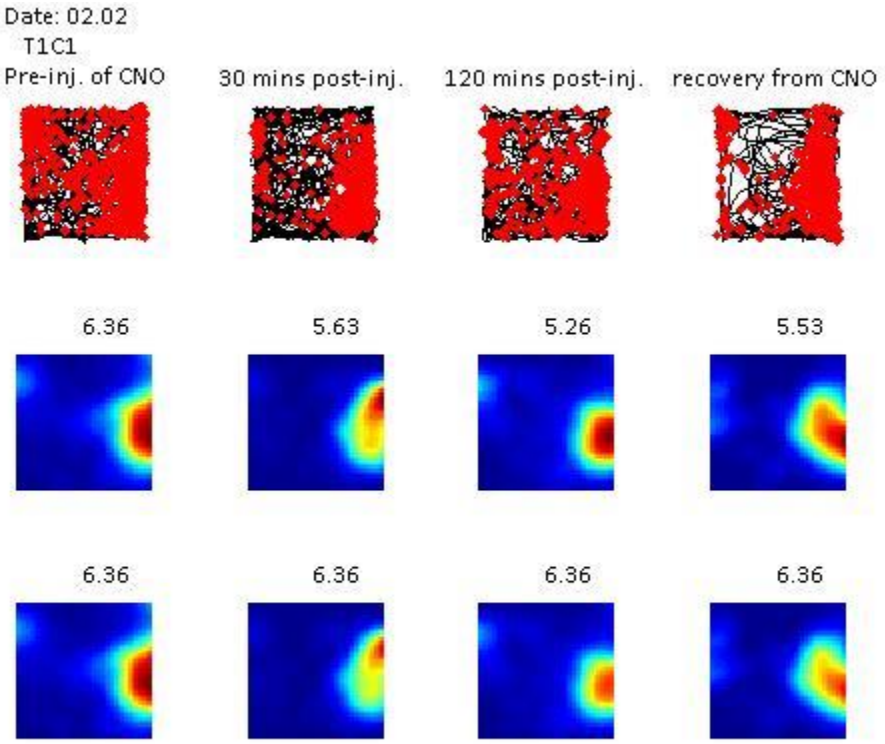
Date: 02.02
T1C1
Pre-inj. of CNO
30 mins post-inj.
120 mins post-inj.
recovery from CNO
6.36
5.63
5.26
5.53
6.36
6.36
6.36
6.36

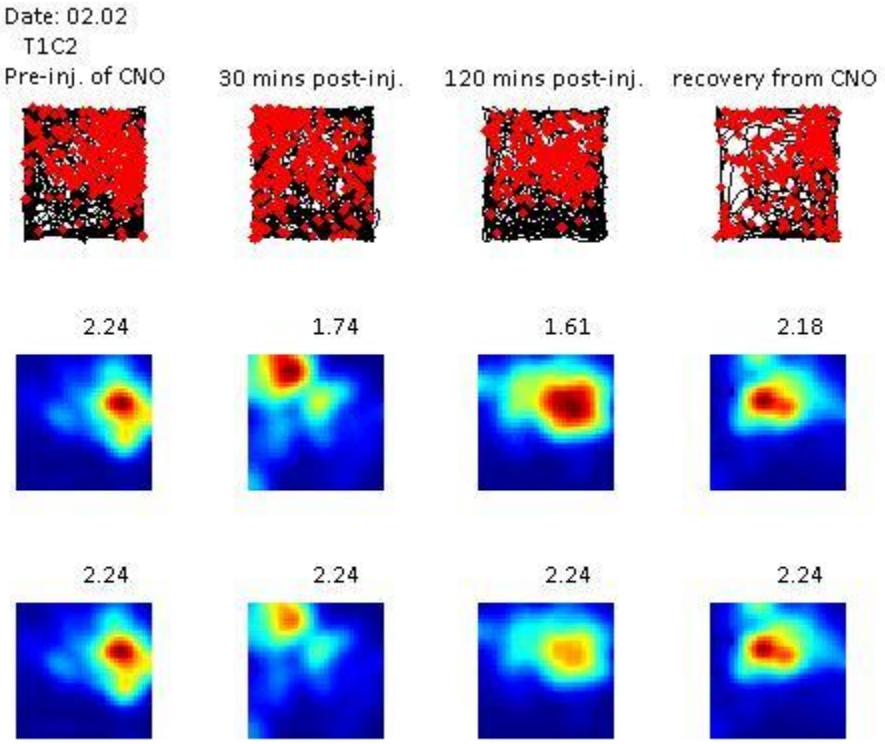
Date: 02.02
T1C2
Pre-inj. of CNO
30 mins post-inj.
120 mins post-inj.
recovery from CNO
2.24
1.74
1.61
2.18
2.24
2.24
2.24
2.24

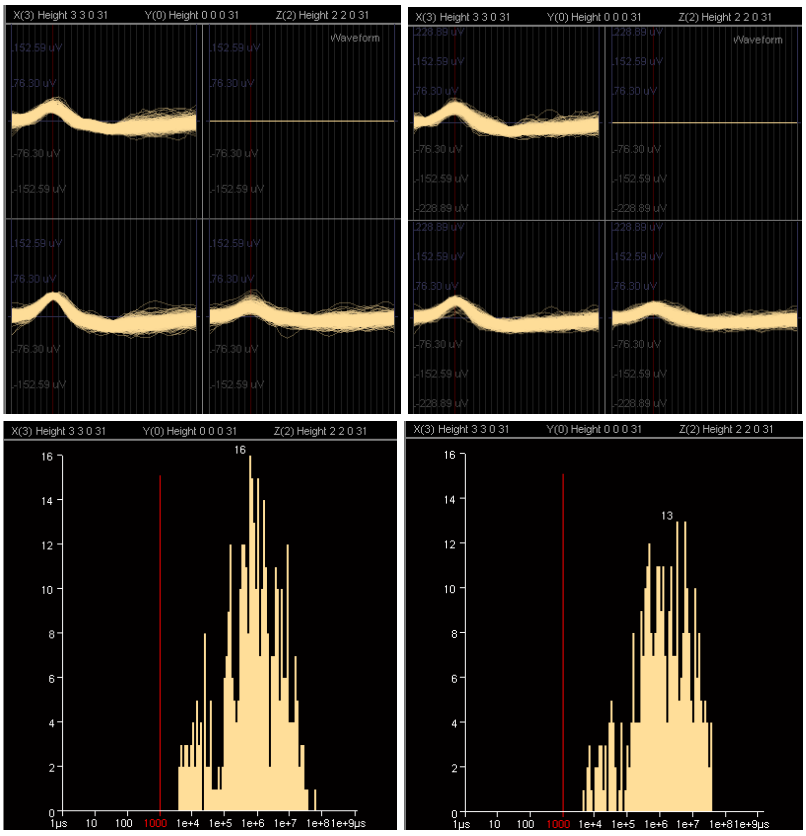
X(3) Height 3 3 0 31
Y(0) Height 0 0 0 31
Z(2) Height 2 2 0 31
vWaveform
16
13

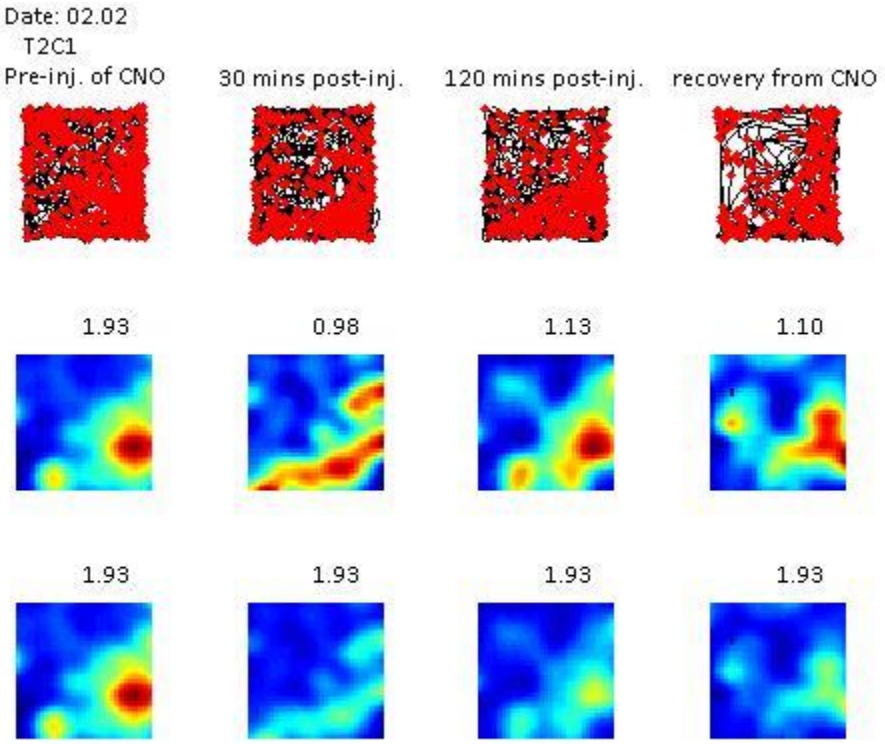
Date: 02.02
T2C1
Pre-inj. of CNO
30 mins post-inj.
120 mins post-inj.
recovery from CNO
1.93
0.98
1.13
1.10
1.93
1.93
1.93
1.93

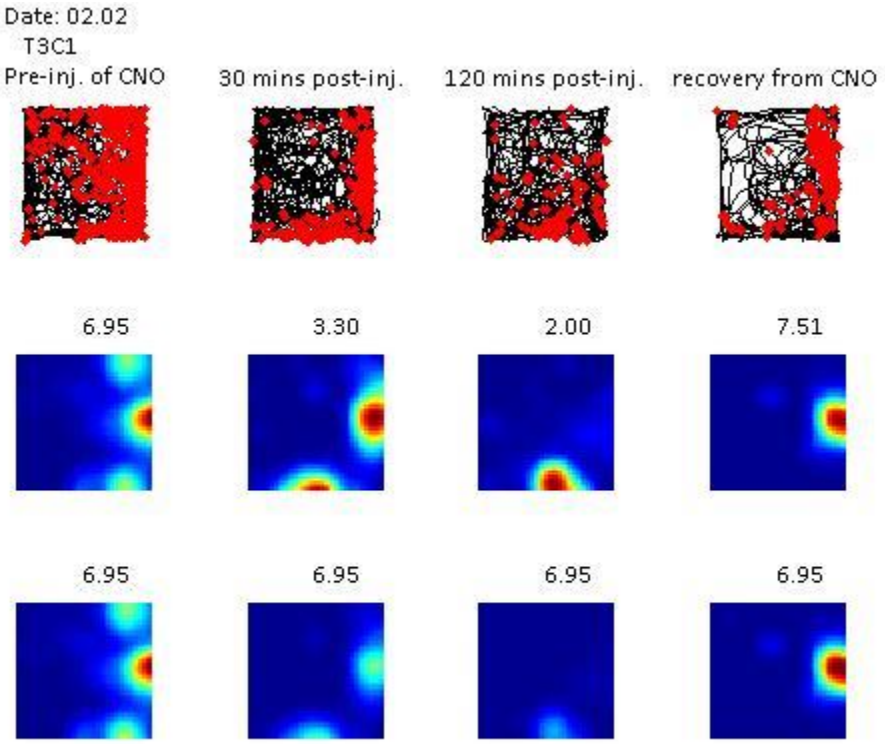
Date: 02.02
T3C1
Pre-inj. of CNO
30 mins post-inj.
120 mins post-inj.
recovery from CNO
6.95
3.30
2.00
7.51
6.95
6.95
6.95
6.95

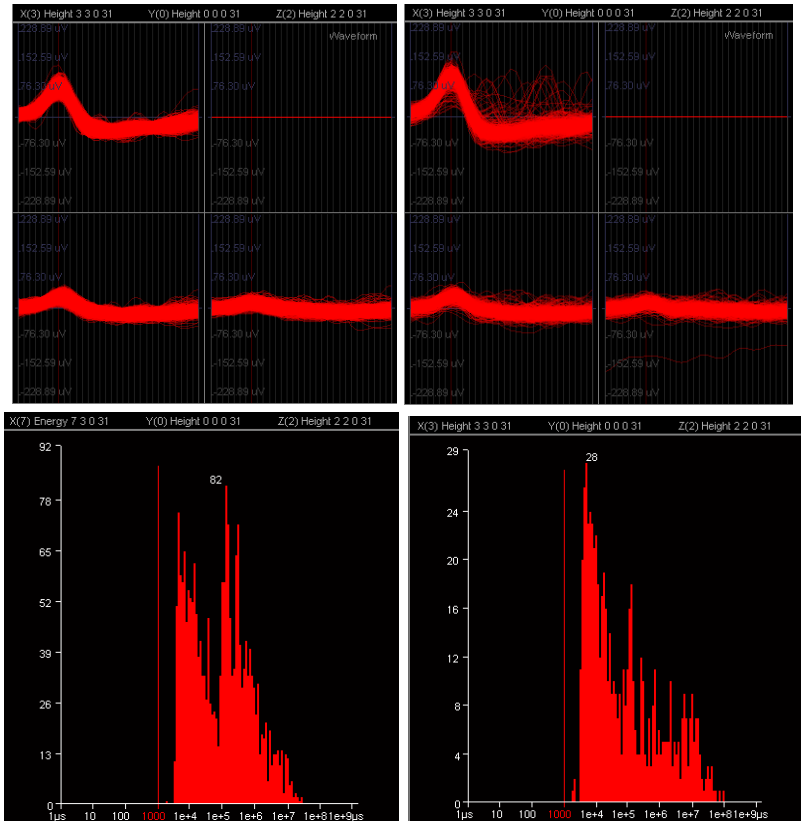
X(3) Height 3 3 0 31
Y(0) Height 0 0 0 31
Z(2) Height 2 2 0 31
Waveform
X(7) Energy 7 3 0 31
82
26

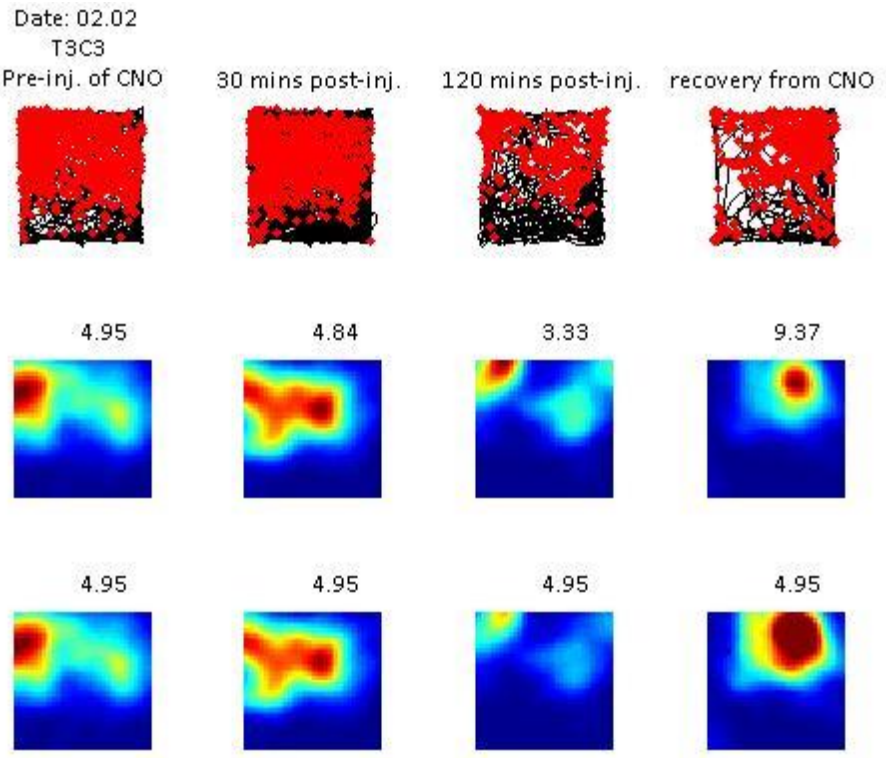
Date: 02.02
T3C3
Pre-inj. of CNO
30 mins post-inj.
120 mins post-inj.
recovery from CNO
4.95
4.84
3.33
9.37
4.95
4.95
4.95
4.95

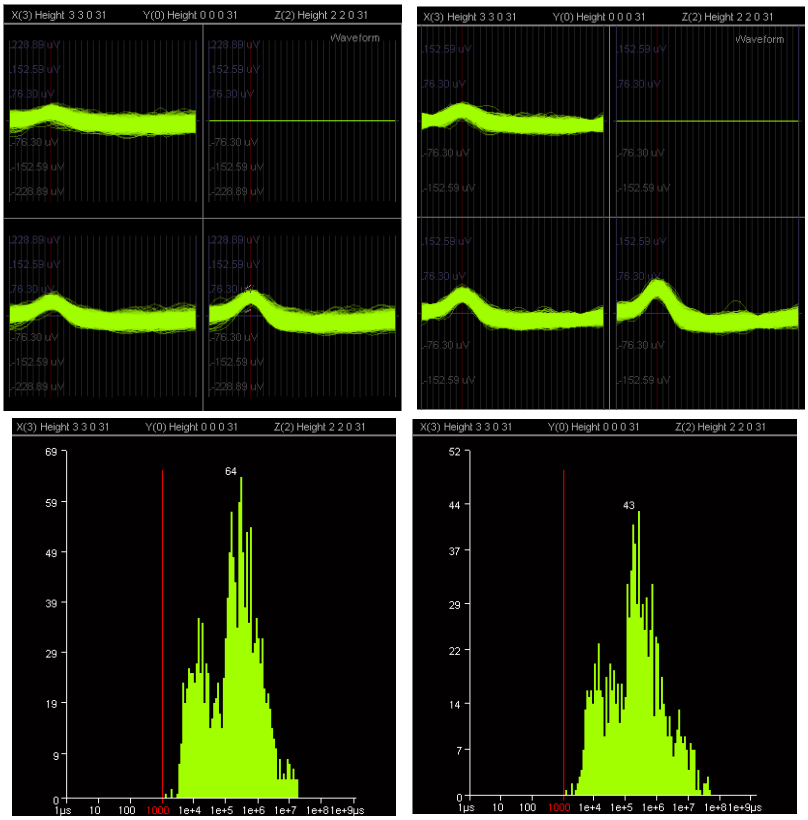
X(3) Height 3 3 0 31
Y(0) Height 0 0 0 31
Z(2) Height 2 2 0 31
Waveform
64
43

Date: 02.02
T3C3

Pre-inj. of CNO	90 mins post-inj.	140 mins post-inj.	recovery from CNO
			
3.63	1.26	0.56	3.99
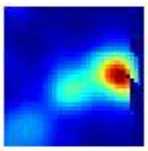	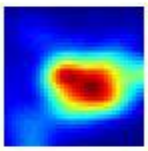	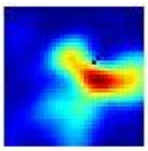	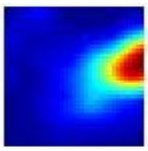
3.63	3.63	3.63	3.63
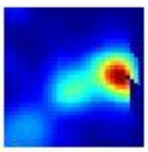	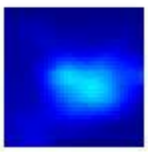	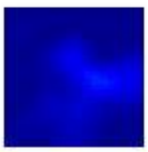	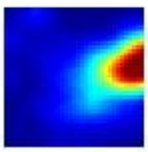

Date: 02.02
T3C3

Pre-inj. of CNO	90 mins post-inj.	140 mins post-inj.	recovery from CNO
			
2.69	1.31	1.13	5.63
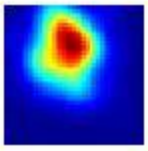	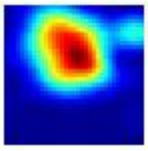	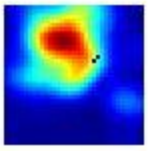	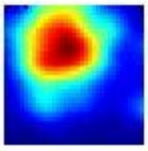
2.69	2.69	2.69	2.69
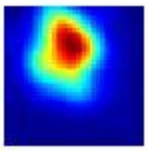	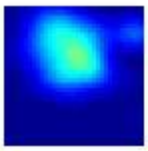	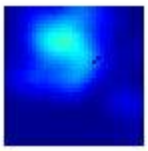	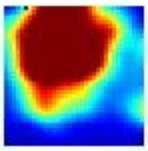

Appendix II

Supplementary Information

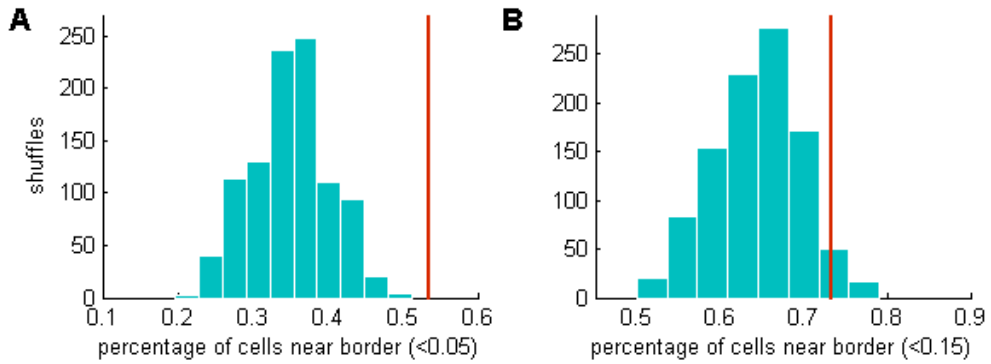

(A-B) Percentage of shuffled data set with cells having its hyperfield located near a border. Real value displayed by red line. (A) "Near border" is defined as less than 0.05 normalized distances from border. (B) "Near border" defined as less than 0.15 normalized distances from border.

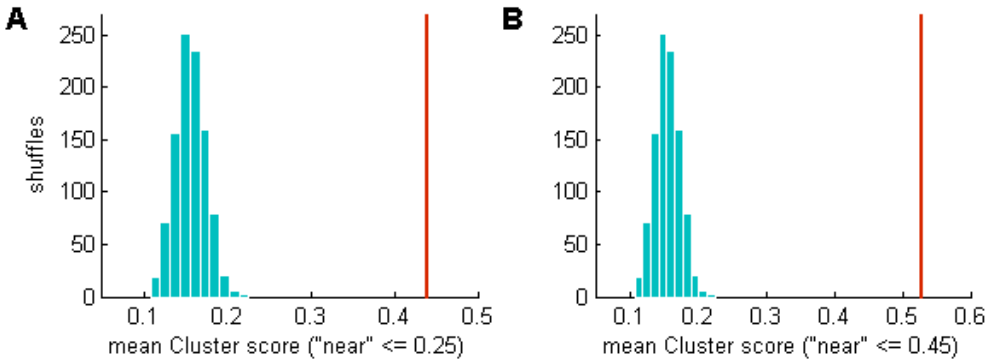

(A-B) shows mean Cluster scores of the shuffled data with real values displayed by the red line. "Nearness" definition for calculating the Cluster score was changed to different values. Results remained significant.

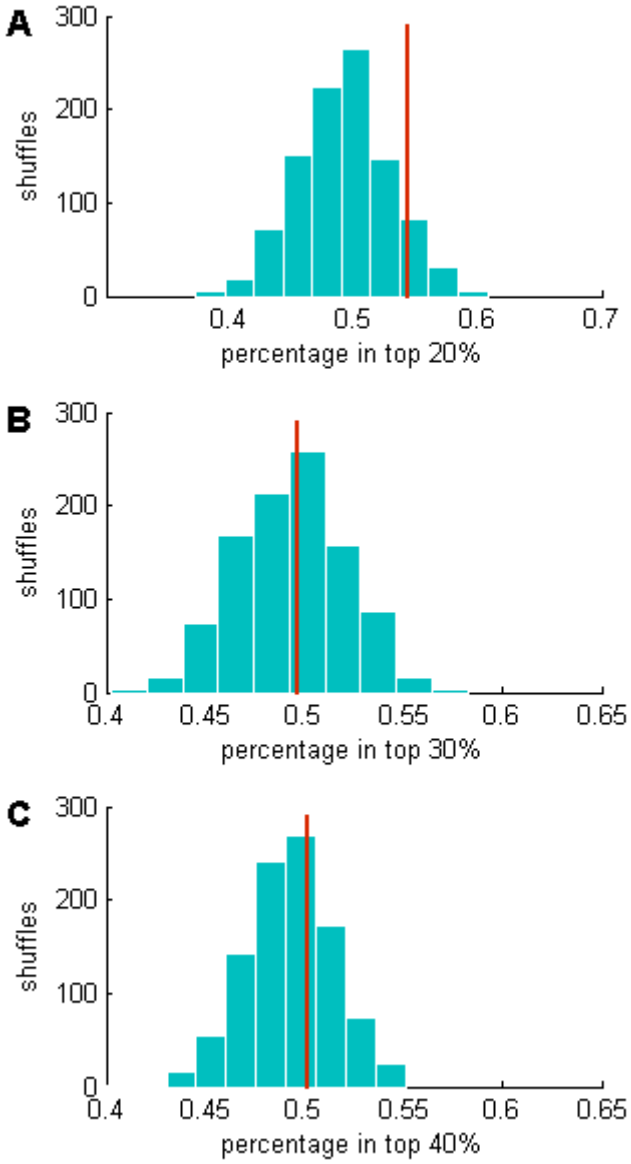

(A-C) The percentage of top maximally-firing fields located at the border of the arena. Top 30% (B), and 40% (C) are shown. Real mean values are displayed with red line. The results are statistically significant in all cases.

References

[1] Carpenter, R. and B. Redd, *Charlas de Café: pensamientos, anécdotas y confidencias (Café Chats: Thoughts, Anecdotes and Confidences)*, in *Neurophysiology: A Conceptual Approach*. 1920, 1967. p. 276.

[2] Suthana, N.A., et al., *Human Hippocampal CA1 Involvement during Allocentric Encoding of Spatial Information.* J. Neurosci., 2009. **29**(34): p. 10512-10519.

[3] Morris, R., *Theories of hippocampal function*, in *The Hippocampus Book*, P. Andersen, et al., Editors. 2007, Oxford University Press: New York, NY, US. p. 581-714.

[4] Schmolck, H., et al., *Semantic knowledge in patient H.M. and other patients with bilateral medial and lateral temporal lobe lesions.* Hippocampus, 2002. **12**(4): p. 520-33.

[5] Scher, A.I., et al., *Hippocampal shape analysis in Alzheimer's disease: a population-based study.* Neuroimage, 2007. **36**(1): p. 8-18.

[6] Cajal., S.R.y., *Histologie du Système nerveux de l'Homme et des Vertébrés*. 1909.

[7] Taube, J.S., R.U. Muller, and J.B. Ranck, Jr., *Head-direction cells recorded from the postsubiculum in freely moving rats. I. Description and quantitative analysis.* J. Neurosci., 1990. **10**(2): p. 420-435.

[8] Taube, J.S. and J.P. Bassett, *Persistent neural activity in head direction cells.* Cerebral Cortex, 2003. **13**(11): p. 1162-1172.

[9] Yoder, R.M., et al., *Both visual and idiothetic cues contribute to head direction cell stability during navigation along complex routes.* Journal of Neurophysiology, 2011. **105**(6): p. 2989-3001.

[10] Blair, H. and P. Sharp, *Visual and vestibular influences on head-direction cells in the anterior thalamus of the rat.* Behav Neurosci., 1996. **110**(4): p. 643-60.

[11] Fenton, A.A., et al., *Unmasking the CA1 ensemble place code by exposures to small and large environments: more place cells and multiple, irregularly arranged, and expanded place fields in the larger space.* J Neurosci, 2008. **28**(44): p. 11250 - 62.

[12] Muller, R.U. and J.L. Kubie, *The effects of changes in the environment on the spatial firing of hippocampal complex-spike cells.* J. Neurosci., 1987. **7**(7): p. 1951-1968.

[13] May-Britt Moser, E.I.M., *Crystals of the brain.* EMBO Mol Med., 2011. **3**(2): p. 69-71.

[14] McNaughton, B.L., et al., *Path integration and the neural basis of the 'cognitive map'.* Nat Rev Neurosci, 2006. **7**(8): p. 663-78.

[15] Solstad, T., et al., *Representation of Geometric Borders in the Entorhinal Cortex.* Science, 2008. **322**(5909): p. 1865-1868.

[16] Barry, C., et al., *The boundary vector cell model of place cell firing and spatial memory.* Rev Neurosci, 2006. **17**(1-2): p. 71-97.

[17] Tolman, E.C., *Cognitive maps in rats and men.* Psychol Rev, 1948. **55**(4): p. 189-208.

[18] Jeffery, K.J., *Self-localization and the entorhinal-hippocampal system.* Current Opinion in Neurobiology, 2007. **17**(6): p. 684-691.

[19] Hafting, T., et al., *Microstructure of a spatial map in the entorhinal cortex.* Nature, 2005. **436**(7052): p. 801-6.

[20] Fyhn, M., et al., *Hippocampal remapping and grid realignment in entorhinal cortex.* Nature, 2007. **446**(7132): p. 190-4.

[21] Colgin, L.L., E.I. Moser, and M.B. Moser, *Understanding memory through hippocampal remapping.* Trends in Neurosciences, 2008. **31**(9): p. 469-477.

[22] Derdikman, D. and E.I. Moser, *A manifold of spatial maps in the brain.* Trends in Cognitive Sciences, 2010. **14**(12): p. 561-569.

[23] Urban, D.J. and B.L. Roth, *DREADDs (Designer Receptors Exclusively Activated by Designer Drugs): Chemogenetic Tools with Therapeutic Utility* Annual Review of Pharmocology and Toxicology, 2015. **55**: p. 399-417.

[24] Dong, S., S.C. Rogan, and B.L. Roth, *Directed molecular evolution of DREADDs: a generic approach to creating next-generation RASSLs.* Nat. Protocols, 2010. **5**(3): p. 561-573.

[25] Dong, S., et al., *A chemical-genetic approach for precise spatio-temporal control of cellular signaling.* Molecular BioSystems, 2010. **6**(8): p. 1376-1380.

[26] Armbruster, B.N., et al., *Evolving the lock to fit the key to create a family of G protein-coupled receptors potently activated by an inert ligand.* Proceedings of the National Academy of Sciences, 2007. **104**(12): p. 5163-5168.

[27] Hires, A., *Neurons controlled by DREADD*. 2009, Brain Windows.

[28] Farrell, M.S., *Using DREADDs to Isolate Internal Clocks.* Front Integr Neurosci. , 2011. **5**: p. 87.

[29] Pollock, J., D.-Y. Wu, and J. Satterlee, *Molecular neuroanatomy: a generation of progress.* Trends Neurosci., 2014. **37**(2): p. 106-23.

[30] Fortress, A., et al., *Designer receptors enhance memory in a mouse model of Down syndrome.* J Neurosci., 2015. **35**(4): p. 1343-53.

[31] Zhu, H., et al., *Chemogenetic Inactivation of Ventral Hippocampal Glutamatergic Neurons Disrupts Consolidation of Contextual Fear Memory.* Neuropsychopharmacology, 2014. **39**: p. 1880-1892.

[32] Garner, A.R., et al., *Generation of a Synthetic Memory Trace.* Science, 2012. **335**(6075): p. 1513-1516.

[33] *Animal Injection*. Sept 10, 2015]; Available from: http://www.clodrosome.com/animal-injection/

[34] Jeffery, K. *Research*. 2014; Available from: http://www.ucl.ac.uk/jefferylab/research.

[35] Miao, C., et al., *Hippocampal Remapping after Partial Inactivation of the Medial Entorhinal Cortex.* Neuron 2015. **88**: p. 590-603.

[36] van Duuren, E.v.d.P., G, et al., *Pharmacological manipulation of neuronal ensemble activity by reverse microdialysis in freely moving rats: a comparative study of the effects of tetrodotoxin, lidocaine, and muscimol.* J Pharmacol Exp Ther., 2007. **323**(1): p. 61-9.

[37] Olypher, A.V., P. Lansky, and A.A. Fenton, *Properties of the extra-positional signal in hippocampal place cell discharge derived from the overdispersion in location-specific firing.* Neuroscience, 2002. **111**(3): p. 553-66.

[38] Fenton, A.A., et al., *Attention-Like Modulation of Hippocampus Place Cell Discharge.* J. Neurosci., 2010. **30**(13): p. 4613-4625.

[39] Lánský, P. and J. Vaillant, *Stochastic model of the overdispersion in the place cell discharge.* Biosystems, 2000. **58**(1-3): p. 27-32.

[40] Olypher, A.V., P. Lansky, and A.A. Fenton, *Properties of the extra-positional signal in hippocampal place cell discharge derived from the overdispersion in location-specific firing.* Neuroscience, 2002. **111**(3): p. 553-566.

[41] Bonnevie, T., et al., *Grid cells require excitatory drive from the hippocampus.* Nat Neurosci, 2013. **advance online publication**.

[42] Sargolini, F., et al., *Conjunctive representation of position, direction, and velocity in entorhinal cortex.* Science, 2006. **312**(5774): p. 758-62.

[43] Derdikman, D., et al., *Fragmentation of grid cell maps in a multicompartment environment.* Nat Neurosci, 2009. **advance online publication**.

[44] Stensola, H., et al., *The entorhinal grid map is discretized.* Nature, 2012. **492**(7427): p. 72-78.

[45] Bonnevie, T., et al., *Grid cells require excitatory drive from the hippocampus.* Nature Neuroscience, 2013. **16**(3): p. 309-317.

[46] Derdikman, D., et al., *Fragmentation of grid cell maps in a multicompartment environment.* Nat Neurosci, 2009. **12**(10): p. 1325-1332.

[47] Hardcastle, K., S. Ganguli, and L. Giocomo, *Environmental boundaries as an error correction mechanism for grid cells.* Neuron, 2015. **86**(3): p. 827-39.

[48] Barry, C., et al., *Experience-dependent rescaling of entorhinal grids.* Nature Neuroscience, 2007. **10**(6): p. 682-684.

[49] Stensola, T., et al., *Shearing-induced asymmetry in entorhinal grid cells.* Nature, 2015. **518**(7538): p. 207-212.

תקציר בעברית

הנוירונים המווסתים מרחבית בתוך המערכת ההיפוקמפלית במוח נחשבים למערכת המאפשרת גיבוש של זכרון ותפיסה של המרחב הפיסי. הנוירונים הללו כוללים בין השאר את תאי המקום, שהינם נוירונים פירמידליים בהיפוקמפוס שיורים כאשר החולדה חוצה איזור מסויים של המרחב, את תאי כיוון הראש, שהינם תאים היורים כאשר החולדה מסתכלת לכיוון מסויים, את תאי הגבול, היורים כאשר החולדה קרובה לגבולות הקופסה ,ואת תאי הגריד, בקורטקס האנטוריינל, שיורים בתבנית מחזורית הקסגונלית. תאי הגריד שומרים על דפוסי הירי שלהם בתוך הסביבה, וניתן לאפיינם ע"י הפרמטרים השונים של הגריד אותו הם יוצרים. יש עדויות לקיומם של תאים מווסתים מרחבית ביונקים שונים, בנוסף למכרסמים. נכון להיום תאים כאלה נמצאו גם בעטלפים, בקופים ובבני אדם.

מחקרים הראו שהנוירונים הללו משחקים תפקיד משמעותי בניווט מרחבי ובתפיסה של מקום העצמי במרחב. המערכת נחשבת גם למעכת ה"ג'י פי אס הפנימי", מכיוון שהיא מתפקדת כמערכת המאפשרת לחיה לבנות מפה קוגניטיבית בתוך המוח. מעבר לתפקידם במיפוי המרחב, נוירונים אלו כנראה מעורבים גם ביצירה ובגיבוש של הזכרון.

תכונות הירי של תאים אלה נוטות להיות יציבות ואמינות כאשר החיה נמצאת באותה הסביבה. התאים פעילים כאשר החיה עוברת דרך השדות הרצפטיביים של התאים, ושקטים כאשר החיה מחוץ לשדות אלה. כדרך לאיתות על שינוי, הנוירונים משנים את מקומות השדות הרצפטיביים שלהם כאשר החיות מושמות בסביבות אחרות. לתכונה זאת של הנוירונים קוראים "מיפוי מחדש".

במחקר זה בדקנו עד כמה השדות הרצפטיביים של התאים הללו נוטים להיות יציבים, חזקים ואמינים. בדקנו זאת בשתי שיטות: גישה כימו-גנטית בה השתמשנו ב-DREADDs (רצפטורים מתוכננים במיוחד להפעלה ע"י סמים מתוכננים) להשתקה של תאים היפוקמפליים, וגישה חישובית, בה חקרנו את דפוסי הירי של תאי גריד בודדים.

DREADDs הם רצפטורים המצומדים ל-G-protein ומגיבים באידאל באופן בלעדי למולקלות סינטטיות קטנות מסויימות, בעוד שהם אדישים לליגנדים טבעיים. הרצפטורים הללו מאפשרים שליטה מרחבית וזמנית בנוירונים באמצעים לא חודרניים. בנוסף, תוצרי התהליך הם הפיכים, ללא נזק למערכת. השתמשנו בסוג אינהיביטורי של DREADD כדי להשקיט את הפעילות ההיפוקמפלית של תאי המקום ולבדוק את את האפקטים של התהליך על השדות הרצפטיביים של

תאי המקום לאחר התאוששות. באופן ספציפי, התעניינו בשאלה האם התאים חזרו למקומם המקורי או עברו תהליך של מיפוי מחדש. מצאנו שבחלק מהמקרים התאים שמרו על מקומם המקורי לאחר ההתאוששות, ובמקרים אחרים התאים עברו תהליך של מיפוי מחדש.

בחלק השני של המחקר, בדקנו את דפוסי הירי של תאי גריד רבים שנלקחו ממאגרי נתונים. רצינו לבדוק את מידת השונות בין שדות רצפטיביים שונים של אותו תא גריד. מצאנו שהשונות בירי בין שדות שונים באותו תא היתה גדולה מהצפוי ע"פ שיטות ערבול סטטיסטיות. ניסינו לבדוק את המקור לשונות הזאת. מצאנו שעיקרה נובעת משדה אחד דומיננטי שחזק מהאחרים. השדה החזק נטה להיות קרוב יותר לגבול המרחב, מה שרמז שהשדה יכול היה לשמש כעוגן (pivot) לקביעת האוריינטציה והפאזה של הגריד.

הממצאים הללו מראים שהשדות הרצפטיביים של תאי מקום ותאי גריד הם לא סטטיים כפי שחשבו לפני כן. דפוסי הירי של תאי המקום משתנים לאחר מניפולציה הפיכה באמצעים פרמקולוגיים. בנוסף, תאי גריד מראים קצבי ירי לא אחידים בין השדות השונים. שני החלקים מצביעים על כך שאינפורמציה נוספת מתווכת בנוסף לדפוס הירי המרחבי הטהור. תהליכים אלה מצביעים על חוסר אחידות וחוסר יציבות של המערכת מעבר לצפוי.

המחקר נעשה בהנחיית דורי דרדיקמן במחלקה ל מדע המוח, פקולטה רפפורט לרפואה- הטכניון - מכון טכנולוגי לישראל.

אני מודה לטכנין על התמיכה הכספית הנדיבה בהשתלמותי.

יציבות ושונות של דפוסי ירי עצביים מווסתים מרחבית

חיבור על מחקר

לשם מילוי חלקי של הדרישות לקבלת התואר מגיסטר
למדעים ברפואה

רֶבֶקָה אִיסְמַקוֹב

הוגש לסנט הטכניון - מכון טכנולוגי לישראל

חשון תשע"ו, חיפה, נובמבר 2015

יציבות ושונות של דפוסי ירי עצביים מווסתים מרחבית

רֶבֶקָה אִיסְמַקוֹב